1-1-2014

Correlation Effects In Nanoparticle Composites: Percolation, Packing And Tunneling

Rupam Mukherjee
Wayne State University,

CORRELATION EFFECTS IN NANOPARTICLE COMPOSITES: PERCOLATION, PACKING AND TUNNELING

by

RUPAM MUKHERJEE

DISSERTATION

Submitted to the Graduate School

of Wayne State University,

Detroit, Michigan

in partial fulfillment of the requirements

for the degree of

DOCTOR OF PHILOSOPHY

2014

MAJOR: PHYSICS

Approved by:

_____

Advisor Date

_____

_____

_____

_____

DEDICATION

To my Parents

ACKNOWLEDGEMENTS

I would like to take the opportunity to thank everyone who helped me during the course of my graduate studies and the completion of my PhD degree. I express my deep gratitude to my principal supervisor, Professor Boris Nadgorny for the kind of broad vision, guidance and encouragement he provided throughout the journey at Wayne State University. I learned a lot and felt relaxed enough to ask questions and make mistakes. Next, I would like to thank Professor Gavin Lawes for his endless effort on providing scientific suggestions and insights during study of dielectric properties. I am also grateful to Professor Zhi-Feng Huang for his theoretical explanations and series of valuable discussions during study of percolation phenomenon. I also want to thank Professor Ashis Mukhopadhyay for accepting to be a committee member and having useful discussions for my future carrier. Next, I would like to thank Professor Ivan Avrutsky from electrical and computer engineering department for being willing to undertake the arduous task of external committee member.

I am very grateful to Professors Ratna Naik, Jogindra Wadehra, Paul Keyes, J.J. Chang, and Sergei A. Voloshin for their considerable guidance and support in my graduate study and being wise mentors.

I am thankful to my senior group members Dr. Girfan Shamsutdinov, Dr. Pushkal Thapa, Dr. Xiangdong Liu and Dr. Debabrata Mishra for their support and sharing their knowledge and experience with me. I am also thankful to my friends in Physics and other department for wonderful time together and support.

Last but not least, I appreciate the patience, encouragement, help and hope of my parents, brothers and wife Sujata Mukherjee for better future.

TABLE OF CONTENTS

LIST OF TABLES

LIST OF FIGURES

CHAPTER 1 INTRODUCTION

1.1 Scope of the Thesis

The work described in this thesis aims to understand the effect of percolation on various, seemingly unrelated physical phenomena, including the relationship between dielectric permittivity and conductivity of metal-insulator composites, classical and tunneling percolation phenomena, and the effect of percolation on packing in nanoparticles systems. Specifically, we investigated the very large enhancement of the dielectric permittivity of a composite metal – insulator system in the vicinity of the percolation threshold, the appearance of a multistep tunneling staircase in complex nano-composite systems, as well as the surprising relationship between particle packing and the percolation threshold.

Most composites studied in this thesis are made of just two materials. One material is the matrix and the other acts as filler. We have studied the behavior of electrical transport properties in these composite systems as we vary the filler volume fraction. In addition to a classical single percolation threshold which we observed in many metal-insulator composite systems, we also found a percolation tunneling "staircase" with multiple percolation thresholds, which are mainly attributed to tunneling percolation of different orders. Along with the change of metallic concentration, we also found an intriguing packing behavior as we change the size

of insulating nanoparticles. We found that along with the percolation threshold, the packing in the composites also has a strong dependence on the ratio of size of insulating particles and metallic particles. In our further work, we aimed to study the behavior of metallic clusters in a dielectric matrix, which can potentially store energy. We came across many interesting results while we studied metallic-dielectric composites. Developing supercapacitors requires the dielectric permittivity to be 1) very high with low loss and 2) to be frequency and temperature independent which is necessary for storing colossal charge effectively over a wide range of voltages, temperatures and in domain of high frequencies. The focus of our experimental work thus aims to fabricate dielectric material with desirable dielectric response as mentioned above. Again percolation technique was used in which metallic particles were incorporated in dielectric matrix to achieve efficient dielectric material.

1.2 Introduction

We acknowledge the fact that our nature is disordered.[1] It is true that despite of ordered systems being more efficient, stable and easily approachable, their existence is very limited. It is difficult to make or even buy clean, pure and defectless systems with precise physical and chemical characteristics. In real world, engineers and experimentalists actually deal with composites, mixtures, defective crystals and many more disordered systems for the purpose of scientific

development.[2] Here, the disorderness is usually referred to the randomness of inhomogeneous medium. As for example, rain water seeping through porous soil.[3] In this type, randomness is associated with the water since water molecules decide where to go in the soil. This dynamics is usually referred to diffusion. However, the rain water will reach the water bed only if the soil pore is open. In this case the randomness is associated with the soil (medium) since the pore can be open or close independent of each other. In these types of disordered systems, the dynamic and non dynamic properties are mostly explained by percolation phenomenon. In laboratory, a similar situation arises in case of composite systems in which the network of constituent elements governs the transport and tensile properties and agrees well with the percolation theory. This percolation phenomenon is basically a statistical concept and is applied well in understanding much complex disordered system. Now a days there is an increase in experimental activities on composite systems due to its ability of tailoring the physical and chemical properties at low cost. In semiconductor industry there is a huge need of small sized active and passive elements which would be stable and efficient at any temperature. This led us to focus on the development of percolative composite systems. [4]

1.3 Theory of percolation:

Flory (1941) and Stockmayer (1943) were the first to introduce percolation phenomenon while describing the process of polymerization. In the

process of polymerization where small molecules fuse together through chemical bonding to form large network of single molecule lays the foundation of percolation process. The first ever mathematical approach on percolation theory was developed by Broadbent and Hammersley (1957).[5] They showed that the percolation process is the consequence of geometrical phase transition in a random medium and interestingly the change in transport and physical properties of the system follows a universal power law and scaling laws. Generally, percolation process is classified into two categories, lattice (site-bond) percolation model and continuum percolation model. Each of them is explained in details below.

1.3.a The site-bond percolation model

Let us consider a regular 2-d lattice in which each lattice site can be occupied by conducting particle with probability P or can be occupied by insulating particle with probability 1-P. The occupation of each lattice site is independent to the probability of occupation at neighboring sites. In this system, the electric current flows from one end of the lattice to the other only when there is continuous cluster of conducting sites that spans the entire lattice system. Here, the cluster is defined as group of conducting sites that are interconnected and bounded by insulating sites. At low occupational probability P, there is a formation of isolated clusters of nearest neighbor

conducting sites. Since there is no inter connection between the conducting isolated clusters, current cannot percolate through the lattice. The system remains insulating. On the other hand, at high P, the number of individual clusters and there sizes grows to merge with each other and thus forms a single infinite conducting cluster that supports the electrical transport throughout the system. Clearly there is an existence of specific concentration with occupation probability P above which the current percolates and below which it remains insulating. This critical concentration is knows as percolation threshold P_C. The above phenomenon in the system is a site percolation since the clusters are formed by closest neighboring sites. When the bond between the sites are randomly occupied with probability q, and the cluster is formed by nearest neighbor bonds then it is known as bond percolation.[6] The nature of site percolation and bond percolation is shown in the figure below.

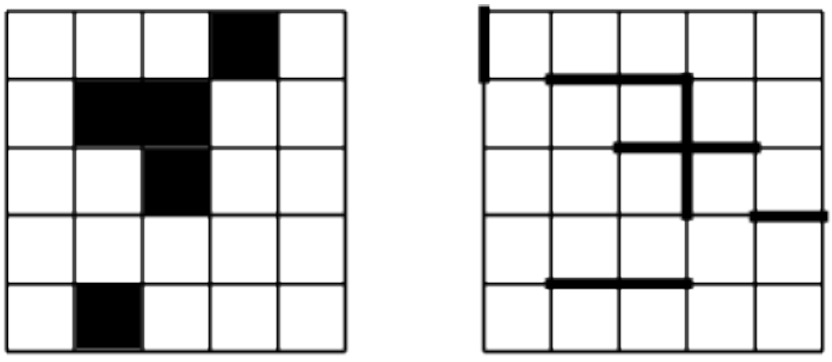

Figure 1.1 Site percolation and bond percolation model in 2 dimensions

Random resistor network and polymerization process are examples of bond percolation. Overall these percolation processes is marked by geometrical phase transition which is different than thermal phase transition in which the transition between two phases appears at critical temperature. The cluster which forms at threshold P_C is known as infinite cluster since its size diverges in the thermodynamic limit. For $P>P_C$, the density of the infinite cluster keeps on increasing since the isolated clusters grows to merge with the infinite cluster. For P=1, the infinite cluster covers all of the lattice sites or bonds. The critical concentration P_C explicitly depends on the dimension (d) of the system, coordination number (Z) and aspect ratio of the constituent particles. As for example, for triangular lattice with Z=6 and square lattice with Z= 4, we have P_C = 0.5 and 0.5927 respectively. Moreover for simple cubic lattice with increase d but same Z=6, we have P_C= 0.3116 which is smaller than the systems with d=2.

1.3.b The continuum percolation model

In case of percolation in continua medium, the distribution of coordination number varies from site to site which indeed makes the problem more interesting. Here the position of the components is not restricted to the discreet sites of a regular lattice.

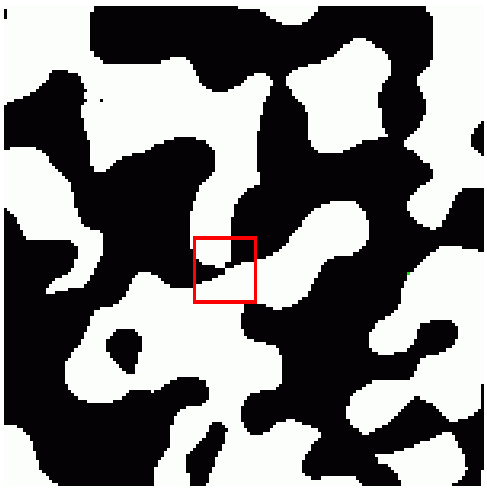

Figure 1.2 Continuum percolation model, distribution in continuous matrix

As for example, let us consider an electrically conductive sheet in which circular holes are punched randomly. Below the critical concentration of holes (P_C), the sheet becomes insulating no matter the sites or bonds are occupied or not. This resembles Swiss cheese and so it is known as Swiss cheese model. This model is appropriate to explain the transport or elastic properties in porous medium.

1.3.c Universal scaling laws

Since the percolation transition is mainly a statistical phenomenon, it is important for a site to have a probable distribution that belongs to percolating cluster. The probability P_∞ that a random site belongs to the infinite cluster has a distribution such that it is zero for $p<p_c$, and $P_\infty \sim (p-p_c)^\beta$ for $p>p_c$. The length of the finite isolated clusters above and below p_c is characterized by correlation length ξ. For $p<p_c$, it represents the length of the connected clusters and for

$p>p_c$, it represents the length scale over which the random network becomes macroscopically homogenous. When p approaches p_c, ξ behaves as $\xi \sim |p-p_c|^{-\nu}$. The other percolation parameters such as cluster mass, backbone mass and transport properties such as effective conductivity and superconductivity are shown in the table below.

Quantity		Exponent	d=2	d=3
Order parameter	$P_\infty(p) \sim (p-p_c)^{\beta}$	β	5/36	0.417±0.003
Correlation length	$\xi(p) \sim \lvert p-p_c \rvert^{-\nu}$	ν	4/3	0.875±0.008
Cluster mass	$M(r) \sim r^{d_f}$	d_f	91/48	2.524±0.008
Backbone mass	$M_B(r) \sim r^{d_B}$	d_B	1.62±0.02	1.855±0.015
Chemical Path	$l(r) \sim r^{d_{min}}$	d_{min}	1.13±0.004	1.374±0.004
Random Walk	$\langle r^2(t) \rangle \sim t^{2/d_w}$	d_w	2.871±0.001	3.80±0.02
Conductivity	$\sigma_{dc}(p) \sim (p_c-p)^{\mu}$	μ	1.30±0.002	1.99±0.01
Superconductivity	$\sigma_S(p) \sim (p-p_c)^{-s}$	s	1.30±0.002	0.74±0.03

Table 1.1 Determination of critical exponents in 2-d and 3-d.

1.4. Electrical percolation in composite systems

In multicomponent composite systems, the electrical transport is mainly characterized as continuum percolation phenomenon. In these systems, percolation transition appears when particles of minor phase (conducting) make a physical contact with each other to form isolated clusters. With the increase of metallic volume fraction (P), the clusters increases in size and when the volume fraction

approaches P_C, it gives rise to infinite cluster that spans the entire system. It is entirely a geometrical effect because it includes the geometry of clusters (size, shape and orientation of the particles) which in turn can modulate the percolation threshold accordingly.[7, 8] This percolation transition is a second order phase transition with percolation threshold being non universal and microstructure dependent. In composite systems, percolation threshold has always been a point of attraction. Many physical properties of composites such as resistivity, dielectric constant, heat capacity, thermal conductivity have a dramatic effect near the percolation threshold. These physical properties of composite systems follow a power law near the threshold (P_C) which is represented in form Properties $\approx |P-P_C|^{\pm e}$, where e is the critical exponent having different values for different physical properties.[9] The fact that the geometry of fillers (minor phase) as well as that of insulating matrix can tune the location of percolation threshold but the critical exponent for a specific dimension (2-d or 3-d) is considered to be universal. Although recently some experiments have confirmed that the critical exponents found to be are non-universal.[10-12] Since the shape size and orientations of filler particles tune the threshold, their filling factor can also affect the nature of conductivity in the composite system. For example, if the conducting particles are spheres and the matrix is insulating, then the filling factor of spheres can be used to study the electrical conductivity in disordered composite powders. The first ever

measurements of electrical conductivity on powdered samples were carried out by Malliaris and Turner by using polyethylene particles of radius R_P = 150μm and metallic nickel particles of radius R_N =4-7μm.[13] They found that the electrical resistivity of this composite system dropped by 20 orders of magnitude at a percolation threshold which itself depends on the ratio of insulating particle t metallic particle (R_P/R_N). If the particle size ratio of insulating to metallic powder is $\lambda=R_P/R_N$, then in the composite involving n_c conductive particles and n_i insulating particles, then the volume fraction of the conductive phase is given as

$$P= n_cR_N^3/(n_cR_N^3+n_iR_i^3)=n_c/(n_c+n_i\lambda^3)$$

Clearly, the conductive percolation threshold P_C, is a monotonic decreasing function of λ and as $\lambda\rightarrow\infty$ P_C approaches a limit.[14] Fitzpatrick et al. also did an explicit study on percolation and electrical conduction in random closed packed spheres. A fraction of spheres were aluminum and rest others were insulated acrylic plastic spheres. This composite system was pressed between two aluminum electrode and conductivity measurements were carried by an ohmmeter at high resistance and wheatstone bridge at low resistance. They noticed that the conductivity of the system vanishes at particular volume fraction of conducting spheres.[15] A more systematic and extensive study on conducting properties of packing of particles were carried out by Ottavi, et.al.[16] They observed that with the

increase of pressure on the composite system, the conductivity increases and percolation threshold decreases with the increase of coordination number. They found that the effective conductivity (g_e) follows a power law near P_C $g_e=(P-P_C)^{\mu}$, where μ is found to be 1.7±0.2 which agrees well with the three dimensional percolation process. It is found that for R_i/R_c (R_i being the size of insulating particle, and R_c is the size of conducting particle) >>1, the conducting phase fillers fills the interstitial space between the insulating phase particles, thus forming a continuous percolating cluster of conducting phase. Following this law, much small percolation threshold can be achieved in spherical shaped composite systems. This size effect on percolation threshold was evident when small Ni particles were forced into the gaps between large insulated ferrite particles and P_C of 0.095 was achieved as a result of large size ratio.[9]

1.5. Dielectric properties of composites

There is a growing demand for the new composites that meet the requirements of miniaturization and multifunctionality such as cellphones, digital camera, supercapacitors, chemical sensors, biological equipments and many other eco friendly applications.[17] Development of composites with high dielectric permittivity and low loss has proved very promising for high tech applications in electronic devices. Memory and capacitance based energy storage devices can acquire more amount of energy and can deliver it instantaneously when high

dielectric materials are used. This led us to find new promising materials or to work on the methods to improve dielectric response of suitable materials.[18] It is found that in metal-insulator composites, when the metallic volume fraction approaches the percolation threshold there is a dramatic increase in dielectric constant. Along with the conductivity, the dielectric constant (K) of the composites diverges as $K \propto |P-P_C|^{-S}$, where s is the critical exponent and its value is found to be close to 1 in 3d systems. Large enhancement of dielectric constant is observed in many systems such as polymer based composite system, Ni/$BaTiO_3$ composites and many other ferroelectric ceramics and polymers.[19-21] These types of polymers are easy to make since it requires low processing temperature and are compatible with blended ceramic powders such as $BaTiO_3$. In ceramic /polymer composites there isn't much enhancement of dielectric constant (K~60). Such enhancement was observed at high metallic volume fraction (P>0.5). The disadvantage of having high volume fraction is that it reduces the flexibility of final polymer composite system and it degrades the permittivity quality due to presence of voids. A number of other composite systems also showed dramatic change in dielectric response at room temperature which is shown in the table below.

Composites	Dielectric constant(K)	Dielectric loss(tanδ)
$Ba_{0.75}Sr_{0.25}TiO_3$/Ag	24,000@10KHz	0.038
$Pb(Zr_{0.97}Ti_{0.03})O_3$/Ag	1,700@1KHz	0.05
$Na_{0.5}Bi_{0.5}TiO_3$/Ag	5,500@100Hz	0.05
$SrTiO_3$/Pt	2,150@100Hz	0.09
$Ca[Li_{1/3}Nb_{2/3})_{1-x}Ti_x]O_3$ $_\delta$/Ag	$4x10^5$@1MHz	0.01
$Bi_{1.5}ZnNb_{1.5}O_7$/Ag	~10^5@1MHz	0.01

Table 1.2 Determination of dielectric constant and loss

In these composite systems the increase of dielectric constant near percolation threshold is mainly due to existence of microcapacitor networks.[22] These microcapacitors are formed by neighboring metallic particles separated by dielectric matrix in between them. It is also believed that near threshold, there is a strong increase in the intensity of the local electric field produced by metallic clusters which helps the charge carriers to migrate and accumulate at the metal-insulator interface. Due to the mismatch of Fermi energy, these accumulated charges experience coulomb blockade at the interface and thus becomes localized. This rise to interfacial polarization and is commonly known as Maxwell-Wagner

effect. This effect is highly responsible for the enhancement of dielectric constant in many composite systems. These charges can only relax either by tunneling between closed metallic clusters or by ohmic conduction caused by physical contact between metallic clusters. The dielectric losses in these composites are mainly due to Debye-type relaxation and leakage current. The former takes place when the time constant of the orientation polarization mismatches with the applied field. At low temperature when the polarization freezes, there is usually a peak in dielectric loss which is attributed to Debye type relaxation.[23] In the second case the leakage current is high near the percolation threshold.

1.6. Motivation of the work

Despite the fact that the critical exponents of electrical conductivity is suppose to be universal (depends only on the dimension and not on the details of microstructure and interacting force between the constituent particles), some researchers have found this to be non-universal. This has been confirmed by theorists and some experimental evidence supports it.[24-26] It is found that the equation 1 still remains valid although there is a deviation of exponents from universal value. The main reason for its non-universal behavior is due to introduction of quantum mechanical tunneling. This type of conduction mechanism is different from the classical one in sense that in the latter case, there is a physical contact between the metallic clusters through which electron flows whereas in the

former case the charge carriers passes through the potential barriers formed due to spatial separation of metallic clusters. As for example, this tunneling mechanism was confirmed by using conducting tip atomic force microscopy in carbon nanofibre/polymer composite systems.[27] It was established that tunneling can occur only through nearest neighbors and all other non-nearest neighbors doesn't count.[24, 28, 29] Our motivation of work was to identify the tunneling region and nature of electrical conduction in both sides of the percolation threshold. We have worked on number of metal-insulator composite systems to study the percolation behavior. The other reason to get involved in number of composite systems is that since the percolation threshold P_C depends on the geometry of the composite components we were trying to establish a relation between the filling factors of the constituent particles and its electrical conductivity.

In metal-insulator composite system, although some work has been done on improving the dielectric constant, we have focused on ceramic based composite system whose high dielectric permittivity can be enhanced even further by some more factors. Our goal is to develop a composite system that has very high dielectric permittivity with low loss.

1.7. Outline of the dissertation

The experimental procedures and the details of materials used have been discussed in chapter 2. It includes various metal-insulator composite systems with different sizes and shapes of constituent particles. Some of the composite systems were synthesized in the lab. The details of their fabrication are discussed. Scanning electron microscopy (SEM), Energy dispersive x-rays (EDX) and Transmission electron microscopy (TEM) and X-ray diffractometer (XRD) have been used for material characterization. A detail of four point contact technique is also discussed in this chapter.

Chapter 3 discusses about types of percolation behavior in composite systems. Determinations of percolation threshold from temperature dependent measurements have been discussed. The nature of critical exponents was also discussed in these composite systems.

Chapter 4 introduces the concept of filling factor in these composite systems. The dependence of filling factor on insulating to metallic particle size ratios is discussed in details. The relation between percolation thresholds and filling factor has been discussed. The scaling law of these filling factors has also been shown here.

Chapter 5 shows the dielectric behavior of Calcium Copper Titanate (CCTO) material prepared by both solid state and sol gel process. The behavior of dielectric permittivity as a function of temperature and frequency is discussed here.

Chapter 6 shows the frequency dependent dielectric behavior in a composite system at room temperature. The ac conductivity at different frequency is shown and discussed in details. We observed enhancement of dielectric constant with increasing metallic volume fraction.

Chapter 7 includes the conclusion of the project works and discussion about the future projects.

CHAPTER 2 MATERIALS AND EXPERIMENTAL TECHNIQUES

Preparation of composite powders and synthesis of some high dielectric materials are discussed in this chapter. The experimental techniques used for conductivity measurement and dielectric measurement are discussed here in details. Characterization of composites and materials were performed with the help of SEM, EDX, TEM and XRD. The theory behind each of this spectroscopy is mentioned in this chapter.

2.1 Materials

The materials used for our experiments are for the purpose of making metal-insulator composite system. Some of the insulating powders used are Al_2O_3 (aluminum oxide), K_2CO_3 (potassium carbonate), PMMA (poly-methyl-methacrylate), $LiCoO_2$ (lithium cobalt oxide), CCTO (calcium copper titanate) and the ones used as metallic powders are CrO_2 (chromium oxide), MgB_2 (magnesium boride) and RuO_2 (ruthenium oxide). The aspect ratio of these components is all different. SEM image gives the details of each of the particles morphology which is mentioned latter.

2.1.1 Chromium Oxide (CrO_2)

The bulk CrO_2 is usually a black microcrystalline powder. CrO_2 converts into Cr_2O_3 at around 400^oC temperature. It has a rutile crystal structure with a tetragonal symmetry.

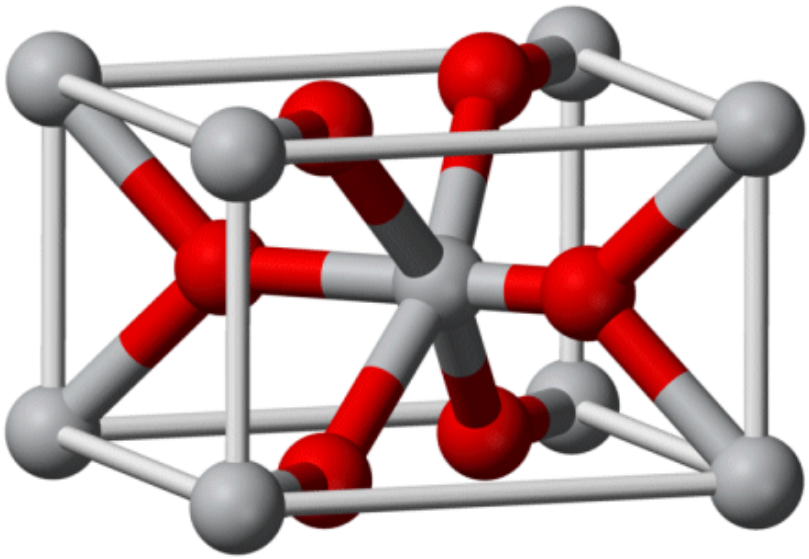

Figure 2.1 Rutile structure of CrO_2, the gray spheres resemble chromium atom and red spheres represents oxygen atom.

Chromium atoms (gray spheres) has a octahedral coordination whereas oxygen atoms (red spheres) shows trigonal planar coordination. Chromium dioxide is a metallic solid and has excellent electrical conductivity.[30] CrO_2 has a thin layer of Cr_2O_3 around it which makes the material more resistive at low temperature.[31] The temperature dependent electrical property is shown below.

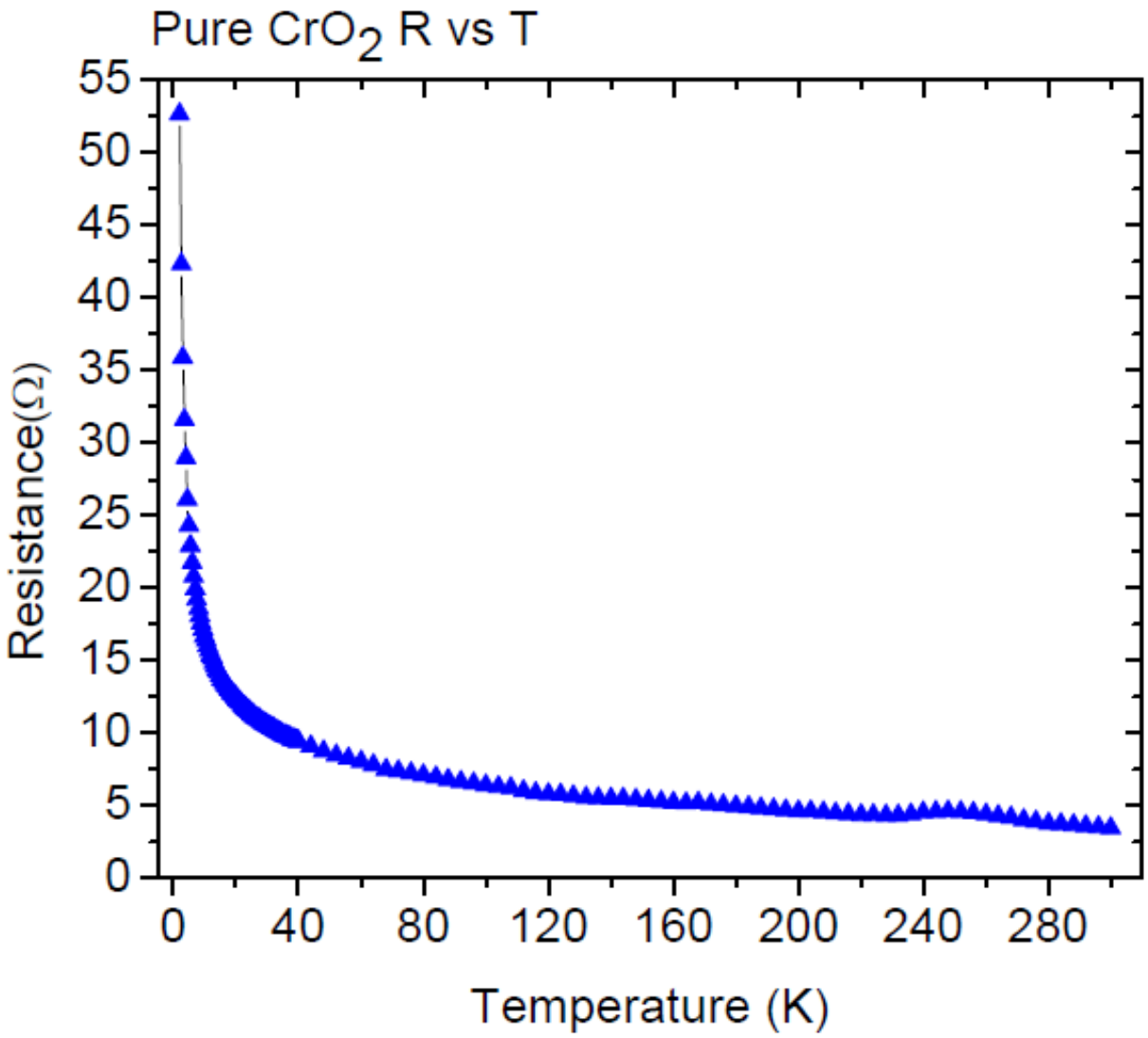

Figure 2.2 Resistance as a function of temperature for bulk pure CrO_2

The size and shape of CrO_2 particles was obtained by SEM which is shown in the latter part of this chapter.

2.1.2 Ruthenium Oxide (RuO_2)

RuO_2 is a deep blue 4d oxide that exhibits metallic Ruthenium-oxygen bonding.[32] It has a rutile structure with melting temperature of around 1235°C. It is most thermodynamically stable compound. RuO_2 has a very high electrical conductivity since its Fermi energy overlaps with the conduction band density of states.[33] At 1100°C, size of the nanocrystals of RuO_2 increases from 50nm to 500nm and becomes isometric in shape. Temperature dependent resistance of RuO_2 is shown in the figure below.

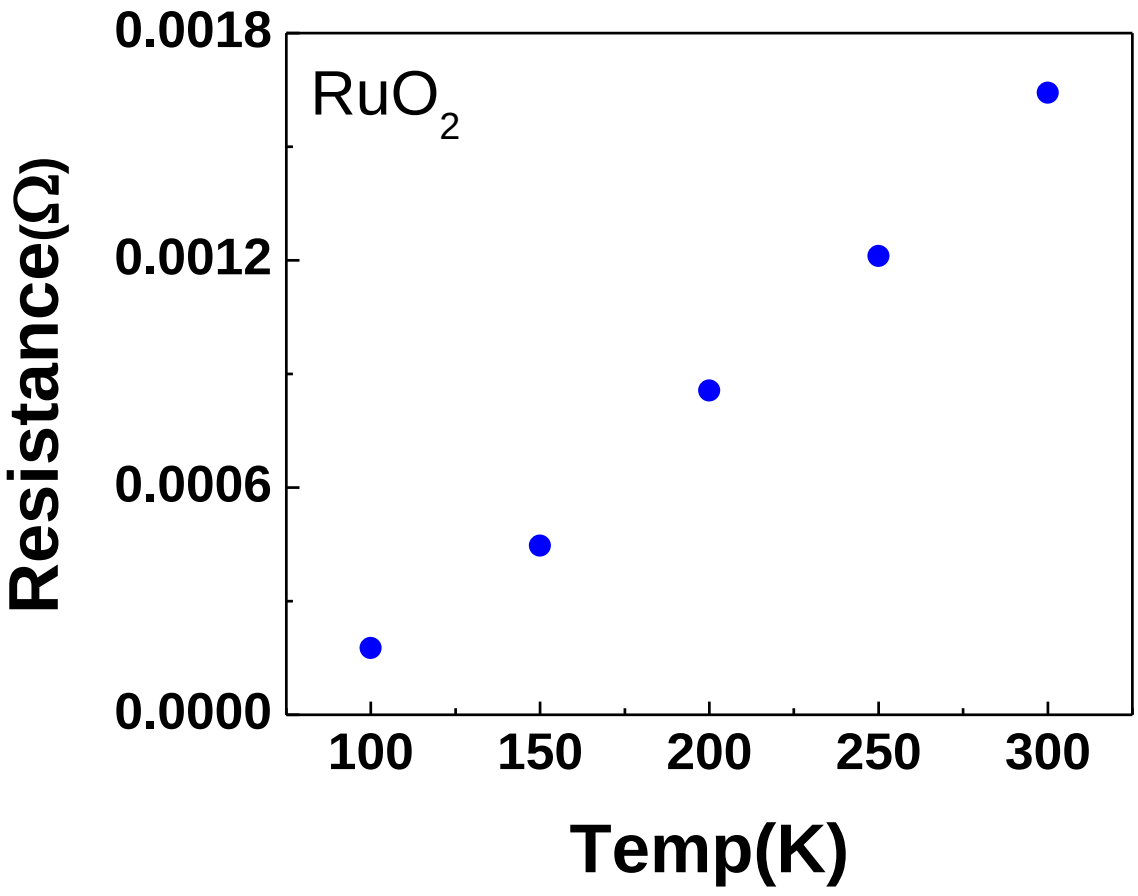

Figure 2.3 Resistance as a function of temperature for pure bulk RuO_2

2.1.3 Magnesium Boride (MgB_2)

MgB_2 is a conventional superconductor with critical constant at 39K.[34] MgB_2 has a hexagonal lattice with two layers of boron and magnesium along the c axis. The structure of boron layer resembles the layer of graphite structure.[35] Boron atoms are at each corner of hexagon and magnesium atoms are located at the centre of the hexagon.MgB_2 shows a strong anisotropy at in the B-B lengths. The atomic distance between the boron planes is considerably longer than the in plane B-B distance. The image of MgB_2 is shown below.

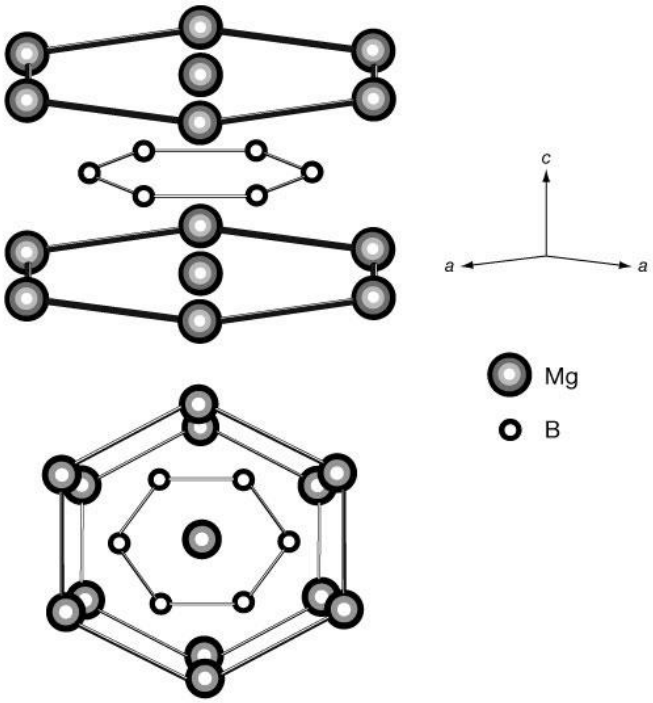

Figure 2.4 Crystal structure of MgB_2, taken from reference 34

2.1.4 Lithium Cobalt Oxide ($LiCoO_2$)

It is a p-type semiconductor with a band gap of 2.7ev. Electrical conduction in a semiconductor is usually a thermally activated phenomenon which exhibits Arrhenius-type behavior.

$$\sigma_T=\sigma_o exp(-E_a/K_BT)$$

where σ is the electrical conductivity, σ_o is the pre-exponential factor, E_a is the activation energy, K_B is the Boltzmann constant and T is the temperature.[36] Structurally layers of lithium lies between slabs of octahedral formed by cobalt and oxygen atoms. The crystal structure of $LiCoO_2$ is shown below.

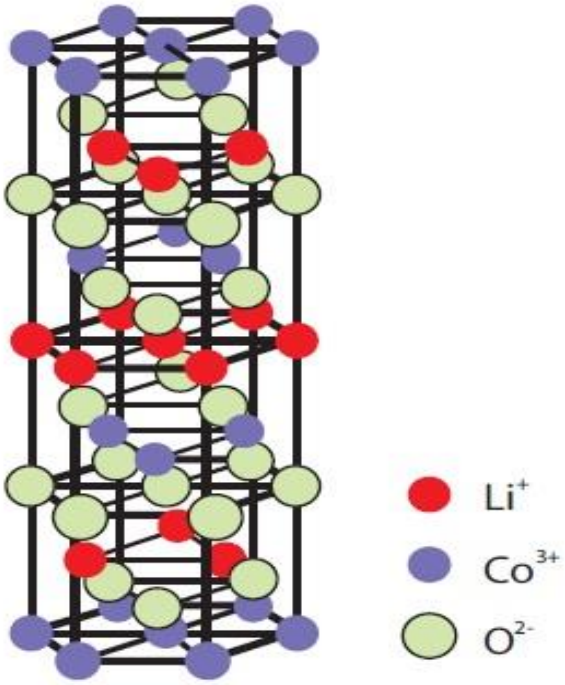

Figure 2.5 Crystal structure of $LiCoO_2$ with respective atoms shown in different colors

2.1.5 Poly-Methyl Methacrylate (PMMA)

It is an insulated transparent thermoplastic polymer white powder with a thin coating of Silicon dioxide (SiO_2). We have used monodispersed spherical particles of PMMA whose size were varied from 500nm to 10micro meter. The structural transformation from methyl mathacrylate to PMMA is shown below.[37]

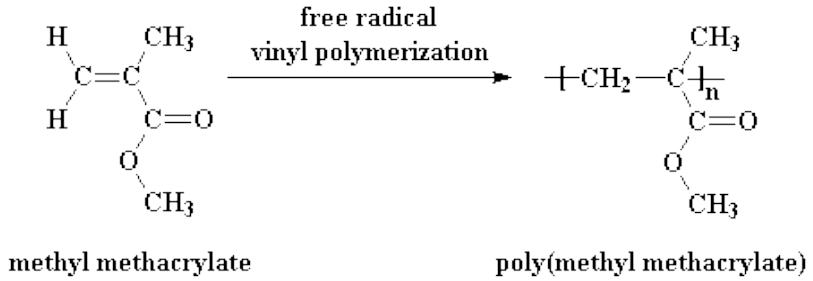

Figure 2.6 Molecular structural transformations from MMA to PMMA

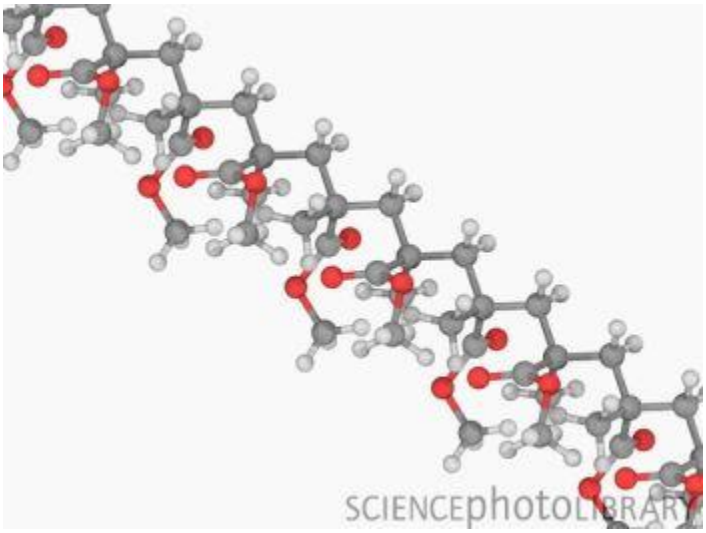

Figure 2.7 Structure of PMMA molecule, taken from Science photo library

2.1.6 Aluminum Oxide (Al_2O_3)

Al_2O_3 has a poor electrical and thermal conductivity but are chemically and thermally stable. Al_2O_3 is also commonly known as alumina. It has different allotropic forms such as amorphous, α and other forms. α- alumina is considered to be the most usual one. In the crystal structure the oxygen ions have an arrangement similar to close-packed hexagonal type with aluminum ions in two –thirds of the octahedral sites.[38] The crystal structure of Al_2O_3 is shown below.

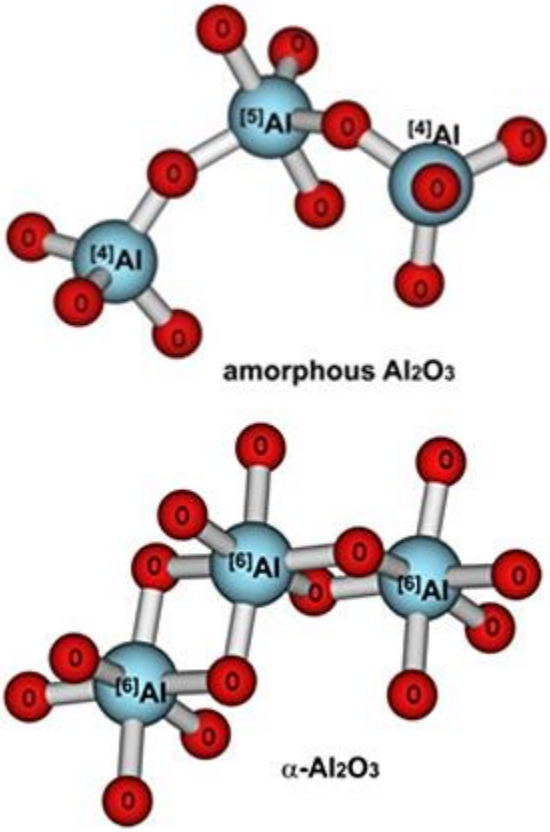

Figure 2.8 Amorphous and α structure of alumina

2.1.7 Calcium Copper Titanate (CCTO)

$CaCu_3Ti_4O_{12}$ (CCTO) is a high dielectric material suitable for energy storage devices. It has a perovskite structure with TiO_6 has octahedral arrangement, copper atoms (green) are bonded to four oxygen atoms (red) and large calcium atoms (purple) are without bonds. The structure is shown below.

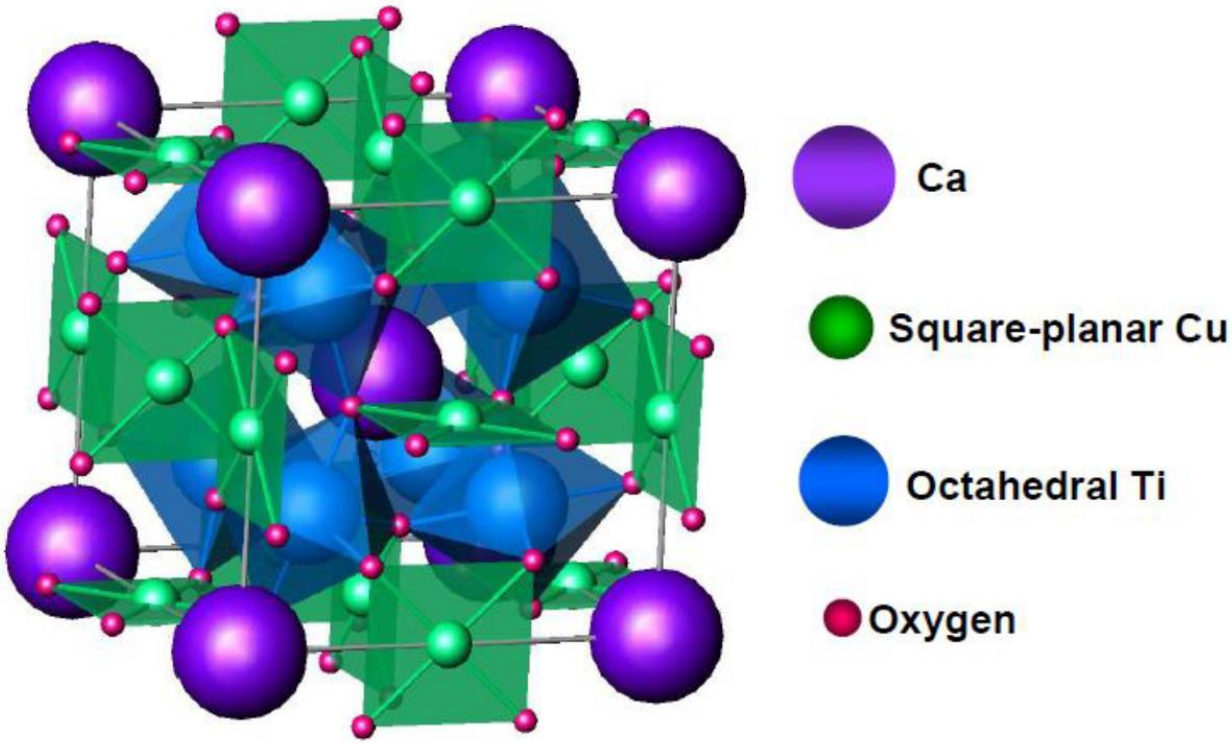

Figure 2.9 $CaCu_3Ti_4O_{12}$: Distorted double perovskite structure

The octahedral tilting is clearly seen which is due to large cation size mismatch between the Ca^{2+} (1.34Armstrong) and Cu^{2+} (0.57Armstrong). $CaCu_3Ti_4O_{12}$ can be synthesized by both solid state and sol gel process. In solid state process powder samples of CCTO were prepared by mixing $CaCO_3$ (99.99%, Aldrich,), CuO

(99.99%, Aldrich) and TiO_2 (99.99%, Aldrich) in a planetary ball mill with acetone using zirconia balls for two hours.[39] The chemical reaction is as follows.

$$CaCO_3 + 3CuO + 4TiO_2 = CaCu_3Ti_4O_{12} + CO_2$$

The mixture was then pre-calcined at 1000°C for 12 hours. RuO_2 (99.99%, Aldrich) was then added at different volume fractions (*f*) and mixed thoroughly with agate mortar and pestle in dehumidifying atmosphere to minimize particle agglomeration. After mixing, pallets of $RuO_2/CCTO_{SS}$ composites were prepared by using a cold pressed die with an uniaxial pressure of 1 GP and then calcined at 1100°C prior to dielectric measurement. To synthesize CCTO composites by Sol Gel technique we used $Ti(OBu)_4$, $Cu(CH_3COO)_2.H_2O$ and $Ca(CH_3COO)_2.H_2O$ reagents as precursors (Aldrich).[40] These starting materials were mixed with hot glacial acetic acid and ethyl alcohol and were stirred with magnetic stirrer for 8 hrs. A xerogel was obtained at 85°C. This xerogel was then pre-calcined at 1000°C for 12 hours.

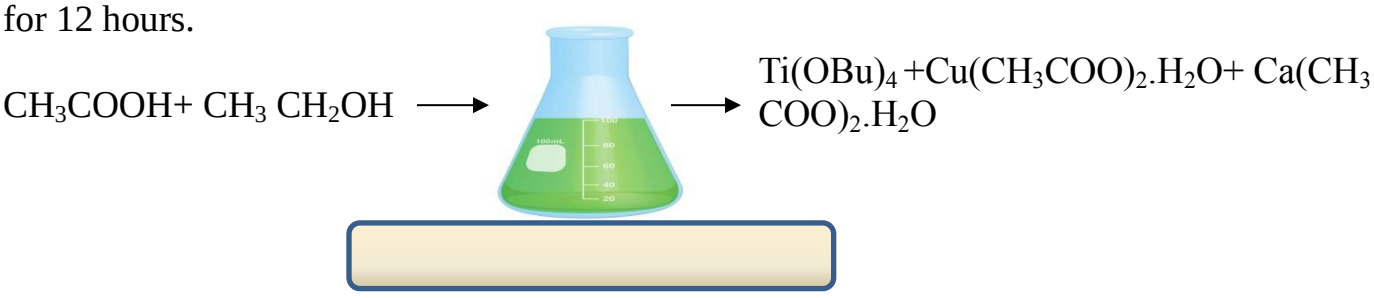

Figure 2.10 CCTO prepared by sol gel process at 85 degree centigrade

2.2 Sample preparation

The metal-insulator composites are mixed according to the weight ratios of metallic component and insulating component. The mixtures of two components were thoroughly grinded with glass mortar and pestle for half an hour. The purpose of grinding is to have a well dispersed homogenous mixture composite and to get rid of agglomerated particles. In case of CrO_2, thorough grinding is recommended since it reduced insulating Cr_2O_3 layer which resides at the outer layer of CrO_2 particles. Along with the grinding, we make sure that the humidity of the surrounding atmosphere has to be low enough so that the moisture doesn't affect our experimental results. Presence of high humidity can increases the resistance of the samples. So to maintain the consistency, we have used LG dehumidifier to keep the humidity lower than 30%. After grinding the mixture, we made pallets with the help of cold press die in which the mixtures were pressed with 20 tons of hydraulic pressure. The pellets have an average thickness of 1mm and 5mm diameter. We used PPMS puck, PPMS and Keithley instruments to conduct our electrical measurements. Silver paste and gold wires were used for four point contact technique at the time of transport measurements. After that the composites were mounted on the PPMS puck with wires attached to the four gold pads of the puck. A set of composite samples were prepared by varying the weight fraction of metallic component. The weight fractions (x) range from 0.01 to1. These weight

fractions are then converted into volume fraction using bulk densities of metallic component (ρ_1) and insulating component (ρ_2). The volume fraction of metallic component is given as

$P= (mx/\rho_1)/[mx/\rho_1+m(1-x)/\rho_2]$

where m is the total mass of the powder. The images of all the experimental techniques we used are shown in the figure below. The filling factor (F) of the composite systems is an important parameter which defined as the total volume in all the clusters both above and below the threshold divided by the simulation or experimental volume of the sample. Mathematically it is defined as

$F= [(m_1 /d_1)+(m_2/d_2)] /(\pi*r^2*t)$

where m=weight of individual powders (metallic or insulating), d= density of respective powders, r= radius of the pallet, t= thickness of the pallet.

Figure 2.11 Mortar and pestle

Figure 2.12 Cold-press die

Figure 2.13 Hydraulic press system

Figure 2.14 Annealing furnace

2.3 Four point contact technique

This technique is used while conducting electrical measurements. In this technique electrical current is passed between two of the probes and the voltage created in the sample is measured with the other two probes. The difference between 2pint contact and 4 point contact is shown with the help of diagram.

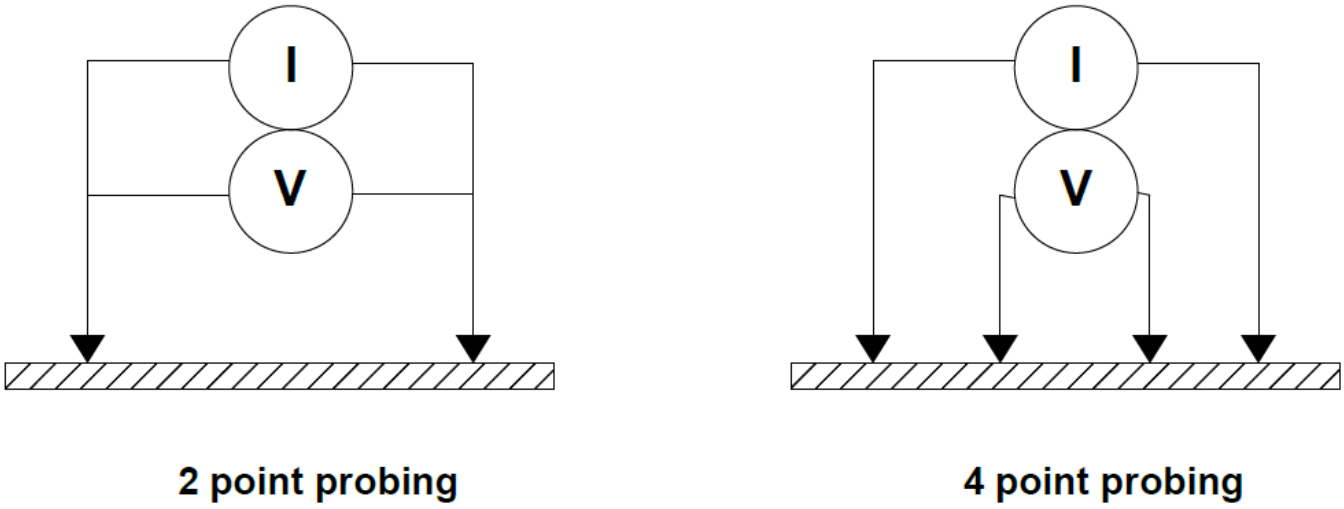

Figure 2.15 Geometrical difference between two point and four point techniques

In 2 point method, current and voltage are measured in the same wire due to which the measured voltage is added with the potential difference created into the wires. Whereas for the 4 point method, since the current and voltages are measured with different wires, the measured voltage is really that circulate within the sample with no current.[41] Since in voltmeter the input resistance is very high, no current can go into the voltmeter which in turn doesn't measure the potential drop within the wires of voltage leads. In this way the electrical measurements turns out to be more accurate.

2.4 Sample characterization techniques

Various characterization techniques were used to confirm morphology, purity and stoichiometry of constituent elements. Before starting the electrical measurements in our composite systems it was required to confirm the shapes and sizes of materials for study of percolation and their corresponding packing in the composites. Moreover, the dielectric material CCTO was fabricated in our laboratory. The extent of its purity and its stoichiometry was required to be confirmed since the material is sensitive to our fabrication procedure. Here below is the list of techniques we used for our material characterization.

2.4.1 Principles of SEM

The scanning electron microscope (SEM) enables the investigation of specimens with a resolution down to the nanometer scale. Here an electron beam is generated by an electron cathode and the electromagnetic lenses of the column and finally swept across the surface of a sample. The path of the beam describes a raster which is correlated to a raster of gray level pixels on a screen. As a consequence the magnification is simply computed by the ratio of the image width of the output medium divided by the field width of the scanned area.

The main signals which are generated by the interaction of the primary electrons of the electron beam and the specimen´s bulk are secondary electrons and

backscattered electrons (BSE) and furthermore X rays. They come from an interaction volume in the specimen which differs in diameter according to different energies of the primary electrons (typically between 200 eV and 30 keV). The SE come from a small layer on the surface and yield the best resolution, which can be realized with a scanning electron microscope. The well known topographical contrast delivers micrographs which resemble on conventional light optical images.

The BSE come from deeper regions of the investigated material thus giving a lower resolution. The typical compositional contrast gives material specific information since the signal is brighter for regions of a higher middle atomic number of the investigated area. As a byproduct of the image giving signals X-rays are produced. They result from ionization processes of inner shells of the atom leading to electromagnetic radiation. The characteristic X-rays give information about the chemical composition of the material. In the conventional scanning electron microscope, which operates in high vacuum, the specimen has to be electrically conductive or has to be coated with a conductive layer (e.g. Carbon, Gold etc.).

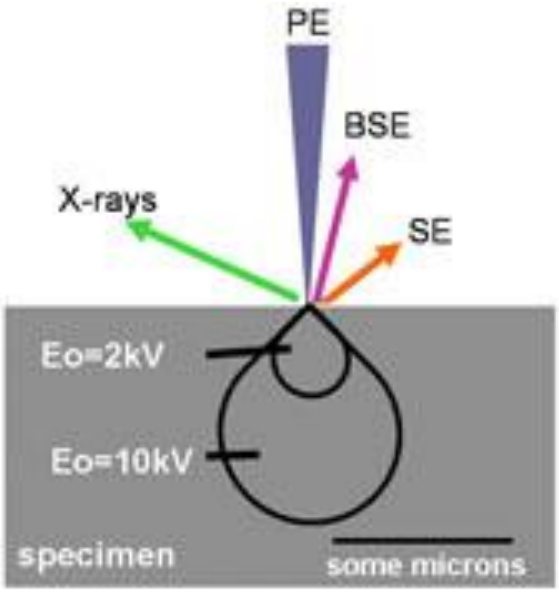

Figure 2.16 Interaction volume in a specimen is shown

2.4.2 Energy Dispersive X-ray (EDX)

EDS makes use of the X-ray spectrum emitted by a solid sample bombarded with a focused beam of electrons to obtain a localized chemical analysis. In principle all elements from atomic number 4 (Be) to 92 (U) can be detected, though not all instruments are equipped for 'light' elements (Z < 10). Qualitative analysis

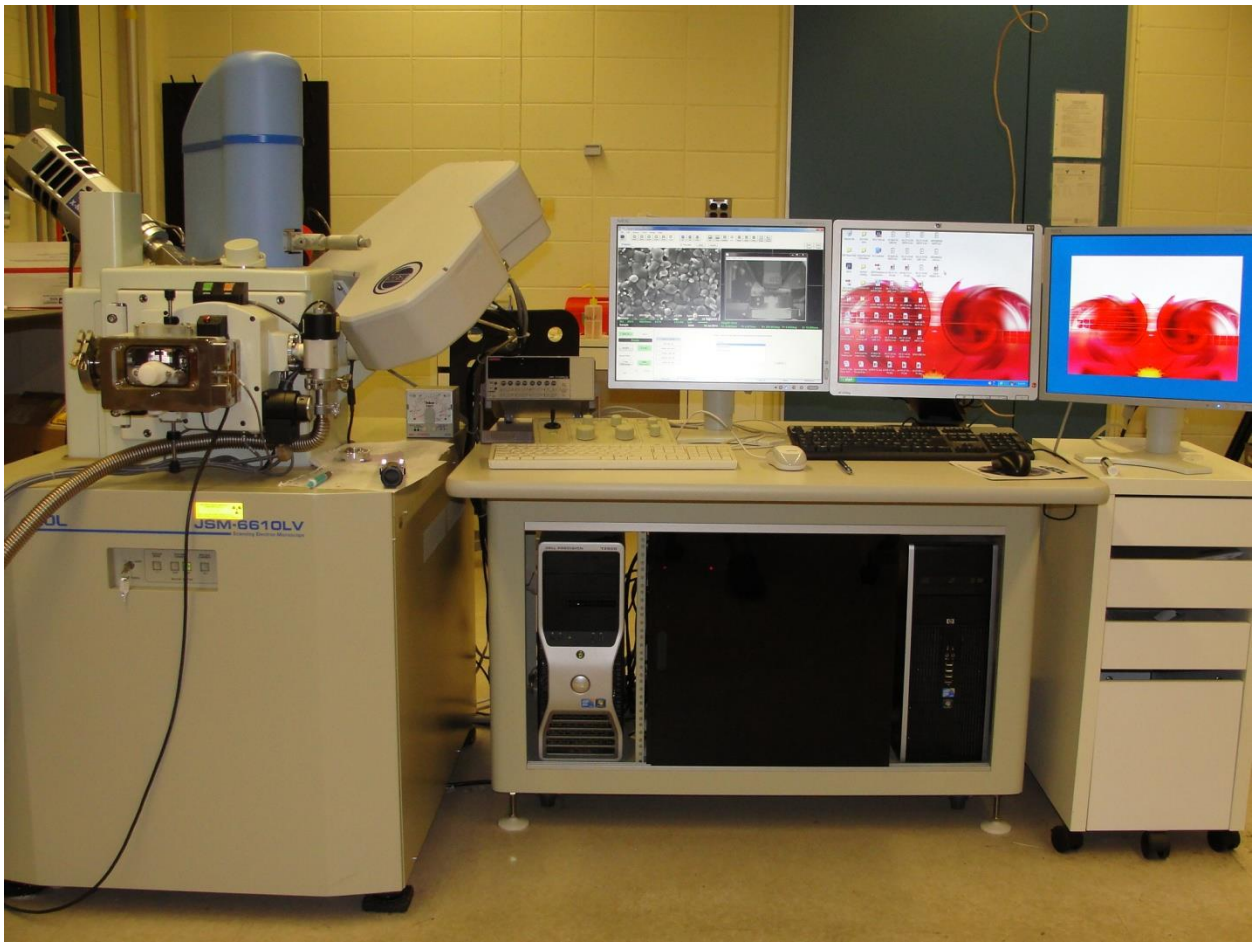

Figure 2.17 SEM microscope compatible with EDX and WDX

involves the identification of the spectrum lines and is fairly straightforward owing to the X-ray spectra. Quantitative analysis for the determination of the concentrations of the elements present requires measuring of line intensities for each element in the sample and for the same elements in calibration Standards of known composition. By scanning the beam in a raster fashion and displaying the intensity of a selected X-ray line, images or 'maps' of element dispersion can be produced. Also, according to the mode selection, images produced by electrons

collected from the sample reveal surface topography or mean atomic number differences. The scanning electron microscope (SEM), which is an electron probe, is thus designed for multitasking such as producing electron images, element mapping and even point analysis, if an X-ray spectrometer is added. There is thus a significant overlap in the functions of these instruments.

Accuracy and sensitivity

The intensities of X-ray are measured by counting photons and the precision obtainable is limited by statistical error percentage. For most of the elements it is usually not difficult to have a precision (defined as 2σ) of better than ± 1% (relative), but the overall analytical accuracy is generally nearer ± 2%, which is due to other factors such as uncertainties in the compositions of the standards and errors in the various corrections which need to be added to the raw data. Along with producing characteristic X-ray lines, the bombarding electrons also produce continuous X-ray spectrum, which limits the detachability of small peaks, owing to the presence of 'background'. Using routine procedures, detection limits are typically about 1000 ppm (by weight) but can be reduced by increasing the counting times

Spatial resolution

Spatial resolution is ruled by the penetration and spreading of the electron beam inside the specimen as shown in the figure. Since the electrons penetrate an approximately constant mass, spatial resolution is thus a function of density. In the case of silicates (density about 3 g cm^{-3}), the nominal resolution is about 2 µm under typical conditions, but for quantitative analysis a minimum grain size of several micrometers is required.

2.4.3 Transmission Electron Microscope (TEM)

The transmission electron microscope is a delicate tool for study of material characterization. Highly energetic beam of electrons is shined through a very thin sample, and the interactions between the incident electrons and the atoms can be used to extract the features such of crystal structure especially dislocations and grain boundaries. Quantitative chemical analysis can also be achieved for stoichiometric materials. TEM can be used to study the atomic layer deposition, their compositions and defects in semiconductors. High optical resolution is required to analyze the quality, structural geometry and density of quantum wells, wires and dots. The TEM and the light microscope operates on same basic principle but the former uses electrons instead of light. Because the wavelength of electrons is much smaller than that of light, the optimal resolution attainable for TEM images is many orders of magnitude better than that from a light microscope.

This is the reason TEMs can be used to reveal the finest details of internal structure - in some cases as small as individual atoms. By the use of cond-

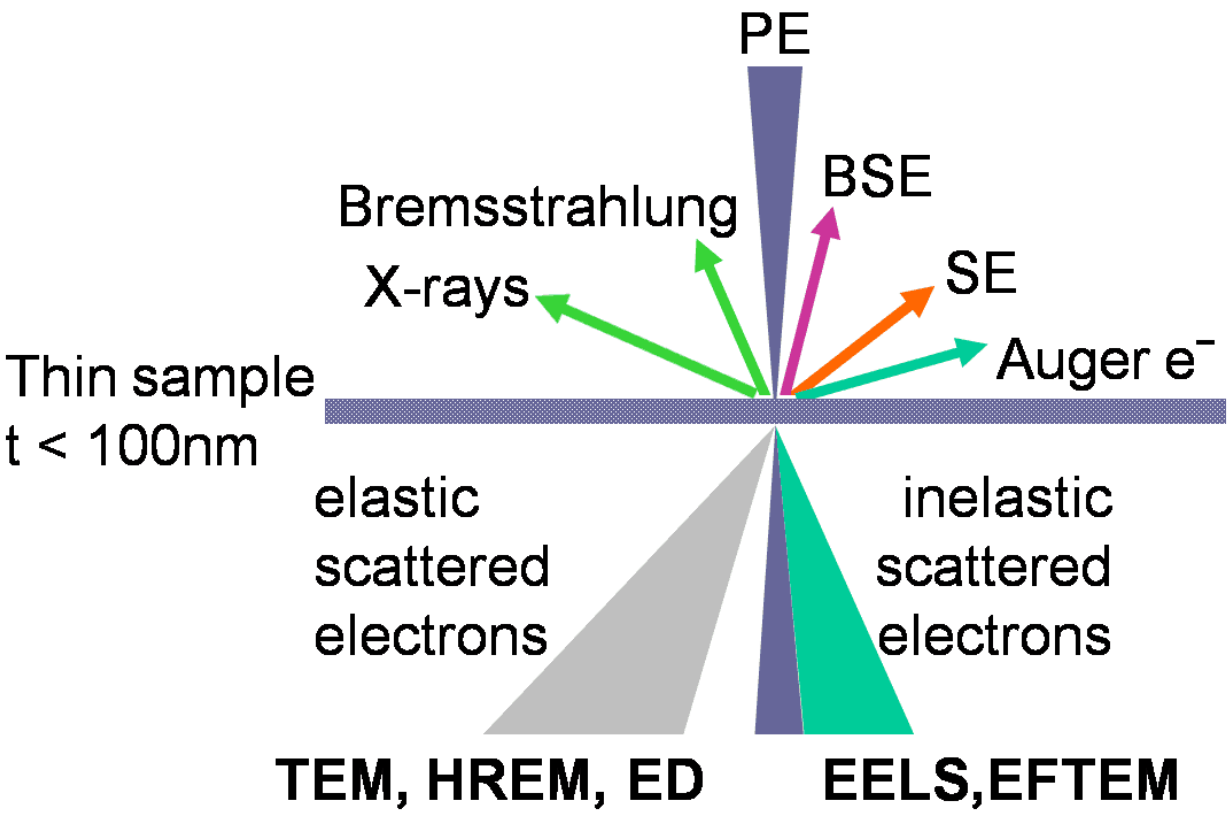

Figure 2.18 Different imaging techniques for all range of energetic particles

enser lens beam of electrons from the electron gun is focused into a small, thin, coherent beam. This electron beam is constricted by the condenser aperture, which rejects high angle electrons. The energetic beam then strikes the sample specimen and parts of it are transmitted depending upon the thickness and electron transparency of the sample. This transmitted portion is focused by the objective lens either into an image on phosphor screen or charge coupled device (CCD)

camera. Optional objective apertures are used to enhance the contrast by blocking out high-angle diffracted electrons. The image then passed down the column through the intermediate and projector lenses, is enlarged all the way.

The image strikes the phosphor screen and light is generated, allowing the image to be visible. The darker areas of the image thus represent those areas of the specimen that fewer electrons are transmitted through while the lighter areas of the image represent those areas of the sample that more electrons were transmitted through. It is to note that a TEM specimen must be thin enough to transmit sufficient electrons to form an image with minimum energy loss. Specimen preparation is an important aspect of the TEM analysis.

2.4.4 X-ray Diffraction (XRD)

Diffraction effects are observed when electromagnetic radiation is shined on periodic structure with wavelength of radiation comparable to lattice spacing. Generally the diffraction effect in crystals and molecules are observed with interatomic distances of 0.15-0.4nm which correspond in the electromagnetic spectrum with wavelength of x-rays having photon energies between 3 and 8kev. Accordingly, optical phenomena like constructive and destructive interference should become observable when crystalline and molecular structures are exposed to x-rays. There are three different types of interaction in the relevant energy

range.[42] Firstly, in the process of photoionization electrons are liberated from their bound atomic states. Since in the process of photoionization, the quantum of

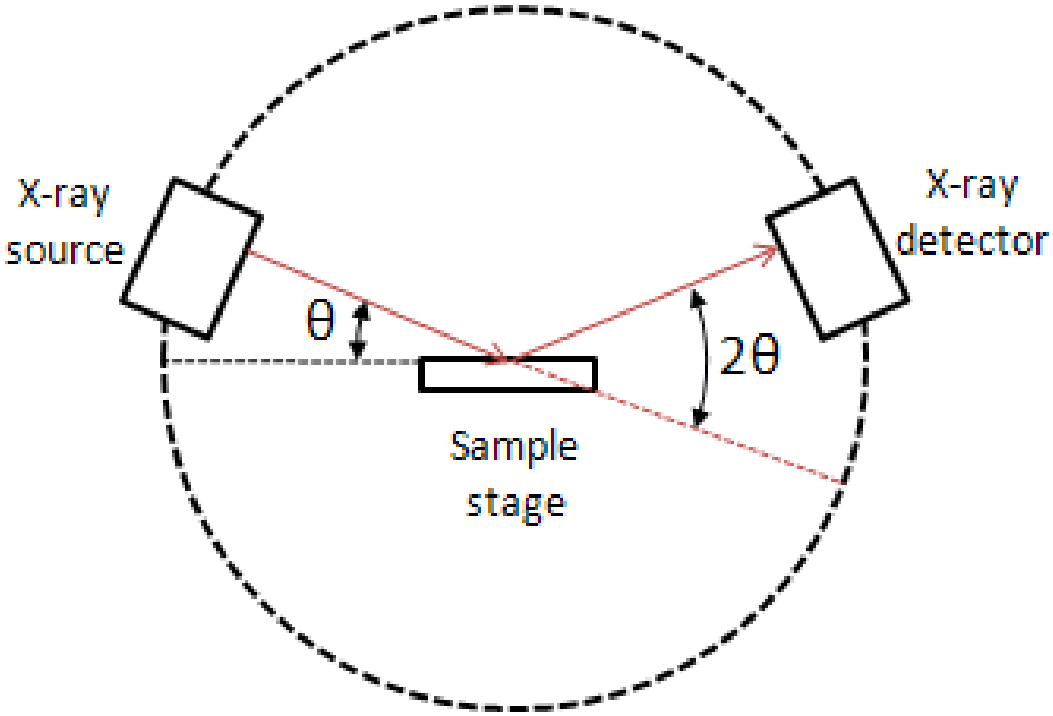

Figure 2.19 Powder X-ray diffractometer

energy and momentum are transferred from the incident radiation to the excited electron. So this kind of photoionization falls in the group of inelastic scattering processes. In the second kind, the incoming x-rays may undergo another inelastic scattering which is known as Compton scattering. Also in this kind of process energy is being transferred to electron which proceeds, however, without releasing electron from the atom. Moreover, X-rays can also be scattered elastically by

electrons which is named as Thomson scattering. In this process, the secondary electron oscillates as Hertz dipole at the frequency of the incoming beam and becomes a source of dipole radiation. The short wavelength λ of x-rays is conserved in case of Thomson scattering in contrast to the two inelastic scattering process mentioned above. It is thus the Thomson component in the scattering of the x-rays that is made use of to study structural details by x-ray diffraction.

We will use all these experimental techniques to study various transport properties in different types of composite systems. To verify the components of the composites in terms of its purity and morphology, it is important to use the material characterization techniques prior to and after each experiments.

CHAPTER 3 ELECTRICAL PERCOLATION IN NANOCOMPOSITES

This chapter introduces the concept of electrical percolation in binary mixture of insulating and conducting phase in granular composite systems. Electrical transport properties in these disordered systems are explained in terms of percolation process. The electrical conduction is mainly attributed to geometrical phase transition which happens when isolated metallic clusters coalesce to form a single infinite conducting cluster that spans the entire system, thus owing to classical type percolation behavior. The universal power law of conductivity is generally a signature of classical percolation. However, some researchers have experimentally found conductivity to have non-universal critical behavior. This unexpected behavior is attributed to non-classical type percolation. Tunneling phenomenon is found to be the origin of non-universality in the composite systems. This urges us to study tunneling conduction phenomenon in details. We have shown that even in the absence of physical connectivity of metallic phase in composite systems, the electric connectivity is still maintained through nearest and non-nearest neighbors via tunneling.

3.1 Introduction

The electrical properties in composites comprising of metallic phase and insulating phase are categorized into two different forms of conduction

mechanism, classical percolation in continuum matrix and tunneling percolation between isolated metallic clusters.[43, 44] In the composites, at high concentration of metallic phase, the metallic grains coalesce to from continuum medium. This continuity is a route to classical percolation and the conductivity follows standard power law with a universal critical exponent which is 2.0. The power law is given as

$$\sigma \propto (P\text{-}P_C)^t \qquad 3.1$$

where σ is the electrical conductivity, P is the metallic volume fraction, P_C is the percolation threshold and t is the critical exponent. On the other hand, it is also observed that even at regime lower than percolation threshold ($P<P_C$), finite conductivity exists.[45] The electrical conductivity in this case is mainly attributed to interparticle tunneling. Earlier experiments have also confirmed that the composites in which conducting Carbon Black (CB) particles are incorporated in an insulating polymer, inter-particle tunneling is the dominant conduction mechanism.[46] Mathematically, the inter-particle tunneling conductivity is given as[47]

$$\sigma_{tun} \propto \exp[-\frac{r-2R}{\xi}] \qquad 3.2$$

where r is the distance between the centers of the spherical conducting particles, R is the radius of the particles and ξ is the typical tunneling range parameter. Although every two metallic particles in the composites are connected through the above equation, but their contribution to the electrical conductivity decreases as r increases. It is also expected that with the metallic volume phase (P) approaches zero, the conductivity decreases and the corresponding dependence will not necessary conform to percolation conductive power law behavior.

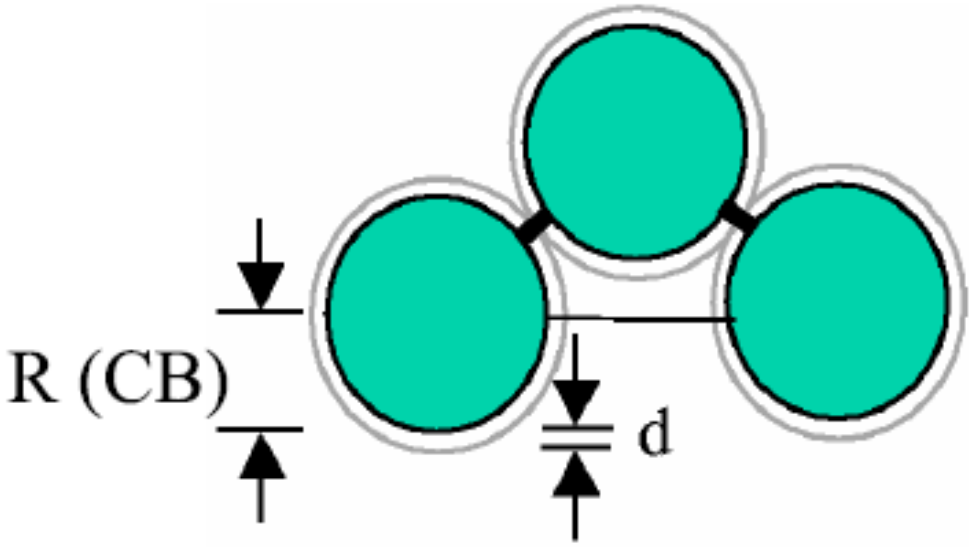

Figure 3.1 Inter-particle connectedness between nearest neighbor is represented as thick black line and far neighbor is represented with thin line. The tunneling length d is shown around the solid core.

From equation 3.2, it suggests that only the nearest neighbor contributes to the electrical conductivity and the contribution from the non-nearest neighbors doesn't count. For non-nearest neighbors, we have r-2R > 2R and for nearest

neighbors we have r-2R ≈ ξ<< R. If R >> ξ, then the corresponding tunneling conduction between non-nearest neighbors indeed yields a negligible contribution to the macroscopic conductivity.[48] It is also found that in metal-insulator composites, the electron tunneling from each conducting particle to another may show both percolation and tunneling behavior depending on parameter D/ξ, where D=2R is the size of conducting particle and ξ is the tunneling length.[49-51] In composites with large conducting particle size (on the order of 1 micron), it shows sharp cutoff of the conductivity at the percolation threshold. So in one case the electrical continuity is well maintained when there is a physical contact among conducting particles. On the other hand even if the conducting particles do not touch each other, their inter particle separation is such that the electron can travel from one particle to another. This tunneling conductance has an exponential decay with the interparticle distance over a characteristics tunneling length ξ, which is on the order of few nanometers, depending on the material properties. This means that unlike classical percolation, tunneling percolation will not have any sharp cutoff conductivity.[52, 53] It is also established that when the microstructure of the composite system resembles the lattice model and when D is several times larger than the correlation length ξ, then multiple percolation thresholds in the composite system would appear.[54] Recently multiple percolation thresholds in Ni-SiO_2 system is observed experimentally.[55] Double percolation is also been observed

experimentally in Ag-SnO_2 nanogranular films.[54] Phenomenon of two percolation or multiple percolation is eventually related and attributed to shape of the filler particles. When rounded shaped SiC particles are used in a matrix of insulated EPD monomer rubber, then slow percolation behavior with only one percolation threshold was observed. Compared to angular shaped filler, percolation threshold was even higher in case of rounded shaped fillers.[56] Percolation is one of the most fundamental and far-reaching physical phenomena, with major implications in a vast variety of fields.[57, 58] The observation of a conductivity threshold in a mixture of a metallic filler in an insulating matrix is one of the simplest manifestations of a classical percolation process, which governs transport and many other properties of the system.[2] In the case of classical percolation, at the percolation threshold with filler volume fraction p_c the geometrical connectivity is beginning to span across the entire system, leading to the appearance of an infinite cluster.[57] Consequently, near percolation threshold p_c the resistivity of a composite can be expressed as $R \propto (p-p_c)^{\mu}$. The critical exponent μ can be considered universal, i.e. material-independent, contingent only on the dimensionality of the system, provided that the local microstructure of a system is isotropic and has only short range correlations.[59] The universality of μ (μ ~ 2 in 3D) can be well described by random resistor network models.[53, 60, 61] Indeed, in many experiments this value lies within a fairly narrow range from 1.7 to 2.[57, 59, 62]. However, in almost half of the experiments μ

deviates from the universal value, often quite dramatically - sometimes exceeding it by almost an order of magnitude.[60] This puzzling behavior has been habitually attributed to various tunneling processes between particles or random clusters.[62, 63] However, at least at first sight percolation and tunneling phenomena are not easy to reconcile. While the definition of a threshold - as a point at which electrical conductivity vanishes - in classical percolation is straightforward, it is conceptually much more difficult to assign a threshold value in the case of tunneling. Strictly speaking, tunneling conductance between particles comprising a percolative network should always exist, albeit exponentially small at larger interparticle distances. Assuming no sharp cut-off and a random distance distribution between particles, one would generally expect variable-range tunneling mechanism to dominate the conductance across such a network, resulting in an exponential-type behavior with no distinct percolative thresholds. On the other hand, multiple percolation transitions can be envisioned in the case of lattice-like microstructure of the composite systems, with specific relationships between the particle size D, the characteristic tunneling length ξ and the interparticle distance r, in which classical percolation transition can be supplemented by a tunneling transition.[51, 53-55] In order to distinguish between these cases experimentally straightforward conductivity measurements may not suffice. For example, in earlier work percolation behavior was studied on carbon black-resin composite systems.[63, 64]

Two distinct regions corresponding to classical and tunneling percolation transitions were identified by linking non-ohmic behavior in one of these regions to a tunneling percolation transition.[63, 65,66] Recently Wei *et al*. reported the existence of two percolation thresholds in $Ag_x(SnO_2)_{1-x}$ nanogranular films from temperature-dependent conductivity measurements.[67] Similarly, by using conductance atomic force microscopy for the Ni-SiO_2 composite system, the first order tunneling percolative behavior (in contrast to higher order ones) was established.[54] In the framework of global tunneling network (GTN), Balberg, Grimaldi and co-workers have studied the tunneling process in some conductor-insulator composites with continuum insulating matrix.[51, 53, 68] Theoretically, it has been well established that in composites, the competition between percolation and tunneling behavior depends solely on the microstructure and the ratio of metallic particle size D to the tunneling length ξ.[53, 59,25]

Additionally, one can envision a series of percolation thresholds due to interparticle tunneling, which has been referred to as a tunneling staircase.[69] In order to implement a system with such properties, local resistivity between the n-th nearest neighbors, ρ_n, should be orders of magnitude higher than that between the (n-1)-th nearest neighbors, ρ_{n-1}, with ρ_n being the highest local resistivity in the system.[69] We note, however, that one can further generalize the condition for tunneling staircase to a multi-component system with different resistivity of

constituents, as long as one type of resistance network dominates at a given composition.

In this context, in addition to a classical percolation threshold resulting from the occurrence of a percolated conducting cluster across metallic oxide RuO_2 nanoparticles that are mixed with another type of particles, $CaCu_3Ti_4O_{12}$ (CCTO), we observe at least two additional tunneling percolation thresholds in a four-step tunneling staircase. Compared to most other percolation systems studied experimentally or theoretically, the nanocomposite system examined here consists of two types of non-spherical particles of different sizes. The system can then be described as a conducting (tunneling) network of one nanoparticle type (RuO_2) packed with another type of semiconducting particles (CCTO), instead of being embedded in a continuum insulating medium as in conventional percolation systems. The observation of a hierarchical nature of percolation staircase in this binary network becomes especially revealing when variable temperature conductivity measurements are utilized. We find that the critical exponents for various tunneling percolation thresholds are strongly temperature dependent, a distinguishing feature of tunneling behavior which has been missing in previous studies of percolation systems.

3.2 Experimental Techniques

Samples of CCTO were prepared via solid state process, by mixing $CaCO_3$ (99.99%), CuO (99.99%) and TiO_2 (99.99%) in a planetary ball mill.[70] In the presence of acetone, the mixture was ball-milled using zirconia balls for 1 hour and pre-calcined at 1000^oC for 12 hours. It was then mixed with different volume fractions *p* of ruthenium oxide RuO_2 of 99.99% metal basic (Sigma Aldrich). Pellets of RuO_2-CCTO composites were prepared by using a cold pressed die with a uniaxial pressure of 1 GPa, and then calcined at 1100^oC prior to resistivity measurement. PPMS (Quantum Design) along with the four-point technique was used to measure the temperature dependent resistivity of the composites. Scanning Electron Microscope (SEM, JEOl, 6610LV) with an EDX detector (Oxford) was used for compositional and morphological analysis. In a separate set of experiments, we have also prepared the host CCTO by a different (sol-gel) technique. This set of experiment yielded similar tunneling behavior also characterized by the presence of a tunneling percolation staircase. The slight differences observed in the values of percolation thresholds and critical exponents are likely to originate from somewhat different microstructure (e.g., of grains and grain boundaries) of CCTO particles.

3.3 Experimental results and Discussions

Figure 3.2 shows a typical micrograph of the distribution of RuO_2 filler in a RuO_2-CCTO composite system. The grain size of CCTO is about 5-10μm and RuO_2 particles are around 400-500 nm.

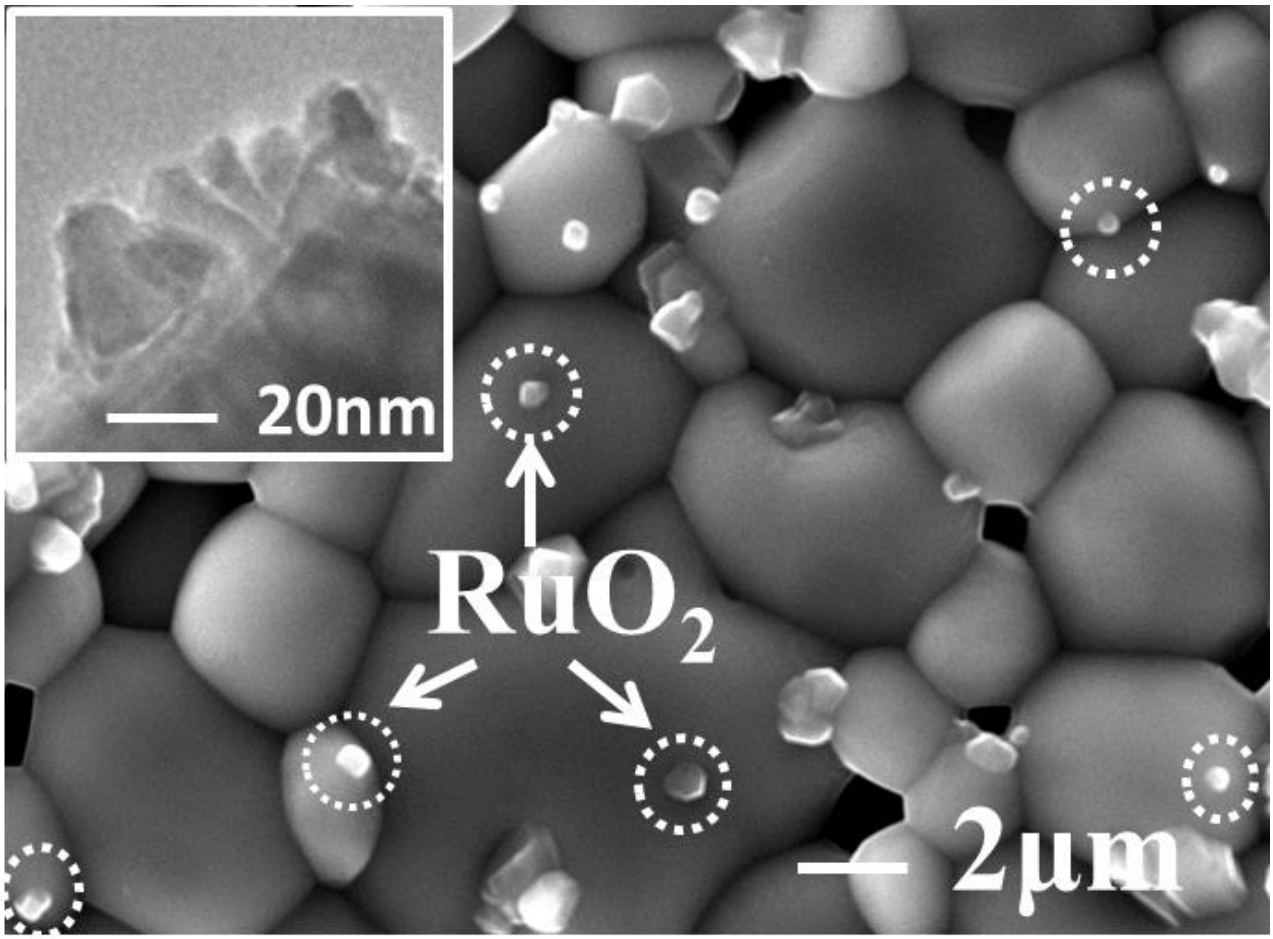

Figure 3.2 SEM image of RuO_2-CCTO composite system, with RuO_2 particles indicated by dotted circles. Inset: High-resolution TEM image of grain structure in CCTO.

By performing a detailed EDX composition analysis, we found that substantial amount of RuO_2 has diffused into CCTO grains. Thus, while nominally our system consists of a bulk semiconducting CCTO and a metallic RuO_2 filler, the real microstructure of this system is more complicated, due to the presence of an insulating surface layer and grain boundaries of CCTO, which is likely to affect percolation tunneling staircase. Figure 3.3(a) and 3.3(b) show the variation in conductance σ with metallic volume fraction p at 300K for RuO_2-CCTO composite systems, with the power law fitting $\sigma \propto (p\text{-}p_c)^{\mu}$ to determine the scaling behavior of different tunneling percolation stairs. Four conductivity stairs can be identified,

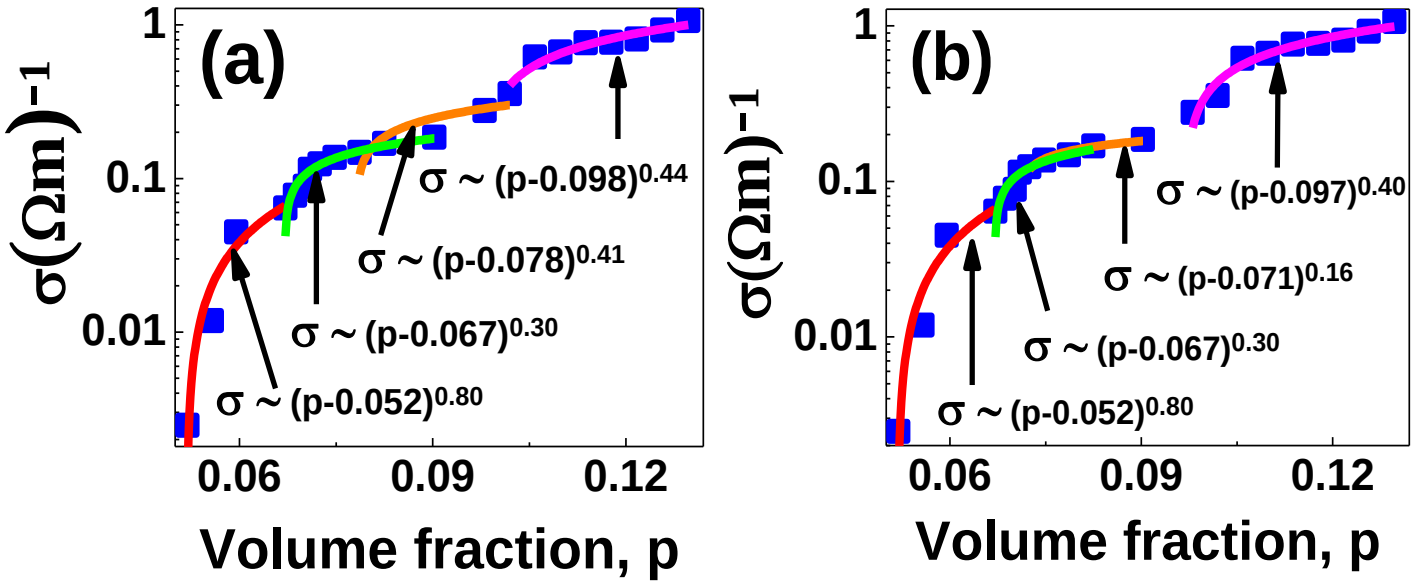

Figure 3.3 System conductivity as a function of volume fraction of RuO_2, as measured at 300K. Two sets of slightly different percolation thresholds are used in the power law fitting, including: (a) thresholds found from the resistance ratio R_{270K}/R_{300K} measurement given in Fig. 3.4(a), and (b) thresholds extracted from the R_{250K}/R_{300K} measurement in Fig.3.4(b).

along with three distinct percolation thresholds and the corresponding critical exponents. Thus the definitive picture of percolation staircase with multiple percolation transitions is presented in this binary particle-packing network, showing a hierarchy of tunneling conductance. We note that while our data is consistent with a tunneling staircase, the accuracy of the scaling fits should be carefully examined. Indeed, the data can be equally well fitted by using slightly different values of percolation thresholds and critical exponents, as shown in Figs. 3.3(a) and 3.3(b). To reveal a more nuanced picture of conduction and to distinguish between classical and tunneling percolation behavior, we use temperature dependent transport measurements (see Figs. 3.4 and 3.5). Since tunneling is typically strongly temperature dependent, it is sufficient in our case to lower the temperature by just 50 degrees below the room temperature to see a significant difference from the room temperature data. At the same time, experimentally one is normally limited by the highest measurable resistance, which sets up the low temperature limit of our measurement.

Such temperature dependent effects are illustrated in Figs. 3.4(a) and 3.4(b), which give the ratio of sample resistance at a given temperature to the room-temperature resistance, i.e. R_{270K}/R_{300K} and R_{250K}/R_{300K} for the temperatures of 270K and 250K respectively, as a function of volume fraction p. Three percolation thresholds, p_C, p_T^1, and p_T^2, can be clearly identified from the inflection points of

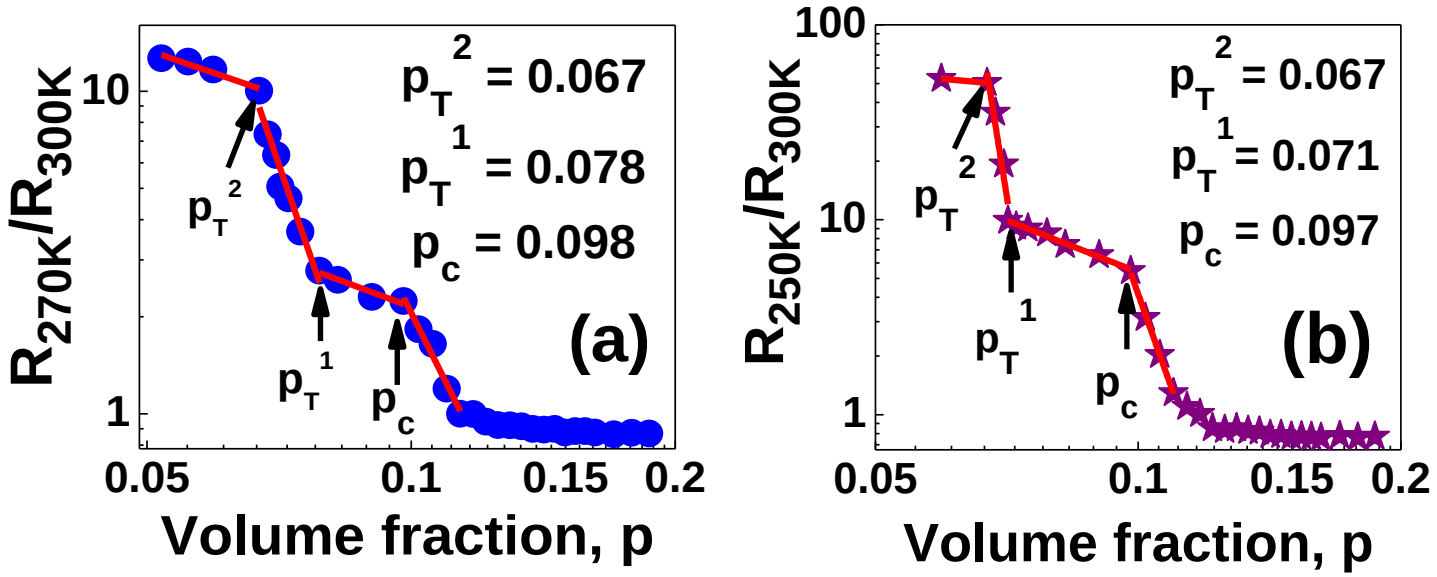

Figure 3.4 Resistance ratios (a) R_{270K}/R_{300K} and (b) R_{250K}/R_{300K} as a function of volume fraction p. Three percolation thresholds, p_T^1, p_T^2 (first and second tunneling thresholds) and p_c (the classical percolation threshold), are identified from the inflection points of the power law fitting in the log-log plots.

the log-log plots. Note that values of these thresholds determined from two independent measurements (R_{270K}/R_{300K} vs. R_{250K}/R_{300K}) are slightly different, leading to different critical exponents as shown in Fig. 3.3. This can be expected from strong temperature dependence of tunneling conductance, which is pivotal for accurate determination of thresholds in systems governed by both percolation and tunneling. An important feature given in Fig. 3.4 is associated with a series of sharp increases in the resistance ratios R_{270K}/R_{300K} and R_{250K}/R_{300K} when going from high to low volume fraction of RuO_2. The first increase occurs from $p \sim 0.12$ to 0.098 (0.097), the first inflection point, followed by a steep rise in the rate of

resistance change. We argue that, in spite of a relatively large resistance ratio near the threshold (R_{250K}/R_{300K} ~ 8), this point corresponds to a classical percolation transition. Indeed, at p ~ 0.11 the resistance ratios approach 1, whereas the ratio R_{250K}/R_{300K} for bulk RuO_2 is approximately 0.75. This implies that some fractions of the active bonds are already tunneling bonds, which have a resistance ratio greater than one. Across the volume fraction range between 0.11 and 0.098 the number of tunneling bonds further increase at the expense of classical bonds between RuO_2 particles. This can also be viewed as the decrease in the number of effective parallel metallic resistors in the matrix. Thus, we can roughly estimate the resistance of such RuO_2 direct conductance paths by calculating the resistance of equivalent RuO_2 "nanowires", $R = 4\rho L/\pi D^2$, where ρ = 40 μΩ·cm is the resistivity of RuO_2, L ~ 5-10 mm (the size of the pellet) is the length of a nanowire near the percolation threshold, and D = 0.5 μm is the average diameter of RuO_2 particles. This results in the resistance of approximately 1-10 kΩ for a few "nanowires" connected in parallel. On the other hand, the resistance measured at the threshold p = 0.098 is around 100 Ω, at least an order of magnitude smaller, indicating that the temperature dependent contribution is largely due to the tunneling conductance. Our conclusion that p = 0.098 (0.097) corresponds to the classical percolation threshold is in agreement with earlier measurement of the dielectric permittivity in this composite system, which also shows a peak at p ~ 0.10.[71]

On the other hand, another two thresholds observed at $p < 0.098$ correspond to tunneling percolation. In contrast to most other systems showing percolation staircase as a result of tunneling between non-contacted conducting particles of various degree of nearest neighbors,[12,16,19] the binary network studied here corresponds to much more complicated tunneling processes, facilitated by surface oxide layers and interior grain boundaries of CCTO. This is further complicated by partial diffusion of Ru into CCTO grains, leading to the complex tunneling percolation effects observed in this system. To examine the origin of these effects, we have taken high resolution TEM images to determine the microscopic structure of CCTO (see the inset in Fig.3.2). We observe nanometer-size grain boundaries, which is within the range required for tunneling processes. Once we identified features of the appropriate size, we can speculate about the hierarchy of the corresponding tunneling processes. For example, the lowest threshold is likely to correspond to the bulk tunneling across the CCTO matrix, as below this point the resistance is practically independent of the composition and hence is largely insensitive to the presence of RuO_2.

The scaling behavior of the staircase (i.e., near various percolation thresholds for the hierarchy of stairs) at 3 different temperatures and the corresponding critical exponents μ are given in Fig.3.5 (a)-(e), with percolation thresholds determined from ratios of R_{270K}/R_{300K} and R_{250K}/R_{300K} as described above. For all

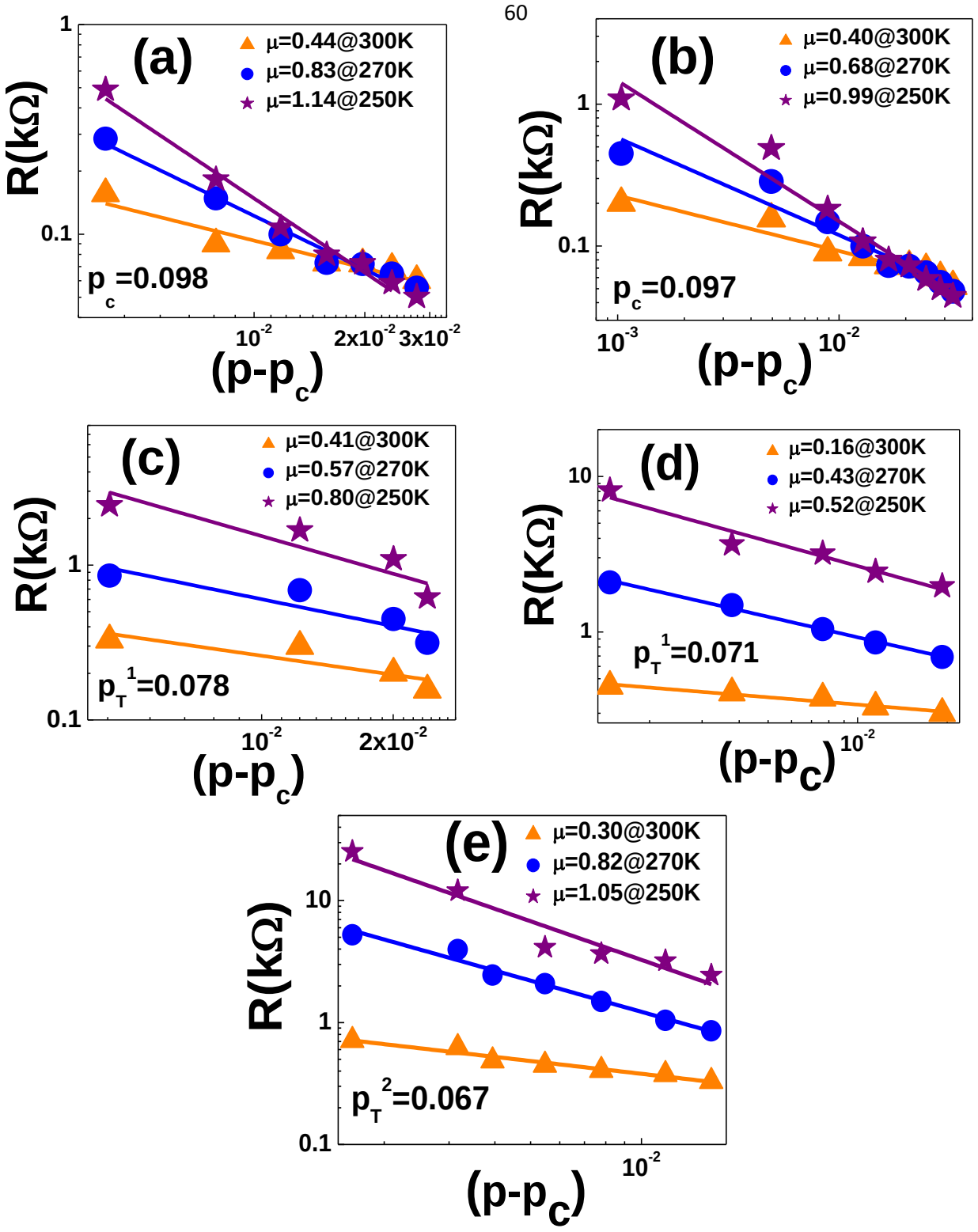

Figure 3.5 Scaling behavior of the sample resistance near different percolation thresholds at temperatures 300K, 270K, and 250K. Values of percolation thresholds determined in Fig. 3.4 are used, with the corresponding critical exponents indicated in each panel.

the percolation stairs, values of the critical exponent for this binary particle network are found to decrease with the increase of temperature, and substantially vary for different thresholds of the tunneling staircase. In addition, for this RuO_2-CCTO composite the critical exponents show a significant deviation from universal values which typically range from 1.7 to 2. We note that, while such nonuniversality of critical exponents, particularly the dependence on p_c and the material type, has been verified experimentally in tunneling percolation[47, 60, 67] and explained theoretically,[60, 72] temperature dependent critical exponents have not been observed before.

3.4 Conclusions

In summary, we have studied the multiple percolation behavior in a RuO_2-CCTO composite system. In contrast to previously studied percolation systems with continuum insulating medium, this system has a complex microstructure and consists of two particle types of large size and conductivity disparity. In addition to a classical percolation threshold, we identify two separate tunneling thresholds based on temperature dependence of tunneling conductance, as well as a hierarchy of four conductivity stairs, supporting the theoretical notion of tunneling staircase in the case of complex microscopic structure of a composite system. The nonuniversality of the scaling behavior in tunneling percolation is examined by temperature dependent transport measurements, showing not only large variations

of critical exponent values, deviating from the universal range for different percolation thresholds and tunneling stairs, but also the new temperature effect on critical exponents. Our study further demonstrates that detailed microstructures and the complexity of multi-component composite systems play a key role in revealing various new phenomena in percolative networks that control system properties and functionalities.

CHAPTER 4 BEHAVIOR OF FILLING FACTOR AND ELECTRICAL TRANSPORT IN PERCOLATIVE NANOCOMPOSITE SYSTEM

We have further investigated the regions of conventional and tunneling percolation in series of metal insulator composite systems in which metallic particle is a thin rod and spherical particles are insulators. It shows existence of two percolation thresholds at lower and higher volume fractions which in turn have a linear dependency to one another. Surprisingly the filling factor in these composite systems which are mixtures of rod and spheres shows a non-monotonic behavior and has a power law dependence on metallic volume fraction. It is also found out that the filling factor maxima has a non-monotonic dependence on ratio of size of spheres to the longitudinal dimension of rods with minima found to be at ratio 8. In contrast the volume fraction which corresponds to maximum filling factor depends on electrical percolation thresholds monotonically.

4.1 Introduction

At the percolation threshold P_C where filler particles form a percolating network in a disordered composite system, has always been considered as point of interest. Due to percolation effects, the huge significant changes in electrical, dielectric and magnetic properties in a composite system are therefore being increasingly exploited in field of magnetic semiconductor, embedded capacitor technology, gas sensors and in spintronics.[31, 73-75] Its immense importance in

scientific fields has motivated us to classify the right percolation threshold which is very necessary and challenging. According to the standard percolation theory the change in resistance R while approaching transition threshold P_C follows a power law behavior, i.e., $R= |P-P_C|^{-\mu}$, where the universal critical exponent μ depends on the dimensionality and the intrinsic conducting property of the composite system.[57, 72] Experimentally, the universal value of critical exponent has been reported to be around 2.0.[63, 76] However, non universality of this critical exponent has also been reported by many groups.[53, 60, 68, 77] Many groups have observed significantly higher values of exponents: 2.8, 3.5, 5.1, 6.3, 9.5 and 9.7.[59, 63, 78]. Tunneling percolation is the origin of non universality in which tunneling conductance has an exponential decay with interparticle distance without having sharp cutoff or threshold.[60, 68] It has also been established that if P_C is defined at the volume fraction where Ohmic conductance is more dominating than non-Ohmic behavior, then universality is preserved.[63] The purpose of our research is to find out whether a mixture of conducting rod shaped and non-conducting spherical particles preserves the universality in ohmic and non-ohmic regions of volume fraction in random metal insulator composite system. We have reported the existence of two percolation thresholds P_T and P_c where P_T is the first order tunneling percolation threshold at which there is an onset of enhanced conductivity due to tunneling with critical exponent μ to be found close to theoretical value thus

preserving the universality and P_c is the classical percolation threshold at which ohmic conductivity dominates the tunneling behavior showing value of critical exponent different and smaller than universal value which is μ=2.00. Earlier, extensive studies have been done on continuum percolation and analytical dependence of percolation threshold on particle shape anisotropy.[79]

In our studies we have also found that the filling factor (F) in composites comprising of a mixture of rod spherical shape particles also follows a power law at both above and below the filling factor threshold. In a composite network, filling Factor is defined as the total volume in all the clusters both above and below the threshold divided by the simulation or experimental volume of the sample.[80, 81] It is well known that in a composite material when two components differ significantly in size, it results in two coexisting networks of particles.[82] In our case, filling factor for systems with different ratio of spherical particle size to length of rod particles have been found out. Non monotonic behavior of filling factor supports the idea of two different networks of constituent particles. Scaling the filling factor for random composite systems helped us to find the nature of its universality and also to understand its coupling with electrical percolation threshold which has been our main focus. This universality is quit important because it gives the whole new approach that goes far beyond the phase transition problems in statistical physics.

4.2 Experimental Technique

The commercial available metallic powders such as CrO_2, MgB_2, and insulating powders such as K_2CO_3, Al_2O_3, CaCO3, PMMA(Poly-Methyl-Methacrylate) were grinded well in dehumidifying environment with humidity less than 25% and were cold pressed under 1gigaPascal pressure to form pallets. The insulating components were of spherical shape with diameters ranging from 50nm to 10µm. Four point contact technique has been used to measure resistance of the composite system in which four silver pads and gold wires were used to make electrical contacts. To verify the shapes and sizes of composite particles, scanning electron microscopy (SEM) has been used to take the images. Quantitatively filling factor is calculated as $F= [(m_1/d_1) + (m_2/d_2)] / (pi*r^2*t)$, where m_1 = mass of insulating powder, m_2 = mass of metallic phase, $d_{(1,2)}$ = density of the respective powders, r= radius of the pallet, t= thickness of the pallet. Volume fraction is measured as $P= (M*X/d_1) / [(M*X/d_1) + (M*(1-X)/d_2)]$, where M= total mass of the composite and X is the required weight fraction. Figure 4.1(a-d) shows Scanning electron microscopy (SEM) images of constituent particles. Figure 4.2 (a-j) shows particles with different size d. Room temperature electrical measurements were done on Keithley instruments. Temperature dependent measurements were carried out by Quantum design Physical Property Measurement System (PPMS).

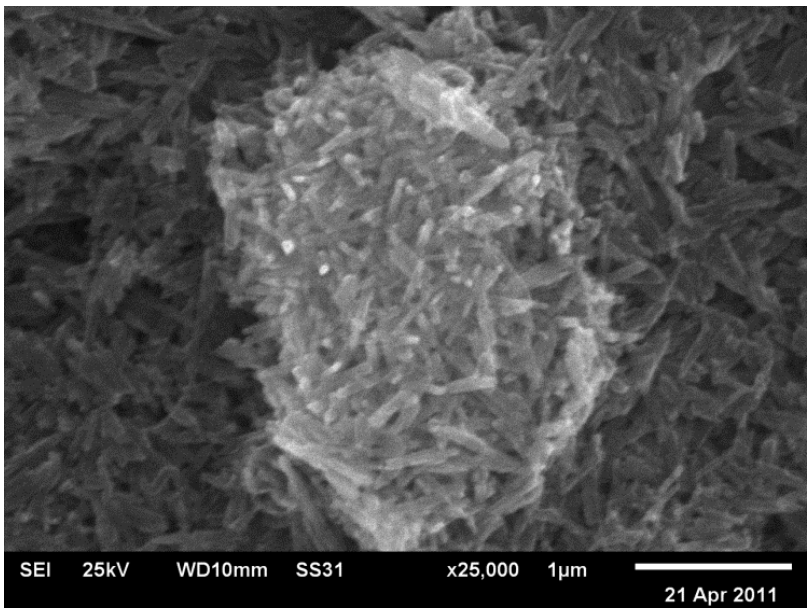

Figure 4.1 (a) SEM image of CrO_2

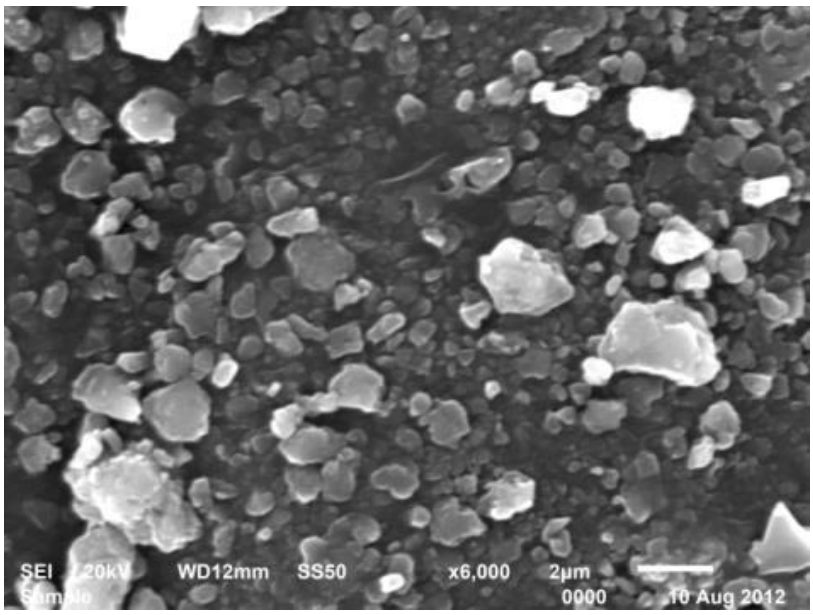

Figure 4.1 (b) SEM image of MgB_2

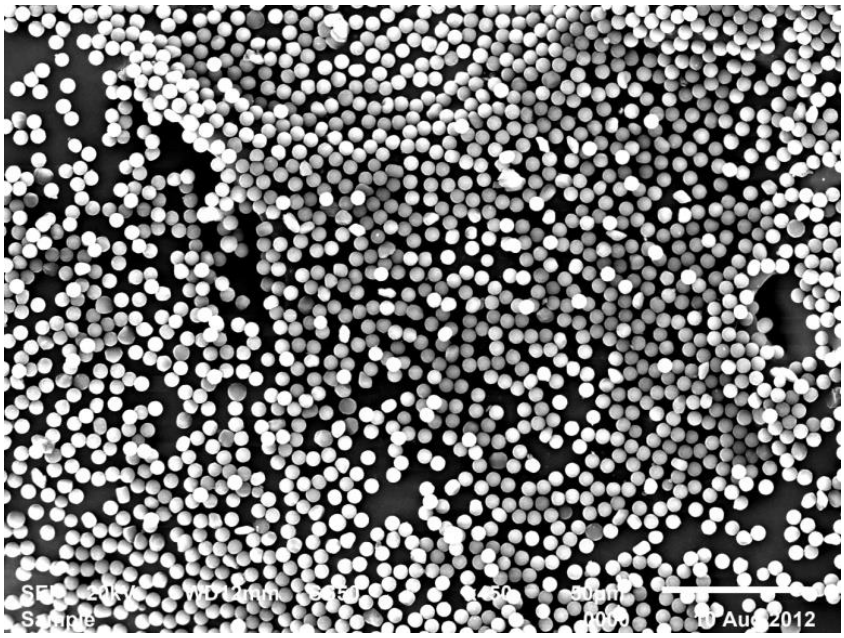

Figure 4.1 (c) SEM image of PMMA

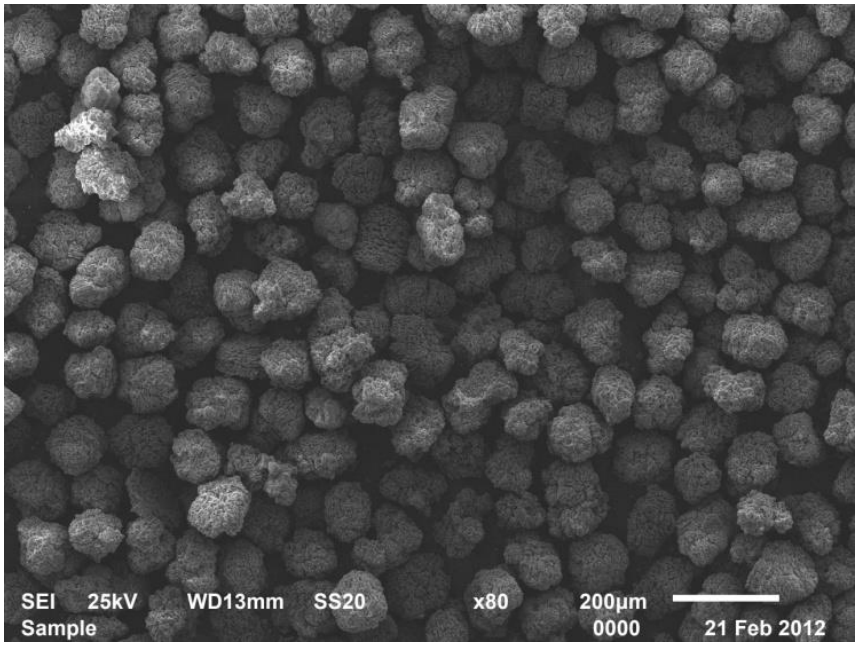

Figure 4.1 (d) SEM image of Al_2O_3

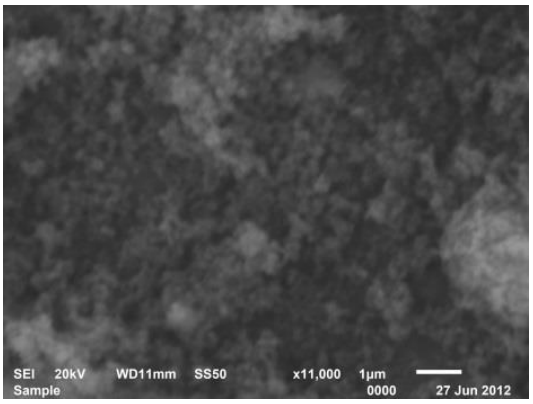

4.2 (a) d=30nm

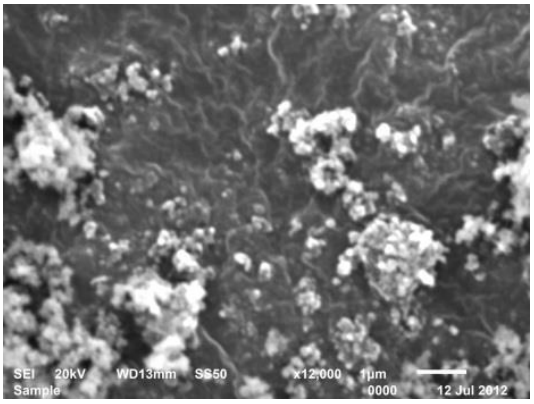

4.2 (b) d=200nm

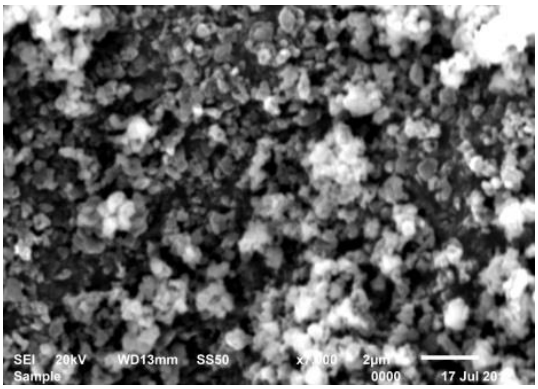

4.2 (c) d=350nm

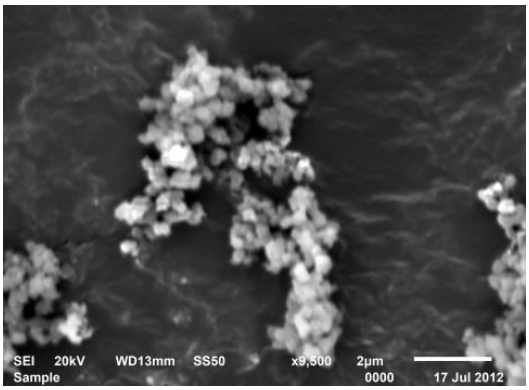

4.2 (d) d=450nm

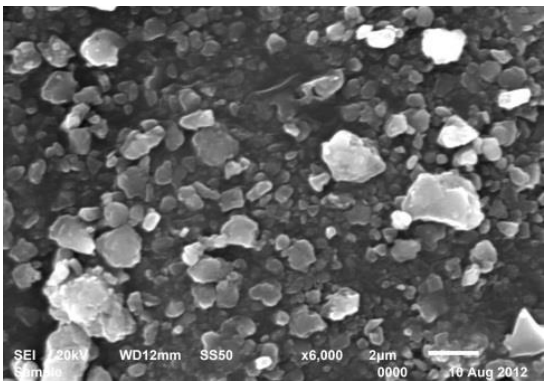

4.2 (e) d=700nm

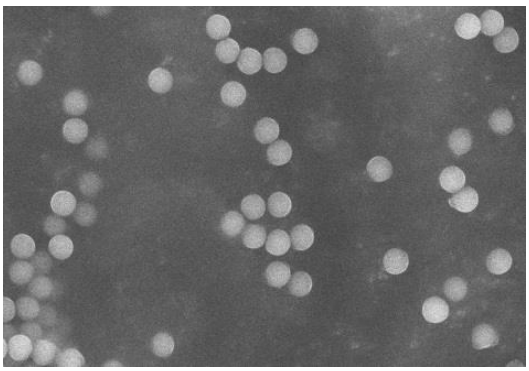

4.2 (f) d=1µm

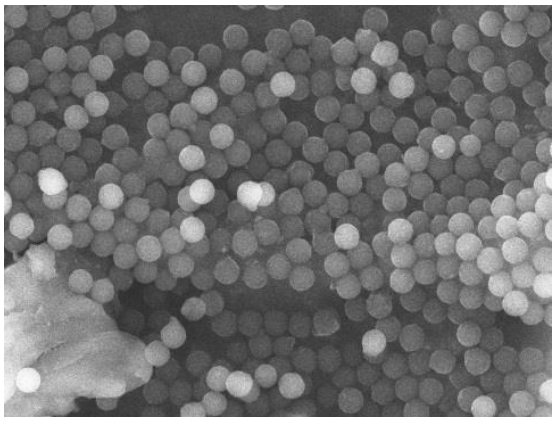

4.2 (g) d=1.5µm

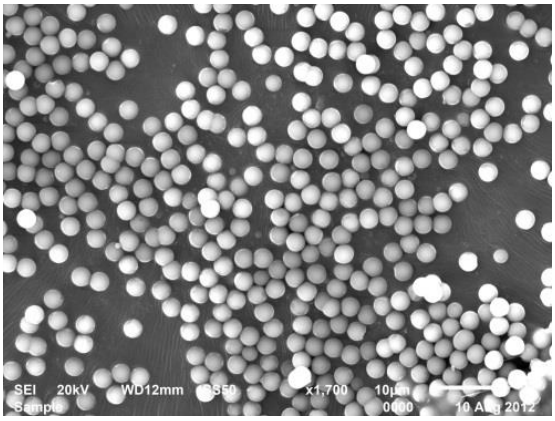

4.2 (h) d=2.5µm

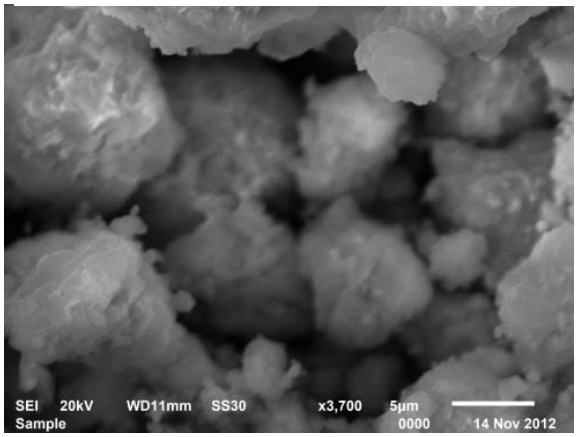

4.2 (i) d=5µm

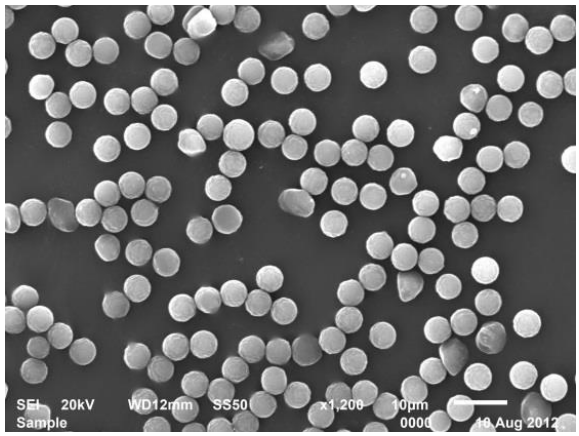

4.2 (j) d=10µm

Figure 4.2 (a-j) Size of spherical particles expressed as d ranging from nano to micro meter.

4.3 Results and Discussions

In composite systems such as $CaCO_3$-CrO_2, PMMA-CrO_2 with ratio of insulating particle size to the metallic particle size (d/D), electrical phase transitions are shown in figure 4.3(a-j). It shows monotonic decrease in resistance with increase in metallic volume fraction. It also reveals that there is an existence of two separate regions at which change in resistance in one region is faster than the other.

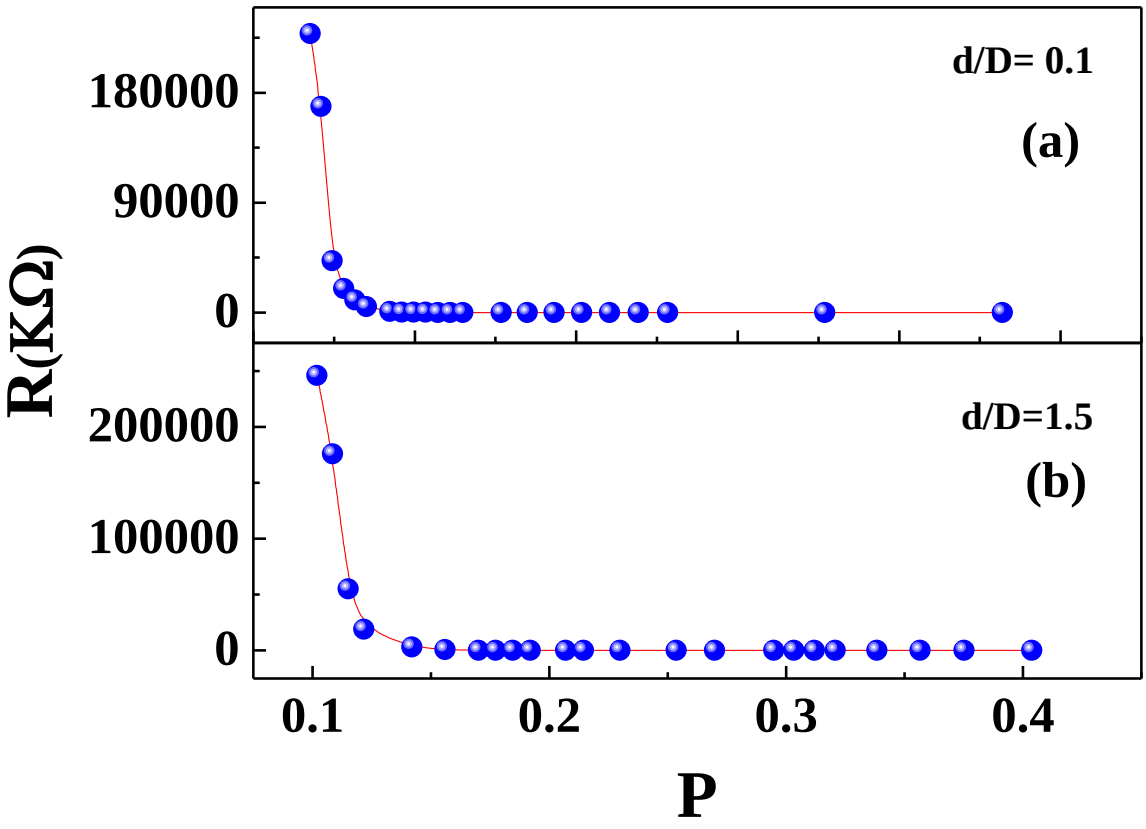

Figure 4.3 Resistance as a function of volume fraction in composite system with d/D ratios (a) 0.1 and (b) 1.5.

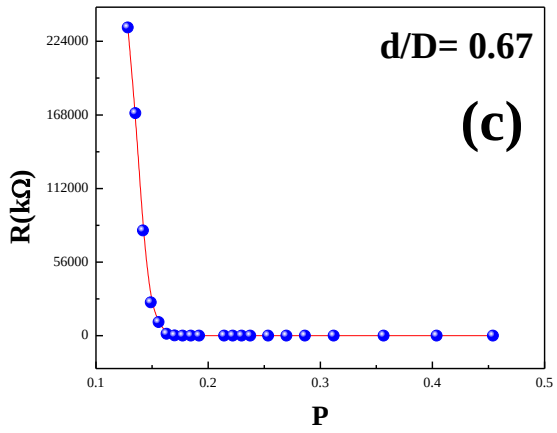

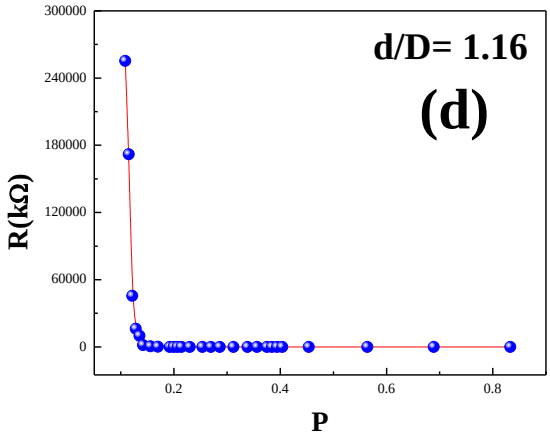

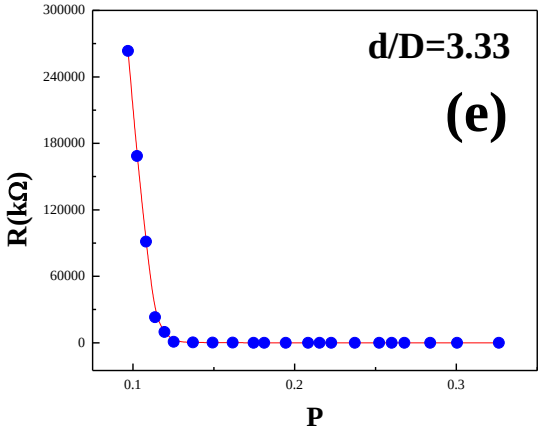

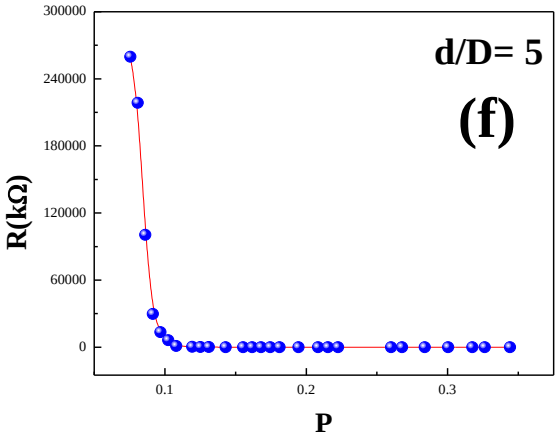

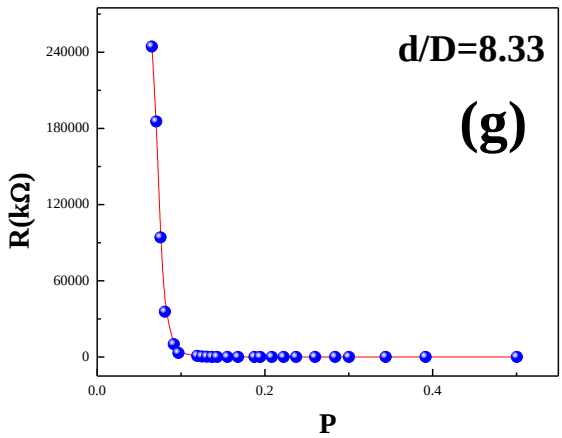

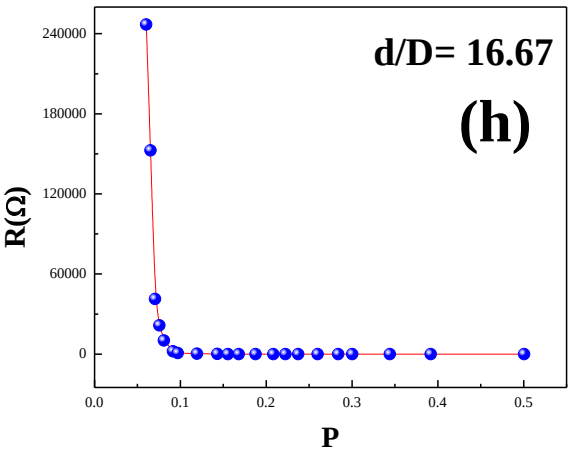

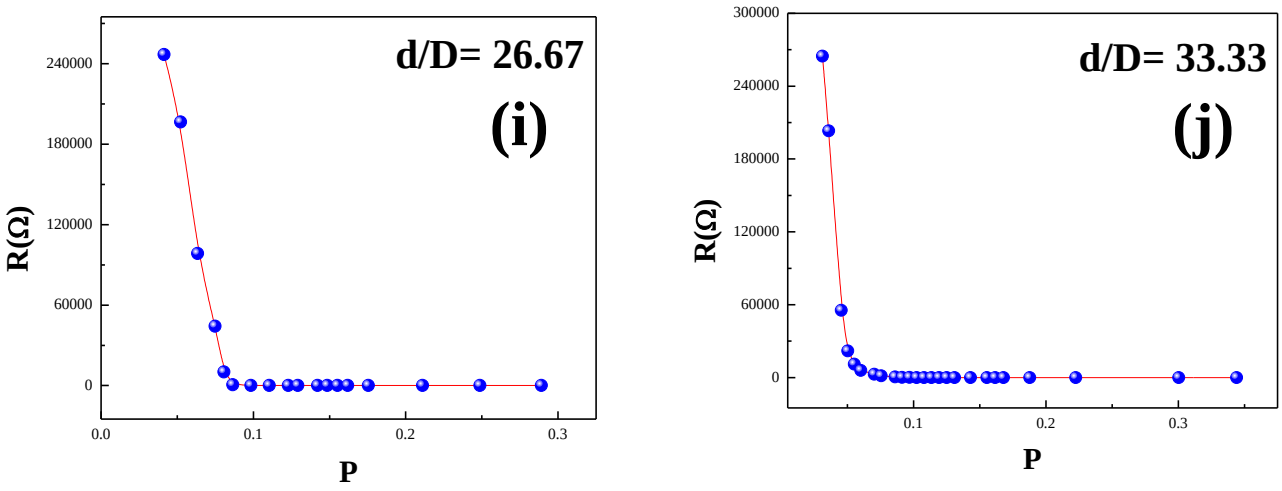

Figure 4.3 (c-j) Resistance as a function of volume fraction in composite system with different d/D ratios.

To find the power law for resistance of the percolating composite systems, the resistance has been plotted as a function of volume fraction of metallic fillers. In the region where first order tunneling dominates with threshold (P_C= P_T), it yields critical exponents of resistance close to universal value (2.0) which is shown in figure 4.4(a-j).

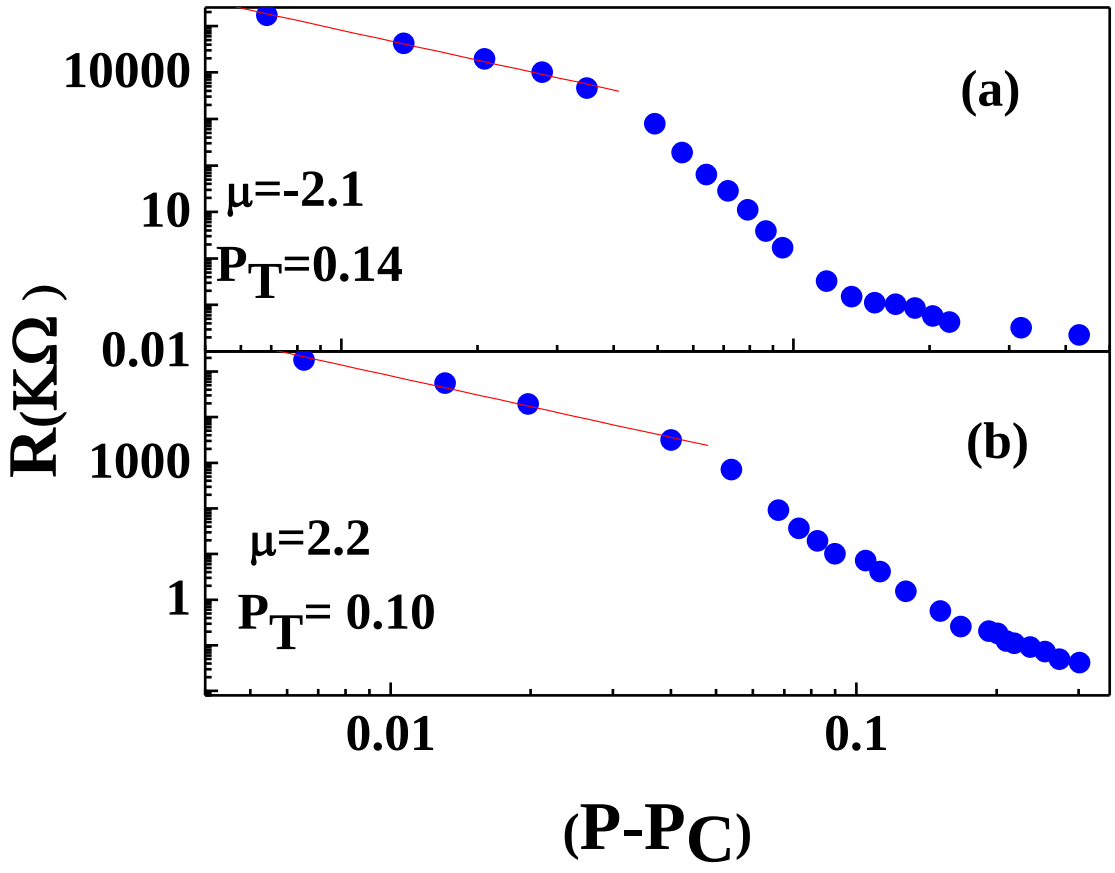

Figure 4.4 Determination of critical exponent μ at low volume fraction by plotting log-log plot in system yields 2.1 for (a) d/D= 0.1 and 2.2 for (b) d/D =1.5.

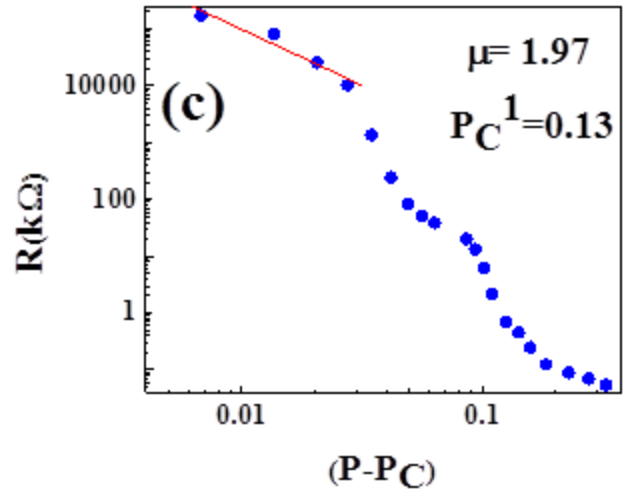

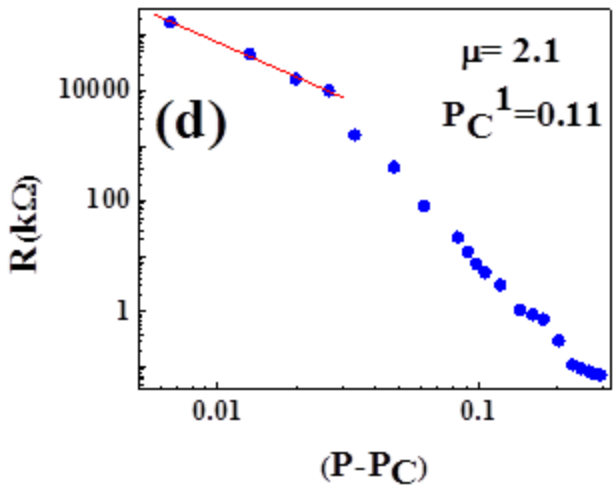

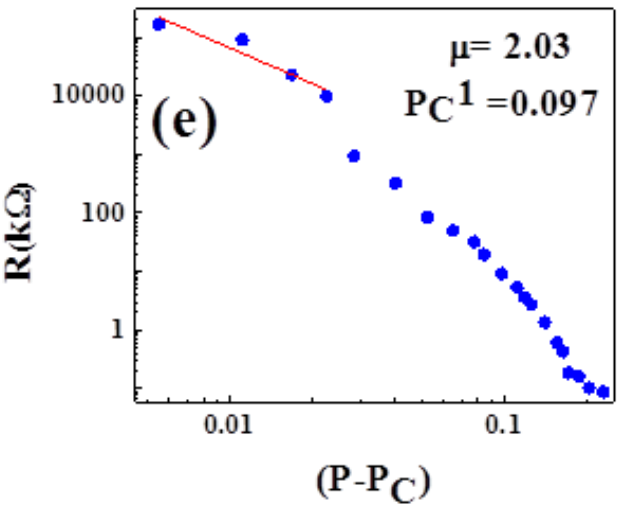

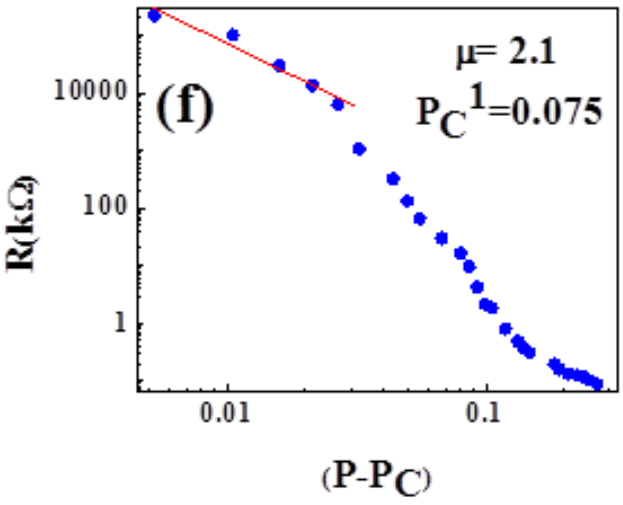

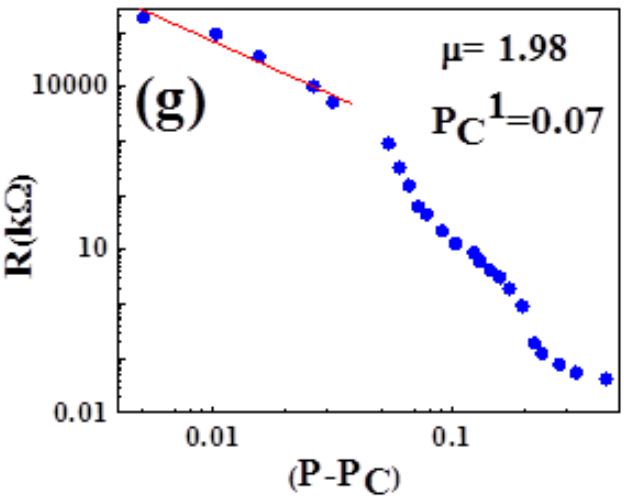

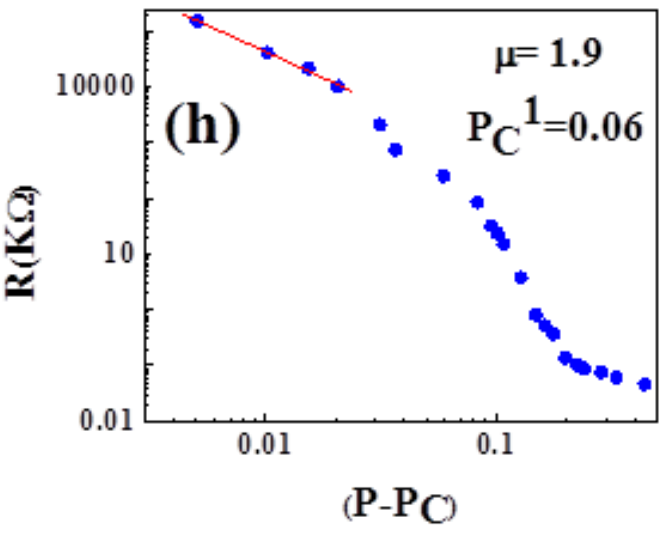

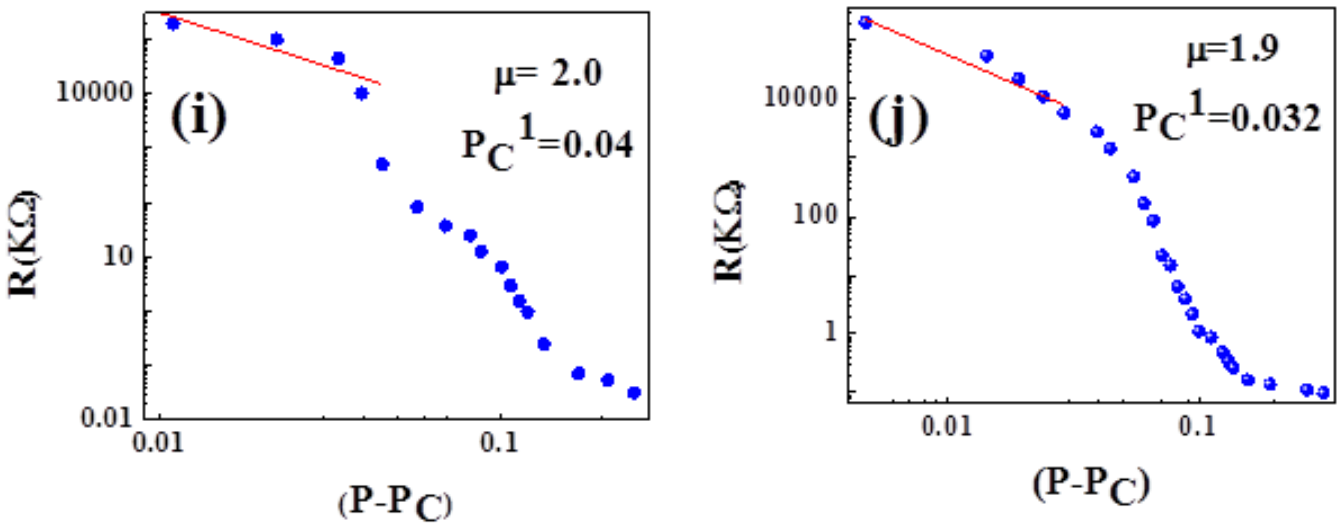

Figure 4.4 Determination of critical exponent μ at low volume fraction by plotting log-log plot in system yields 2.1 for (c) d/D=0.67; (d) d/D =1.16; (e) d/D=3.33; (f) d/D=5; (g) d/D= 8.33; (h) d/D=16.67; (i) d/D=26.27; (j) d/D=33.33.

Here the critical exponent μ is found to be 2.1 and 2.2 respectively. On the other hand at high volume fraction, when classical percolation region with threshold (P_C=P_c) is considered for the same d/D ratio, then the critical exponent is found out to be close to 1 as shown in figure 4.5 (a-j). Moreover, it is established that the critical exponent for resistance increases with lowering of percolation threshold.[72]

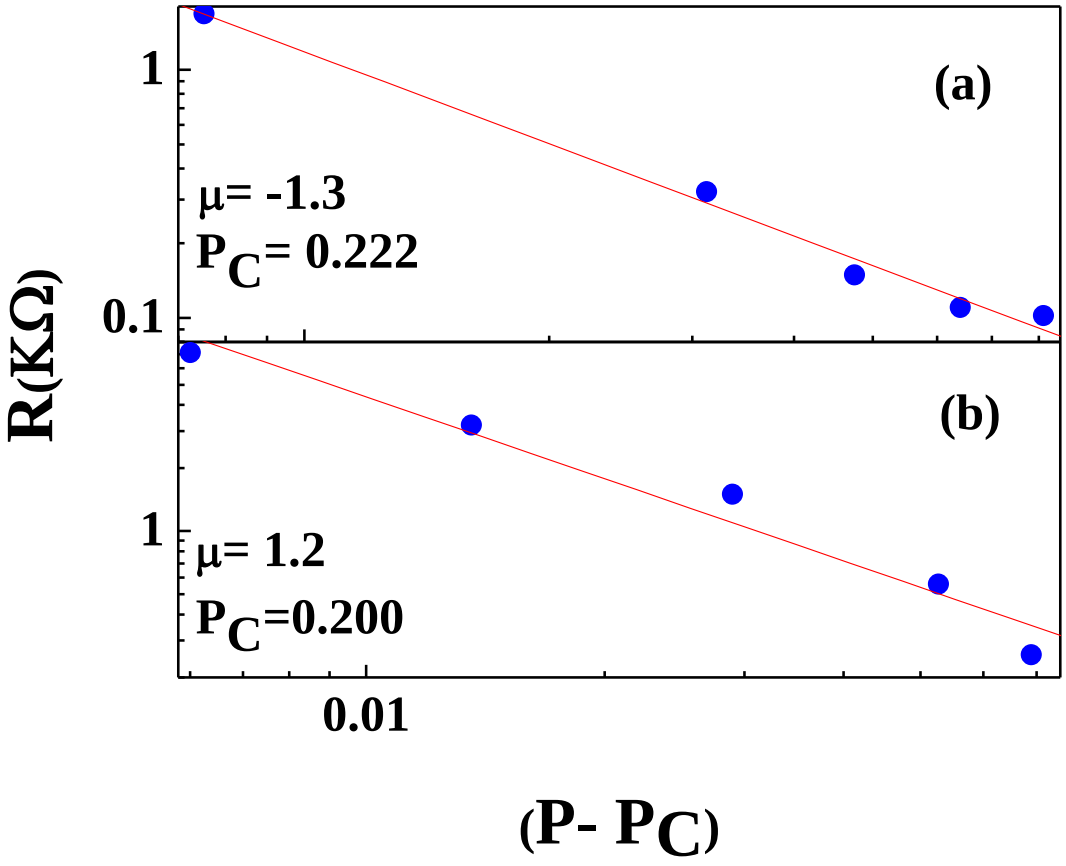

Figure 4.5 Determination of critical exponent μ at high volume fraction by plotting log-log plot in system yields 1.3 for (a) d/D= 0.1 and 1.2 for (b) d/D =1.5.

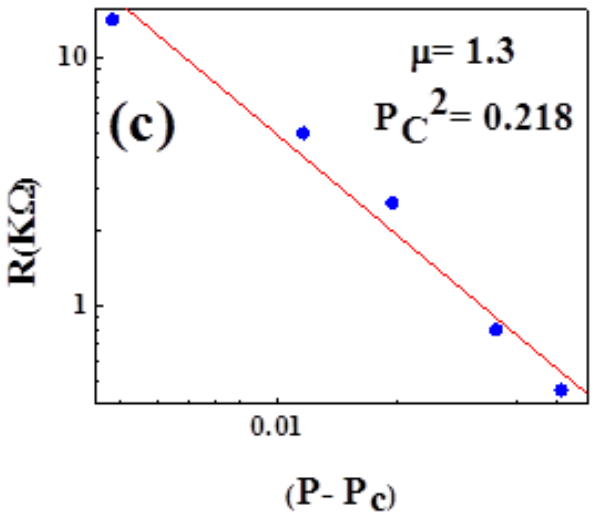

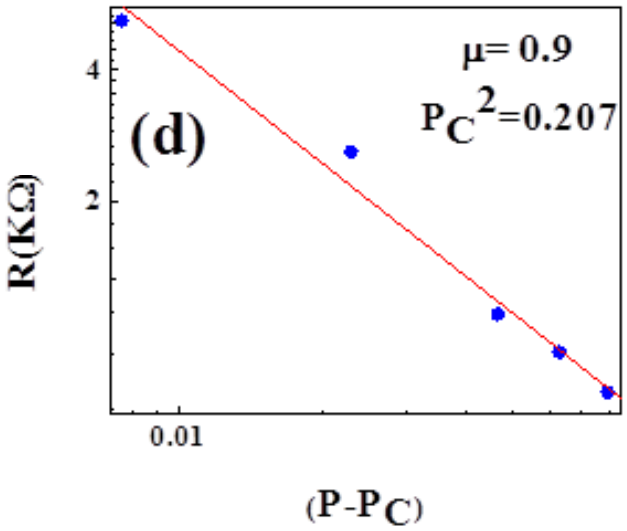

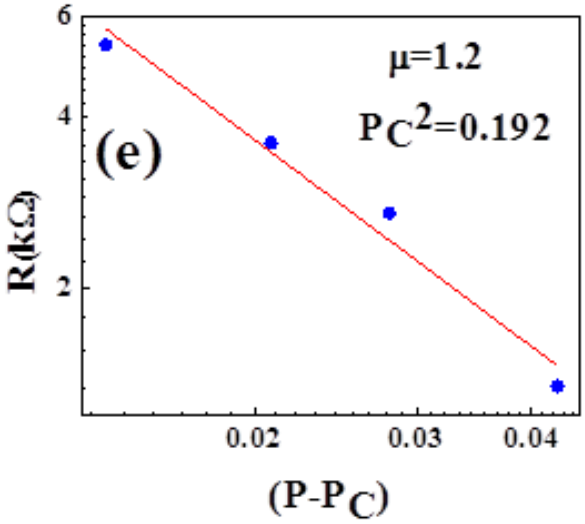

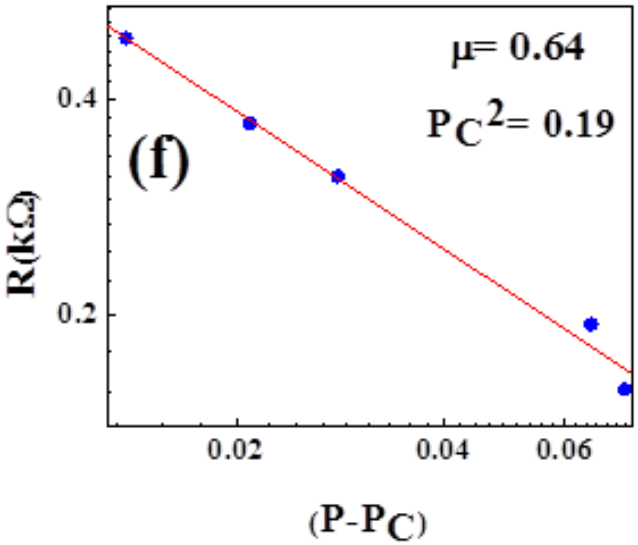

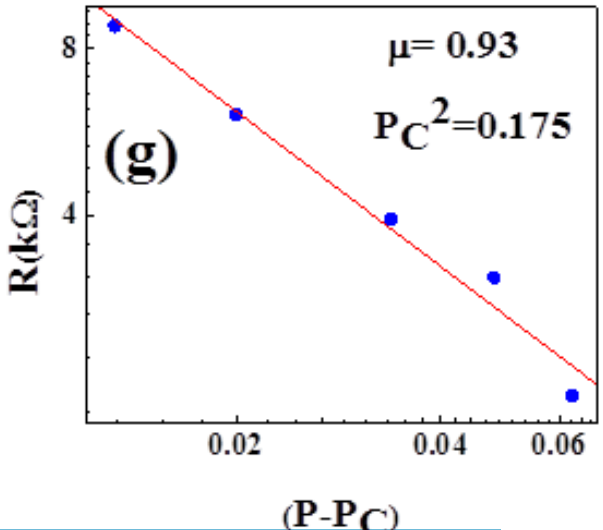

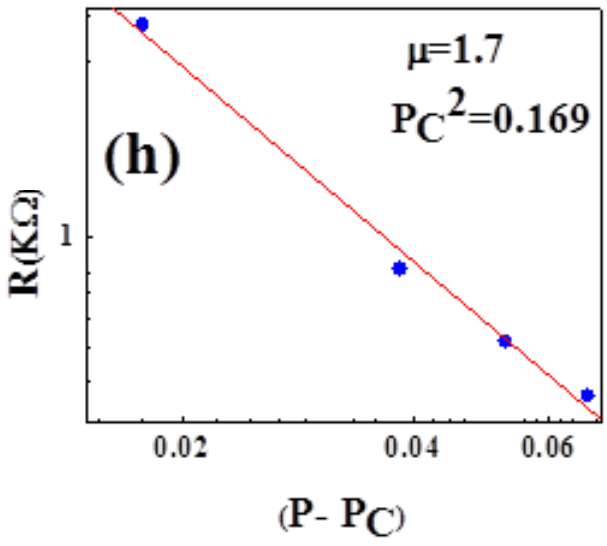

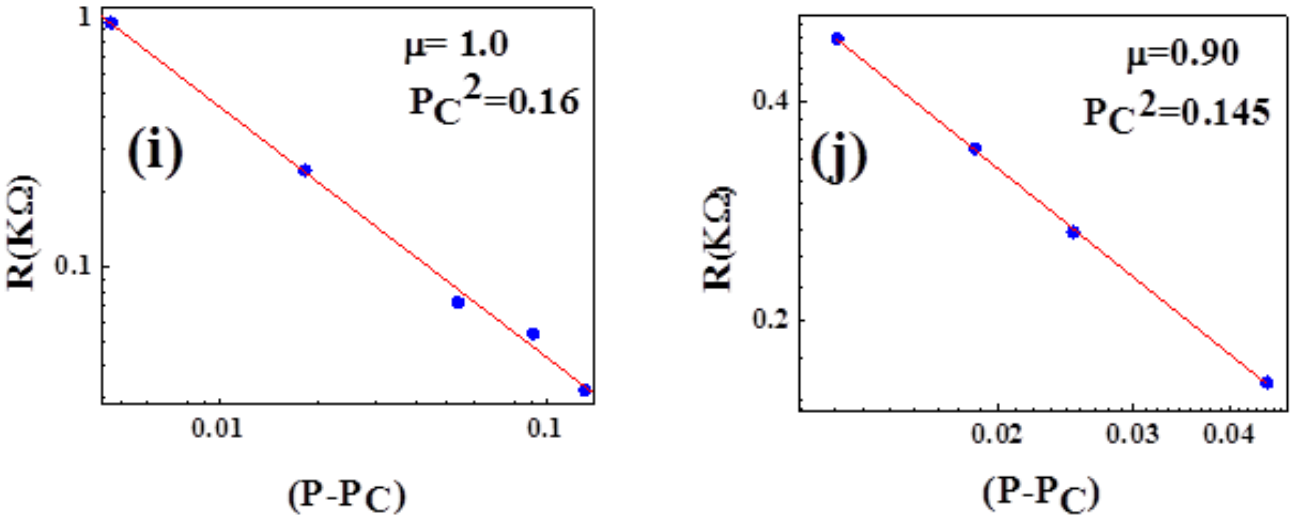

Figure 4.5 Determination of critical exponent μ at high volume fraction by plotting log-log plot in system yields 2.1 for (c) d/D=0.67; (d) d/D =1.16; (e) d/D=3.33; (f) d/D=5; (g) d/D= 8.33; (h) d/D=16.67; (i) d/D=26.27; (j) d/D=33.33.

In tunneling regime, P_T is chosen from resistance Vs volume fraction of metallic phase plot, where above P_T the resistance becomes so high that no conductivity is seen to appear in the composite. On the other hand, at high volume fraction, temperature dependent resistance shows the location of P_c (classical threshold). It is shown in figure 4.6 (a) and (b).

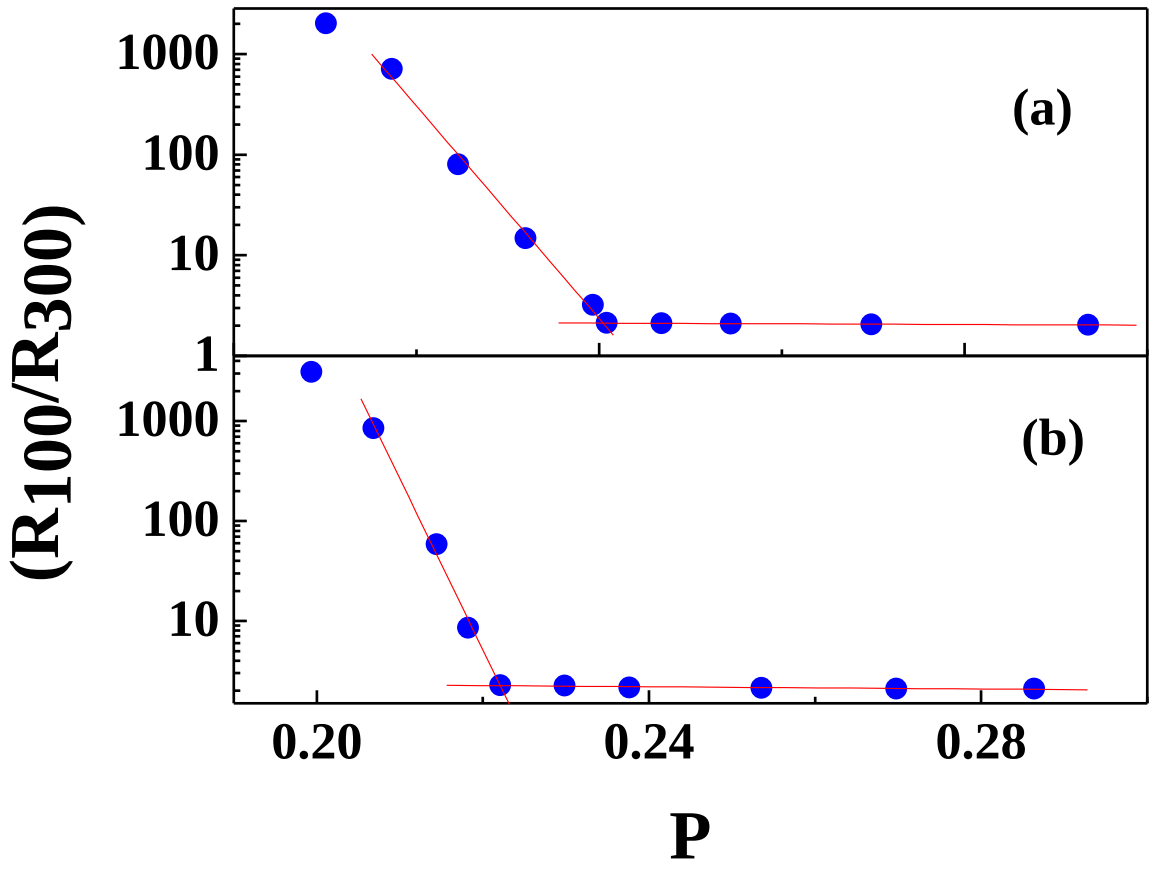

Figure 4.6 Using temperature dependent measurement, P_c is considered at the intersection of two slopes as shown in figure (a) for d/D=0.1 and (b) for d/D=1.5.

In the composite systems, it was found that as the ratio d/D increases, both tunneling threshold P_T and classical threshold P_c decreases exponentially. This is shown in figure 4.7.

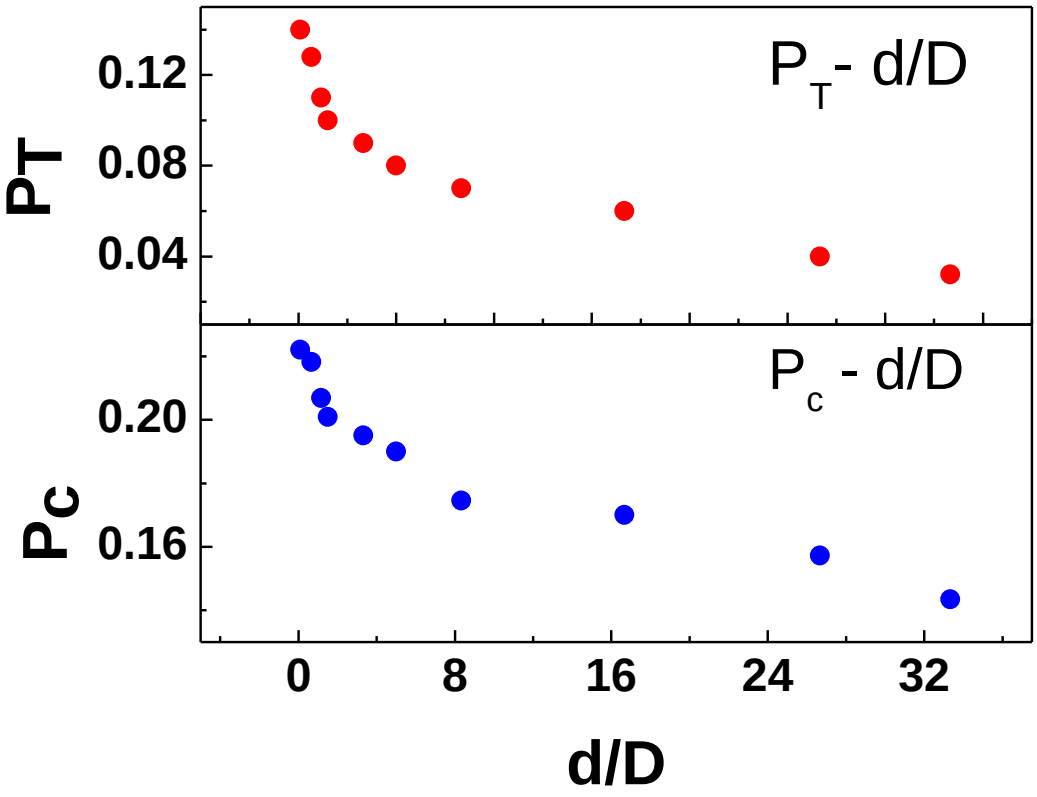

Figure 4.7 Dependence of tunneling percolation threshold P_T and classical threshold P_c as a function of d/D in different composite systems.

The decrease of percolation thresholds can be explained by the following argument. In the random packing of binary particles in composite systems at given volume fraction P (i) the ratio of the surface areas of big insulating particles to the surface area of small metallic particles decrease with increasing d/D ratio and (ii) when d/D increases, the probability of isolation of small metallic particles decrease in the regions occupied by larger insulating particles. Both favors the formation of metallic cluster at low threshold and also supports the fact that at low d/D ratio, the

decrease in threshold is faster than in the regions of high d/D ratio.[83] It is also found that with the increase of ratio d/D, classical threshold P_c depends linearly on

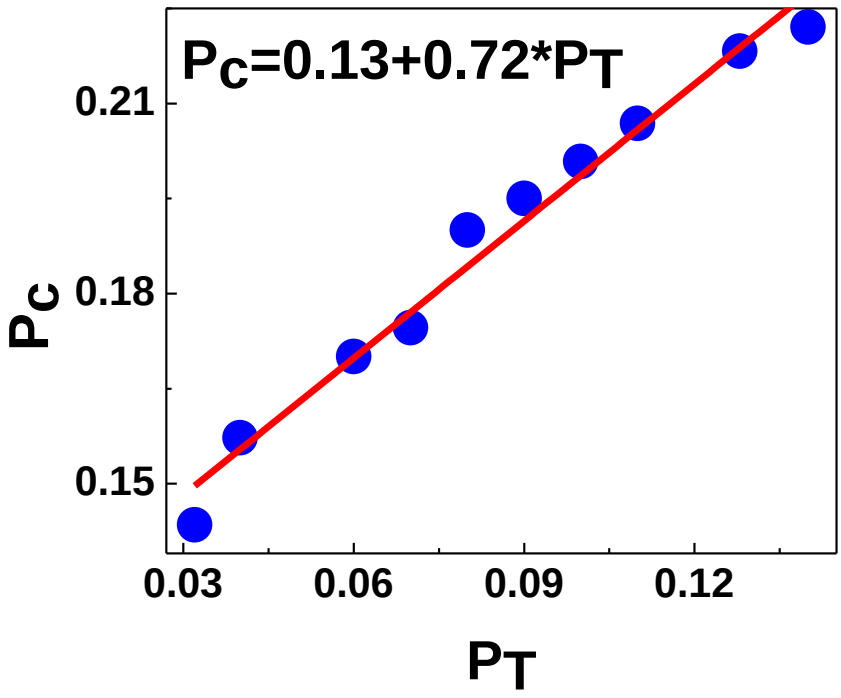

Figure 4.8 Linear dependence of P_c as function of P_T is shown with linear fit.

tunneling threshold P_T. This is due to the fact that both tunneling and classical connectedness originates from same isolated metallic clusters which grow when metallic fraction increases. This is shown in figure 4.8.

Geometrical phase transition in metal insulator composite system has been well understood by examining the characteristics of filling factor in this system of mixtures. Consequently, the filling factor is a geometrical entity that varies not

only by volume fraction of the composites but also by the size and shape of the constituent particles and is sensitive to sample geometry.[31, 81] In our composite samples CrO_2 has a rod like structure with typical length L about 300nm with aspect ratio 7.5 and the size of spherical insulating fillers ranges from nanometer to micrometer in diameter. Many experimentalists have established the property of metallic fillers in insulating matrix, i.e. interparticle connectivity is stronger at low volume fraction for asymmetric conducting fillers with high aspect ratio whereas weaker for low aspect ratio of composite metallic fillers.[84, 85] In our work, we have shown a possible relationship between filling factor and percolation thresholds and there response to the change in ratio of dimensions of the constituent particles. The filling factor (F) of constituent particles in the mixture of rods and spheres with different ratios of d/D is shown in figure 4.9a. When filling factor is plotted as a function of volume fraction it is found that the maximum filling factor of the composite systems i.e. F_C is at the volume fraction P_F which is greater than electrical percolation threshold P_T and P_c. Normalization of filling factor and volume fraction is shown in figure 4.9b.

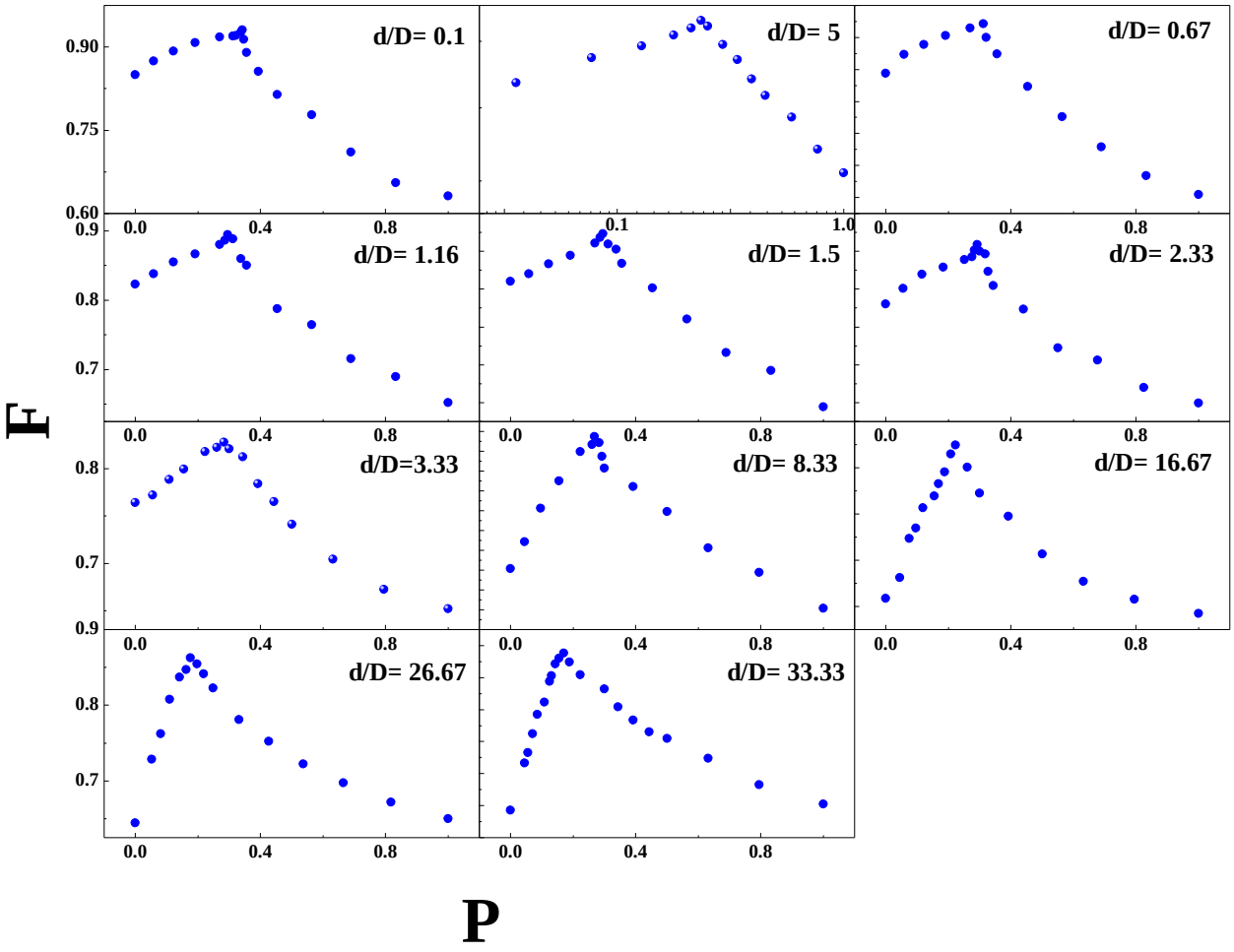

Figure 4.9(a) Filling factor (F) as function of metallic volume fraction (P) in composite systems with different d/D ratio.

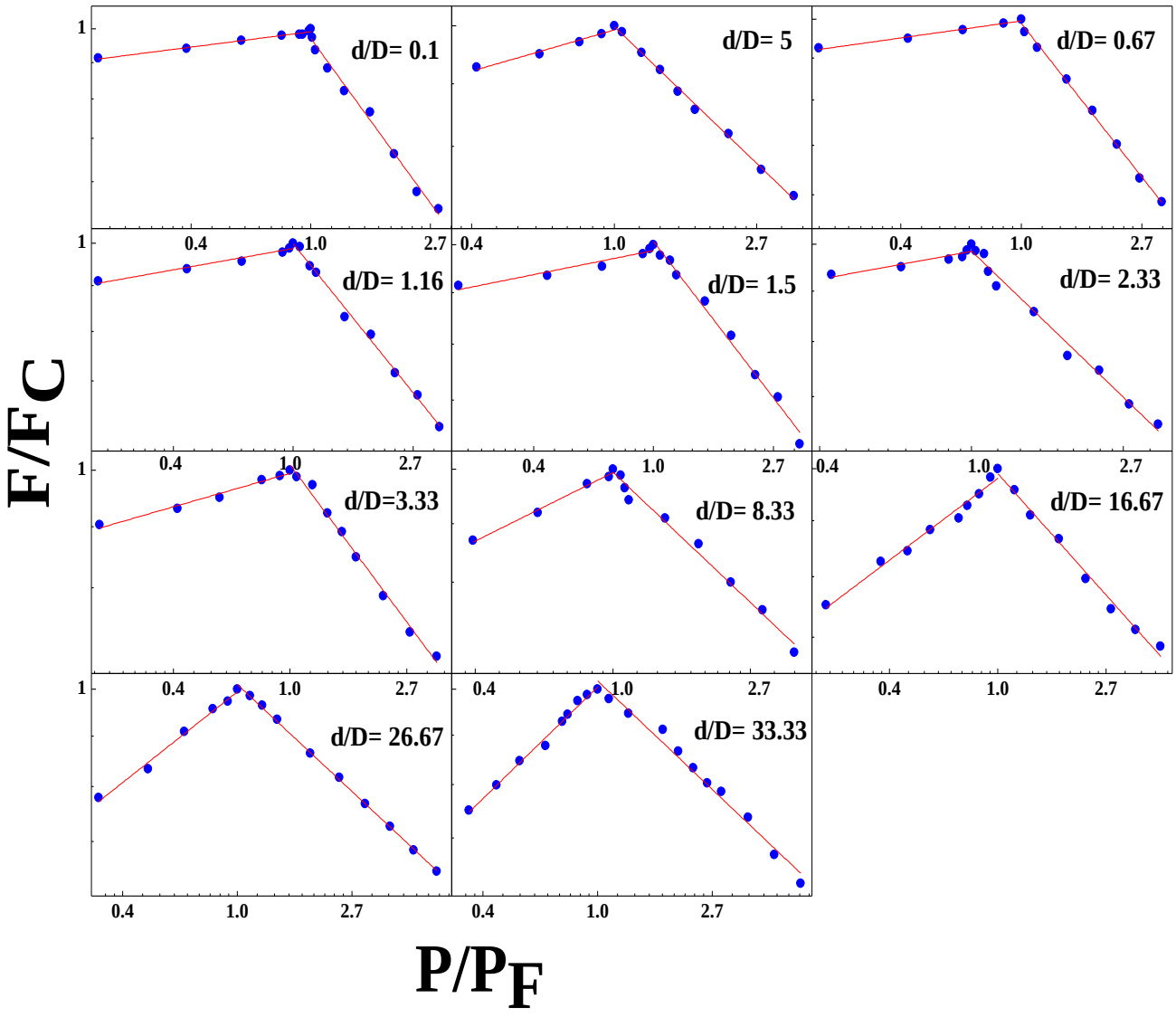

Figure 4.9(b) Determination of slopes using log-log plot of normalized variables.

The dependence of filling factor (F) on volume fraction of metallic particle (cylindrical shape) in binary mixture of spheres and cylinders shows a definite pattern. This pattern is found in all of the binary composite samples. There is a peak in the plot that appears at volume fraction P_F, which signifies that before attaining P_F, the cylindrical particles orient themselves freely in voids and around spherical particles which makes the packing maximum. After P_F, on addition of more cylindrical particles, it hinders the orientation and translation of cylindrical particles around the space in the composite due to which excluded volume around the cylindrical sticks increases and becomes more dominating. This increase of excluded volume drives the filling factor of the composite systems downward. A similar phenomenon was reported by some groups when total packing fraction was plotted as function of rod aspect ratio.[86] They found that density maximum was result of competition between local caging and excluded volume effects and the later one was dominating effect that drives the packing density down.[82, 86] At the threshold, it is expected that the size of largest cluster grows to maximum and then shows a discontinuous behavior.[87] Number of clusters when plotted as function of volume fraction P, it shows a peak at threshold and then decrease on increasing the volume fraction.[87, 88]. Figure 4.10 shows the dependence behavior of the slopes of the filling factor in binary mixtures as a function of size ratio of constituent particles.

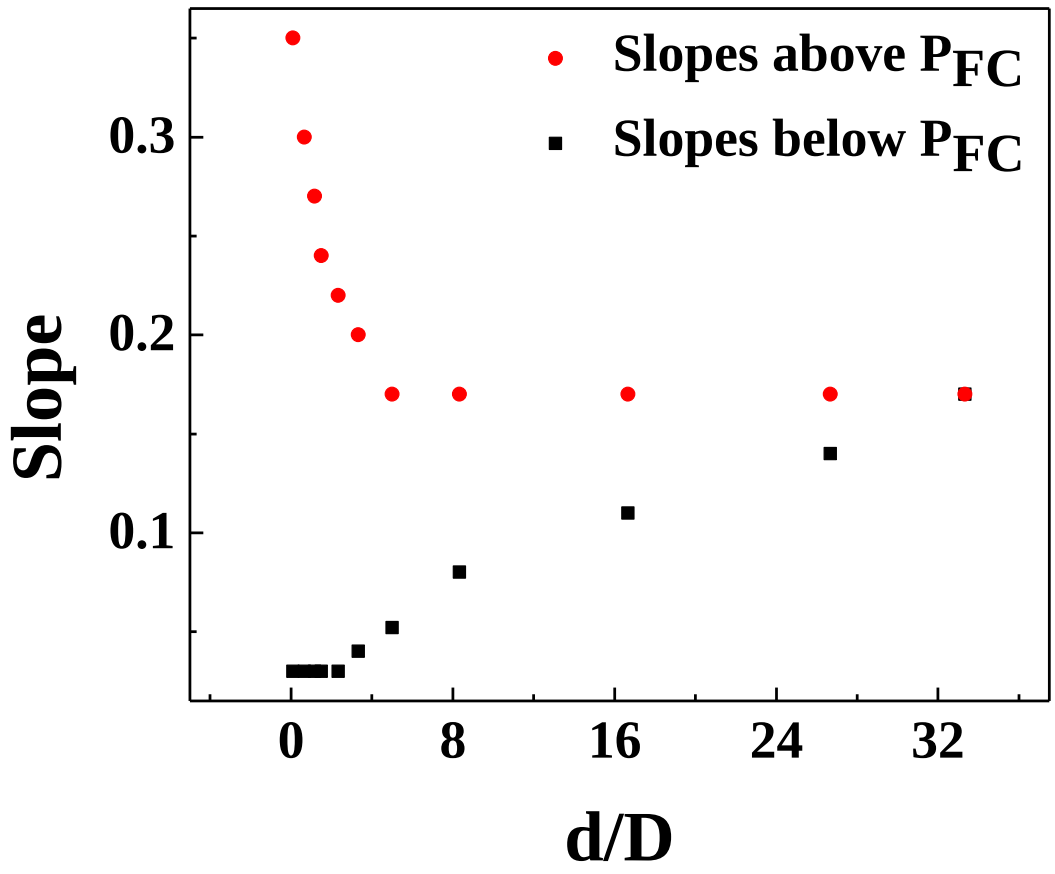

Figure 4.10 Dependence of slope of filling factor in composite systems as a function of d/D. The red circles correspond to the slopes before P_F and black squares corresponds to slopes after P_F.

Figure 4.11(a) shows exponential dependence of difference between variation in slopes of F and saturation slope on ratio of length of metallic particle to the diameter of insulating particle (D/d) before P_F. Exponential fit and log-linear fit are also shown along with fitting equations and parameters. On the other hand, after P_F, the variation of slope of F is found to have exponential dependence on the inverse ratio of constituent particle dimensions which is shown in figure 4.11(b).

Exponential fitting and log-linear fitting is also shown for this case. This idea helps us to find a scaling law between slopes of filling factor before and after P_F as a function of different size ratios of composite particles. The ratio d/D seems dominating in one region (after P_F) whereas D/d dominates before P_F. Before P_F, the saturation slope (α_S) is 0.03 and after P_F it is 0.17.

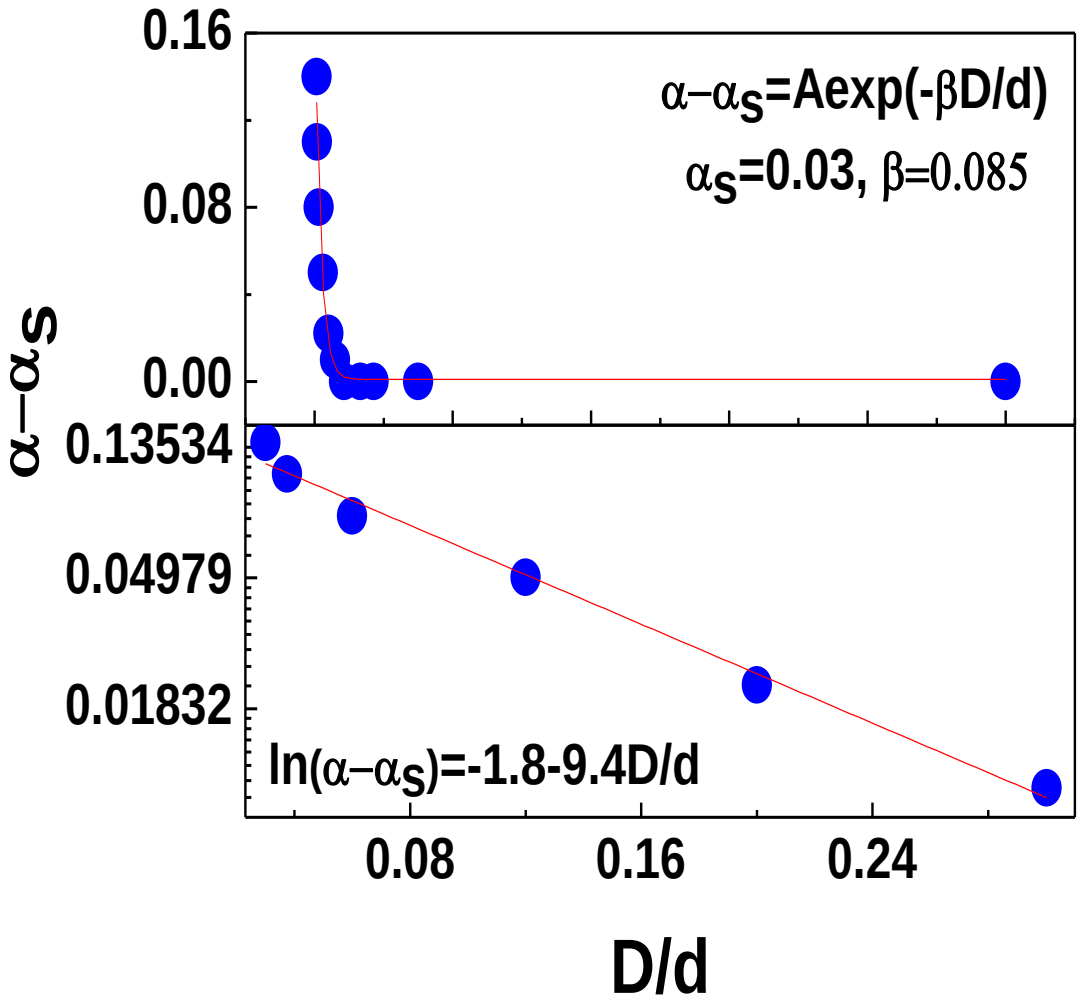

Figure 4.11(a) Exponential dependence of slope of filling factor before P_F with D/d and its log-linear fitting.

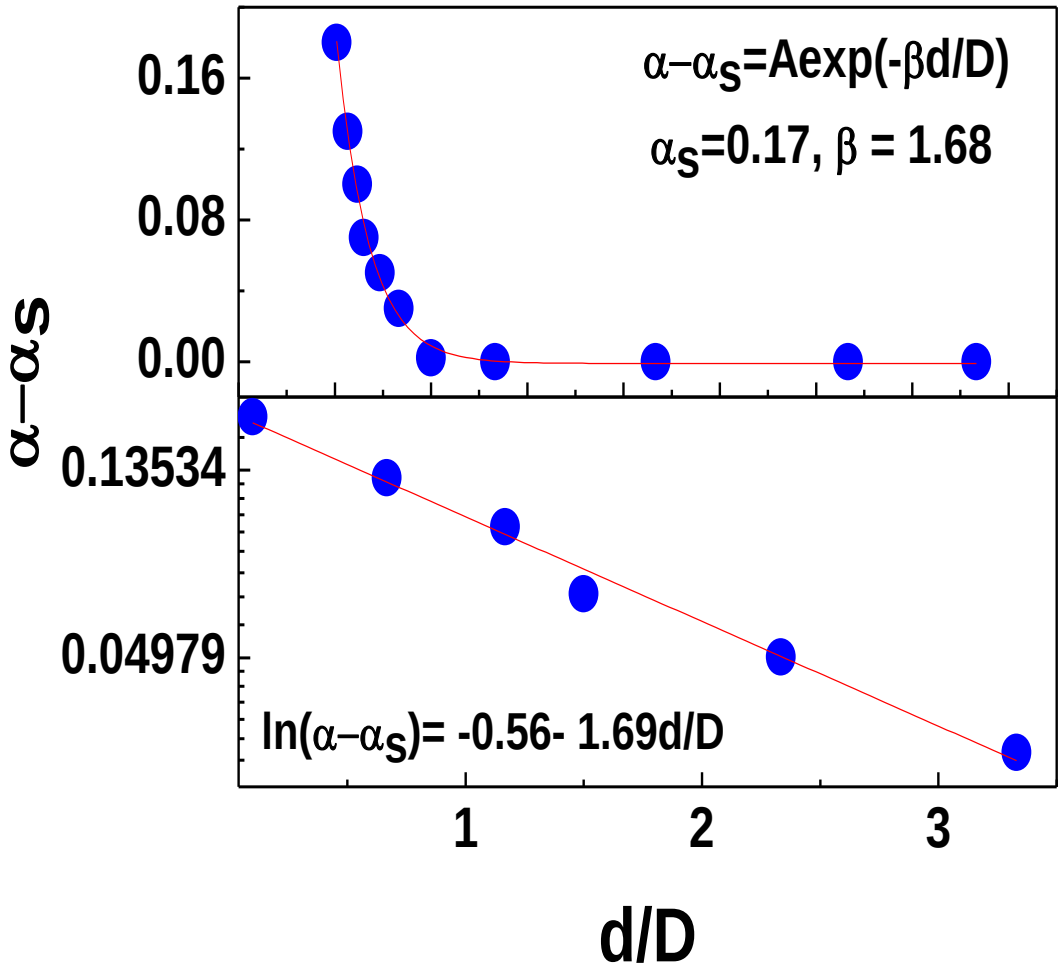

Figure 4.11(b) Exponential dependence of slope of filling factor after P_F with d/D and its log-linear fitting.

Taking natural logarithm of slopes yields straight lines with slopes of magnitude 9.4 and 1.69 before and after P_F respectively. Earlier, Monte Carlo simulations showed that when critical density of continuum percolation systems which composed of discs (2D) and spheres (3D) of two different length is plotted against the relative volume fraction, it yielded a symmetric function.[89] But when filling factor is plotted as a function of volume fraction it followed a typical non-

monotonic asymmetric function. Scaling of the filling factor is plotted in figure 4.12. This is plotted using the above two fitting equations in the plot for before and after $P_{F.}$

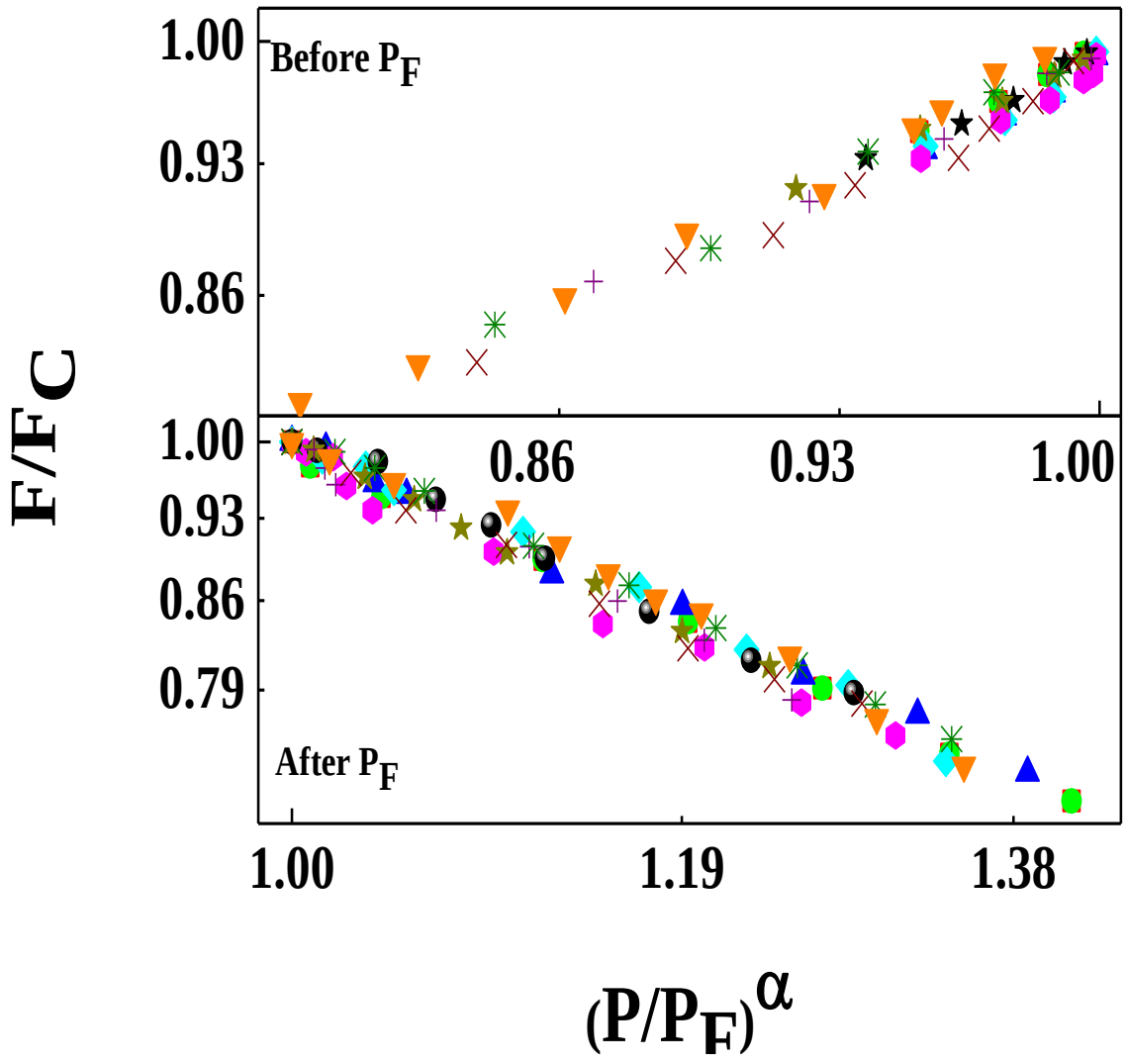

Figure 4.12 Scaling the slopes of filling factor before and after P_F, where α is the slope.

The maximum filling factor F_C at volume fraction P_F is plotted as function of ratio d/D shown in figure 4.13. It is found out that F_C has non-monotonic dependence whereas P_F has monotonic dependence on the ratio of dimension of particles. This non-monotonic dependence can be explained in terms of excluded volume.

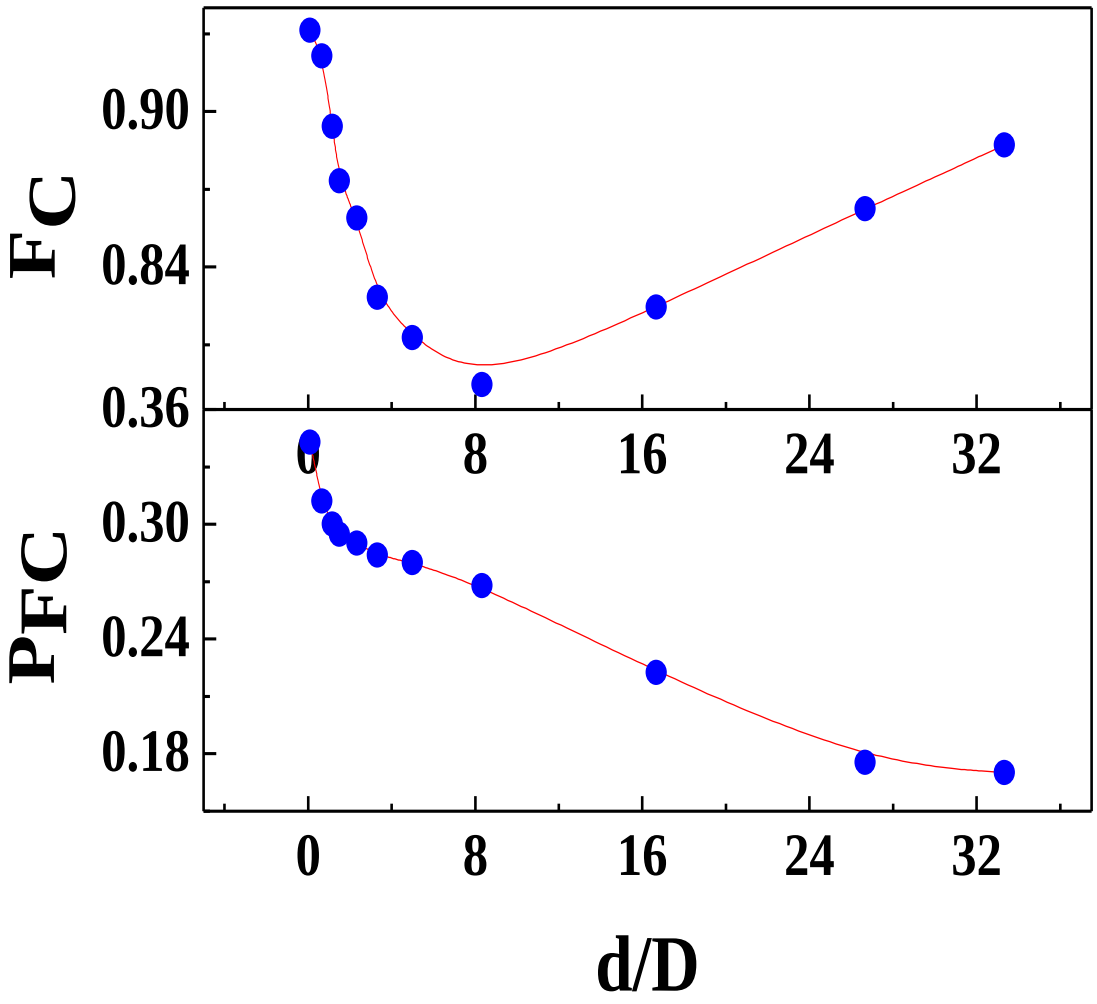

Figure 4.13 The peak of filling factor in composite systems and its corresponding volume fraction P_F is plotted as function of d/D. A minimum is observed in F_C – d/D plot, whereas monotonic dependence is observed in P_F – d/D plot.

Considering the excluded volume of capped cylinders which is V_{Exc} = $(32\prod/3)r^3+8Lr^2+4L^2r<siny>$, where <siny> is the average of siny and y is the angle between two called cylinders.[90, 91] From fig. 4.13, it is found that maximum excluded volume is found around d/D ratio 8 since filling factor is inversely proportional to excluded volume. The dependency of P_F on electrical percolation threshold is shown in figure 4.14. The volume fraction P_F at which maximum filling factor appears has a monotonic dependency with P_C and P_C^T.

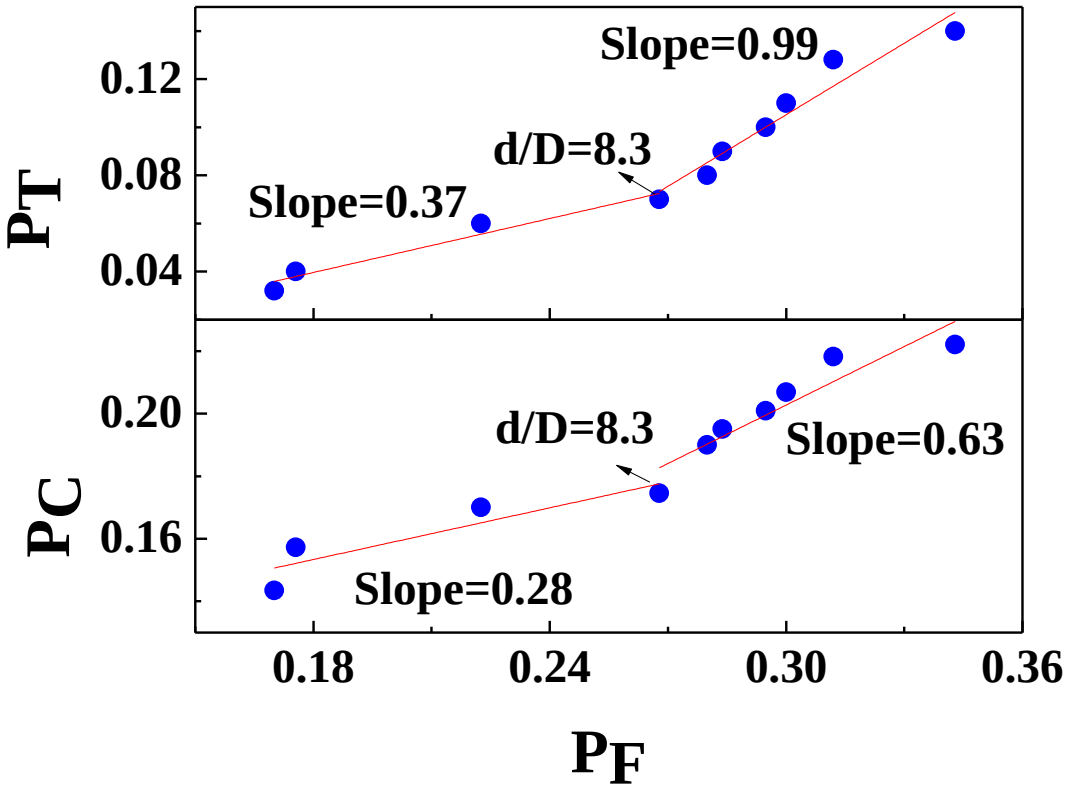

Figure 4.14 Monotonic dependence of P_T and P_C on P_F. A kink in the plot is found to be at 8.3 in both cases.

However when packing threshold i.e. $F_C.P_F$ is plotted as function of particle size ratio (d/D), we observed the decrease of packing threshold is fast at low size ratio but slows down at high size ratio. This is shown in figure 4.15 below.

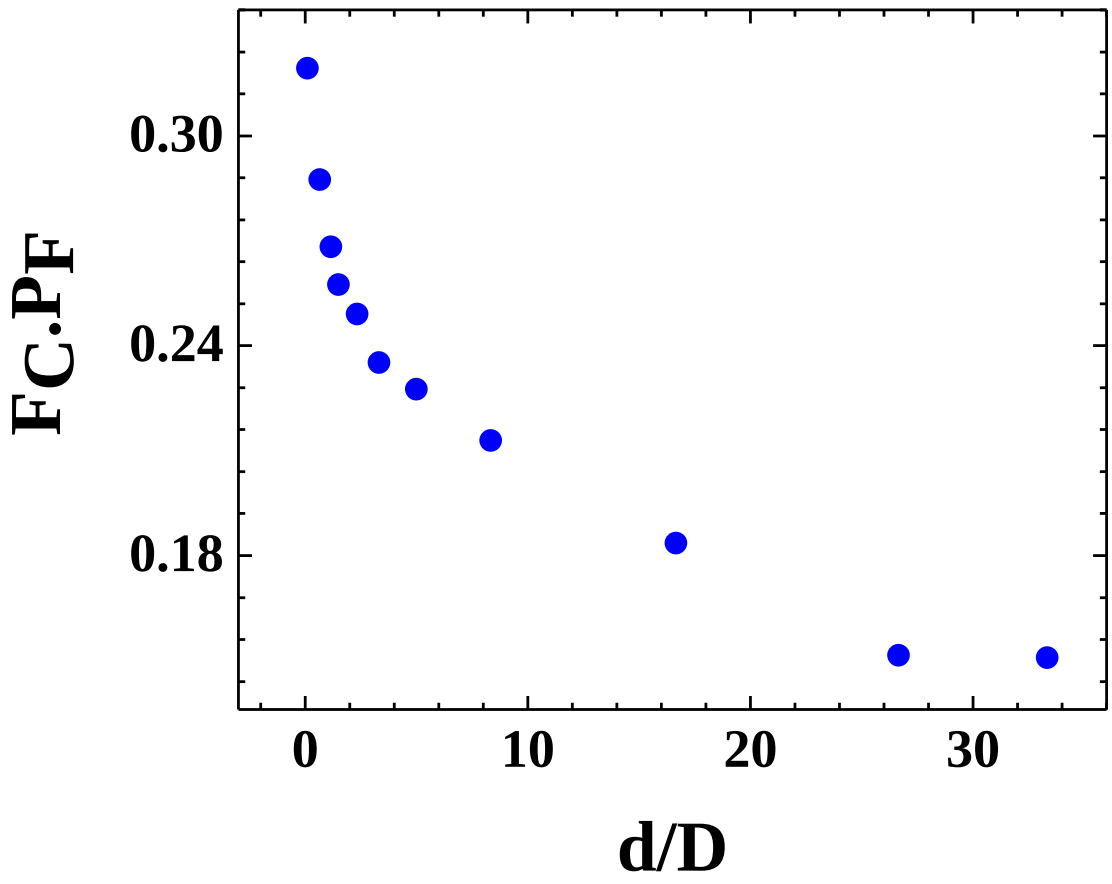

Figure 4.15 Packing threshold is plotted as function of particle size ratios.

4.4 Conclusion:

Existence of two percolation thresholds P_T and P_C have been confirmed. P_T is at the volume fraction where tunneling percolation dominates and P_C is at the volume fraction where ohmic conductance governs. The critical exponent of resistance in two regions is different which further supports the idea of two type of percolation phenomenon in distinct regions. Upper percolation threshold P_T also shows linear dependency with lower threshold P_C. In this paper we have shown the behavior of filling factor as a function of volume fraction in rod sphere composite mixtures. Filling factor shows a peak at P_F in all composite systems which signifies minimum excluded volume since packing density is inversely proportional to excluded volume. Filling factor shows a non monotonic behavior as a function of d/D ratio. Scaling of the filling factor yielded equations that is proportional to exp (-D/d) and exp (-d/D) for $P<P_C$ and $P>P_C$ respectively. It is also found that P_T and P_C have a monotonic dependency as a function of P_F, which suggests that the electrical percolation has geometrical relationship with filling factor.

Chapter 5 DIELECTRIC BEHAVIOR OF $CaCu_3Ti_4O_{12}$ CERAMICS

$CaCu_3Ti_4O_{12}$ (CCTO) is a perovskite like compound which exhibits high value of dielectric constant on the order of 10,000 over a wide range of temperature from 100 to 400K. Such dielectric property of CCTO makes a desirable material for micro-electronic devices such as static and dynamic random access memories and proves to be excellent for high charge energy storage devices. The high dielectric permittivity of CCTO is believed to be arising from both intrinsic effect and extrinsic mechanism. Absence of any structural distortion at low temperature has ruled out CCTO behaving as ferroelectric material. These days ferroelectric oxides such as $BaTiO_3$ or relaxor ferroelectrics like hafnium doped barium titanate ceramics, $Pb(Mg_{1/3}Nb_{2/3})O_3$ are often used as high dielectric material.[92, 93] However these dielectric oxides don't have any temperature stability or doesn't sustain high voltage. Moreover these oxide dielectric materials do not show any giant dielectric permittivity thus limiting their usage on achieving high energy density storage devices.

5.1 Introduction

For high degree of miniaturization of energy storage and memory devices, dielectric permittivity of a material which is an important component of the device needs to be very thermally stable and highly effective. The dielectric permittivity

(K) of a material depends on the dipole polarizability (α) which arises from the orientation of permanent electric dipoles in presence of applied electric field. In metals, since the charge is delocalized the dielectric permittivity is negative (K<0) whereas in case of insulators, the charge carriers are localized which make dielectric permittivity greater than zero (K>0). Recently single crystal $CaCu_3Ti_4O_{12}$ (CCTO) is found to have largest static dielectric constant of nearly 80,000 at room temperature.[94, 95]. Generally, ferroelectric materials which exhibits dipole moment in the absence of external electric field or materials that behaves as ferroelectric relaxor under high electric field at low temperature are believed to show dielectric permittivity above 1000. These ferroelectric can even surpass 1000, increases rapidly with increasing temperature and peaking around ferroelectric phase transition temperature.[96] There are two basic reasons for which CCTO is not considered as ferroelectric material. Firstly, unlike ferroelectric materials, CCTO shows temperature independent dielectric response at low frequency over a wide range of temperature. Secondly, high resolution x-ray and neutron powder diffraction measurement shows that CCTO has centrosymmetric (inversion symmetry) crystal structure, thus ruling out the existence of permanent dipole moment.[97, 98] It is predicted that the high dielectric permittivity in CCTO may have been originated from either intrinsically or extrinsically.[99] By intrinsic, it means that the dielectric response is measured in a perfectly stoichiometric, defect free,

single domain crystal of CCTO. Whereas on the other hand extrinsic effect means the dielectric response is associated with domain boundaries, defects, space charge effect and other crystal imperfections.[97] Some details of intrinsic mechanism and extrinsic mechanism are described below which can help us to understand the origin of high dielectric response.

5.1.1 Intrinsic mechanism

Generally in ferroelectric and relaxor materials, the lattices are unstable with temperature due to which it shows anomalous dielectric response. Due to lack of any experimental evidence of lattice distortion in CCTO, ferroelectricity cannot be held responsible for high dielectric permittivity. Secondly, a relaxor material is characterized by presence of random atoms in sublattices or presence of local polar lattice distortion. In CCTO, Ca/Cu sublattice is well ordered which again rules out the possibility of CCTO to behave as relaxor. Thirdly, it was believed that high permittivity in CCTO might have originated from either free orientation of domains (domains considered to be very small) or motion of domain walls in order to reorient the polarization (domains are considered to be very large). Since CCTO shows wide range of temperature independent dielectric response, the former possibility in CCTO is ruled out. Had the latter possibility is found to be true, then CCTO would have shown magnitude of dielectric constant comparable to that observed in other ferroelectrics containing domains, which is not the case.[97]

Existence of highly correlated electronic ground state can also be held responsible for high dielectric response. Anomalous dielectric permittivity in CCTO could be explained in terms of electronic ferroelectricity since CCTO is an antiferromagnetic Mott insulator with an electronic structure containing localized d states and dispersive s and p bands.[100-102] But experimentally, optical gap in CCTO is found to exceed 1.5eV, which is nearly same as conventional Mott insulator. So, excitons or other low frequency excitations cannot be expected to condense in presence of this robust gap. So existence of electronic ferroelectric state is not possible.

5.1.2 Extrinsic mechanism

It was found that it was easier to understand the origin of high dielectric permittivity if extrinsic mechanisms such as point, planar, line defects, morphology, microstructure or boundary layers are taken into account. It is believed that boundary or interface effects are more dominant than others and play an important role on achieving high dielectric permittivity. Interface effect mainly arises due to presence of antiphase boundaries which separate regions of Ca sublattice shifted by a primitive lattice vector. There is also an existence of twin boundaries due to which the domains with reverse rotation of oxygen octahedra are separated. In CCTO, presence of such interface boundaries is confirmed through neutron diffraction analysis. Suppose the conductance of CCTO is eliminated by

the presence of insulating antiphase or twin boundaries. If ε_{int} represents the dielectric permittivity of the insulating interface and f is the volume fraction of the insulating phase, then ε_{int}/f is the static dielectric permittivity of the material. Assuming $\varepsilon_{int} \sim 10^2$ and $f \sim 10^{-3}$, then overall static dielectric permittivity of 10^5 is possible. Temperature independent dielectric response of CCTO is also possible if ε_{int} and f doesn't vary significantly over range of temperature.

On applying alternate voltage at high frequency, the mean electron conduction path decreases below the average grain size. This is ascribed to an activated behavior of intradomain conductivity (conducting bulk contribution).[103] So interface boundaries can indeed help us to understand all the dielectric behaviors we observe in CCTO. By changing the width of the insulating boundaries, the dielectric permittivity of CCTO can be regulated accordingly.

5.2 Impedance spectroscopy on CCTO

5.2.1 Basic principles of impedance spectroscopy

Temperature dependent impedance spectroscopy (IS) is a powerful tool to understand the factors that contribute to dielectric and resistive properties in a material. In electrically inhomogeneous electroceramics such as CCTO, the dielectric properties of grain boundary (GB) and grain interior (bulk) can be characterized separately with the help of IS.[104, 105] In IS experiments, there is an

applied time dependent alternating voltage U of angular frequency ω with amplitude U_0. Correspondingly, the current response signal I is measured in terms of the amplitude I_0 and phase shift δ. Mathematically, they are represented as

$U(\omega,t) = U_0\cos(\omega t); \quad \rightarrow I(\omega,t) = I_0\cos(\omega t-\delta)$

The phase diagram corresponds to various phase shifts is shown in the figure below.

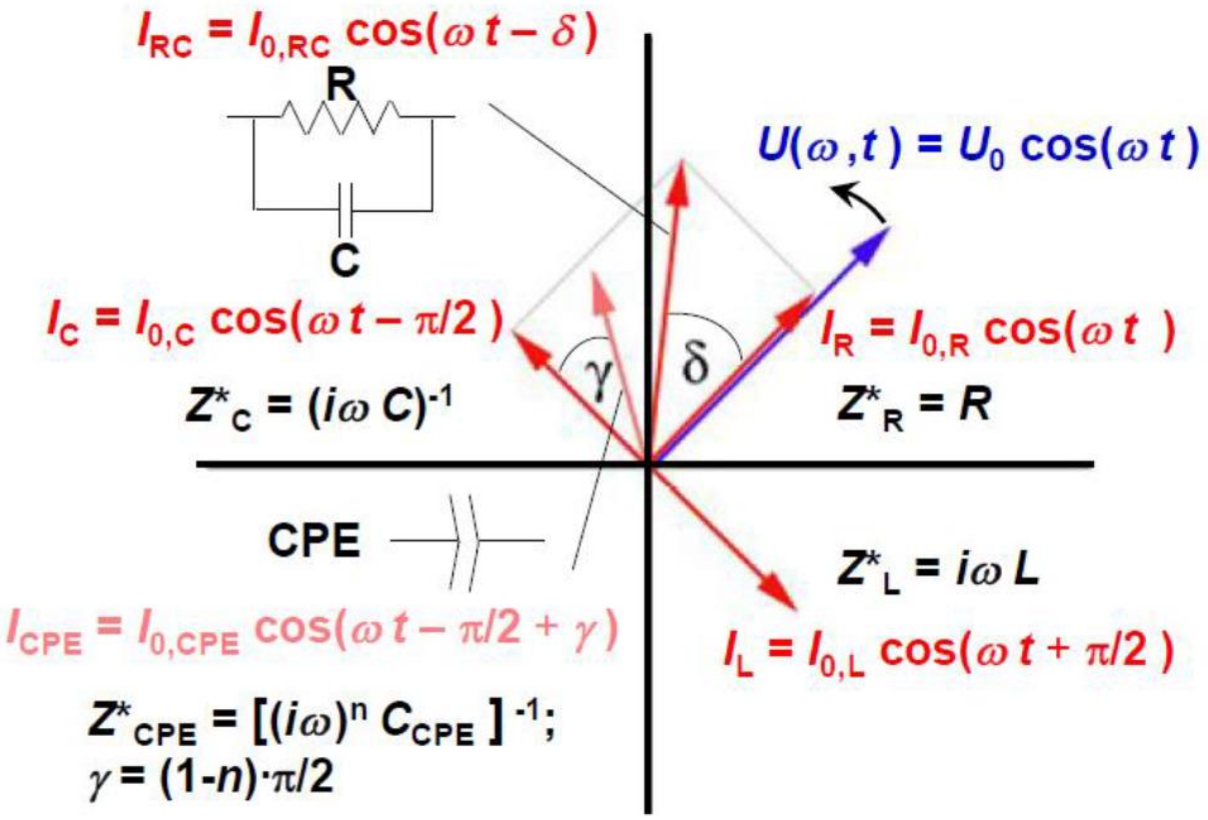

Figure 5.1 Impedance responses of circuit elements on a phase diagram.

Here, the applied voltage is marked in blue and the response current is shown in red. For δ=0, the circuit is purely resistive. For δ= -π/2, the circuit is capacitive and

for $\delta = +\pi/2$, it is inductive. All phase angles which rotates at constant angles with given frequency are considered time independent. The dielectric relaxation processes at GB (grain boundary) and at bulk regions are different as found by IS data analysis. This can be modeled for simplicity as brick work layer model in which GB or bulk type contribution is described by RC element, where resistor (R) and capacitor (C) are connected in parallel.[106] Here, the function of the capacitor describes the ability of a material to store charge and the parallel resistor signifies the leakage current due to un-trapped charge carriers bypassing the capacitor. This is shown in figure 5.1.

5.2.2 Impedance spectroscopy on CCTO ceramic

The structure of CCTO is shown in figure 5.2.a. below where semiconducting grain interiors (bulk) is represented in dark blue and is surrounded by insulating GB boundaries which is represented as colorless. There is no electrical conductivity that can percolate through this structure. IS measurement on CCTO shows that capacitance C drops sharply as a function of increasing frequency (f). The giant dielectric permittivity which is contributed mainly by GB at low frequency has now had a permittivity contributed by bulk reduced to 100 at high frequency. This is shown in figure 5.2.b. This particular behavior is evident in an internal barrier layer capacitance (IBLC) structure since at high frequency alternating voltage, mean electron conduction path decreases below the average

grain size. The dielectric response at low frequency is dominated by insulating GB and at high frequency it is mainly a bulk conducting mechanism.[107] The dielectric relaxation process originated from both GB and bulk is represented as two RC element connected in series which is shown in figure 5.2.c.

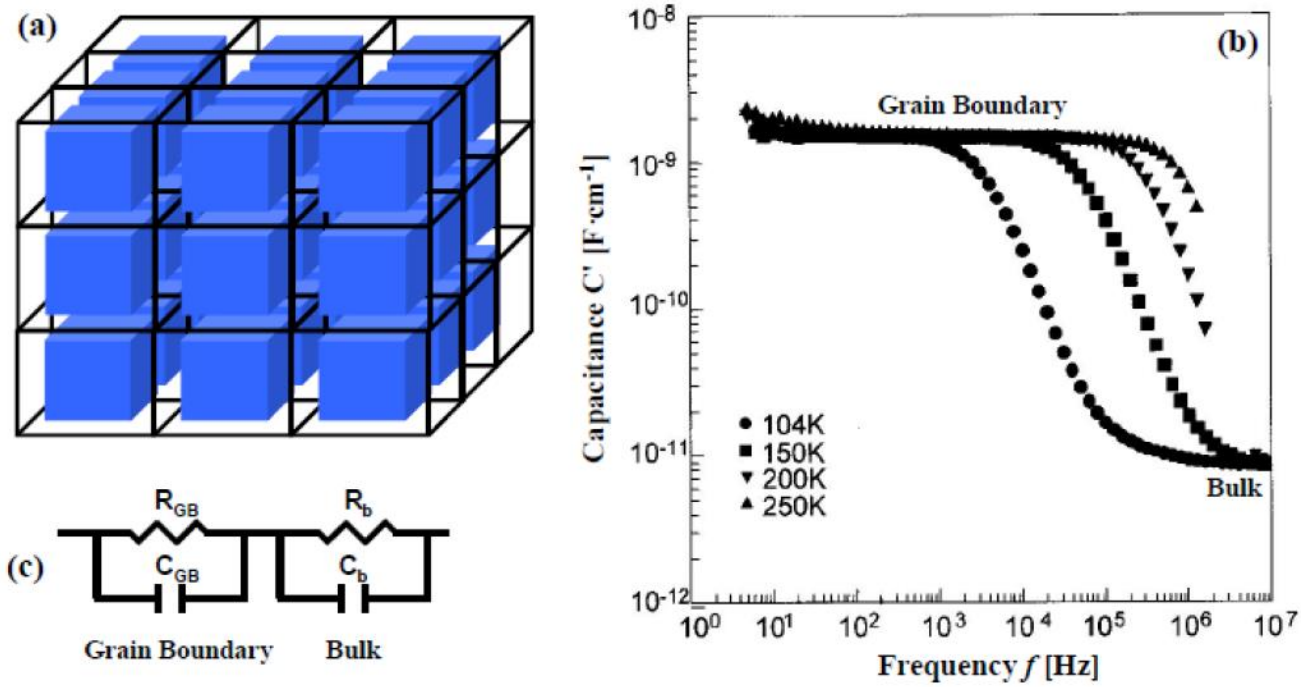

Figure 5.2 IBLC structure of CCTO: (a) Semiconducting grains bulk are represented by blue cubes and insulating GB is represented by colorless cubes.(b) IS shows real part of C as a function of frequency f. (c) To account for GB and bulk dielectric relaxation process, equivalent RC model is shown.

5.3 Influence of Sintering temperature on dielectric CCTO

After preparing CCTO with reagent powders followed by calcinations at 1000°C, six pellets were pressed and sintered at different set of temperatures, T_S = 975, 1000, 1025, 1050, 1075 and 1100°C. They were sintered for 12 hours and were cooled back slowly. For dielectric measurement gold electrodes were used for making contacts. There is increase in GB permittivity with increase in T_S as shown in figure 5.3 below.

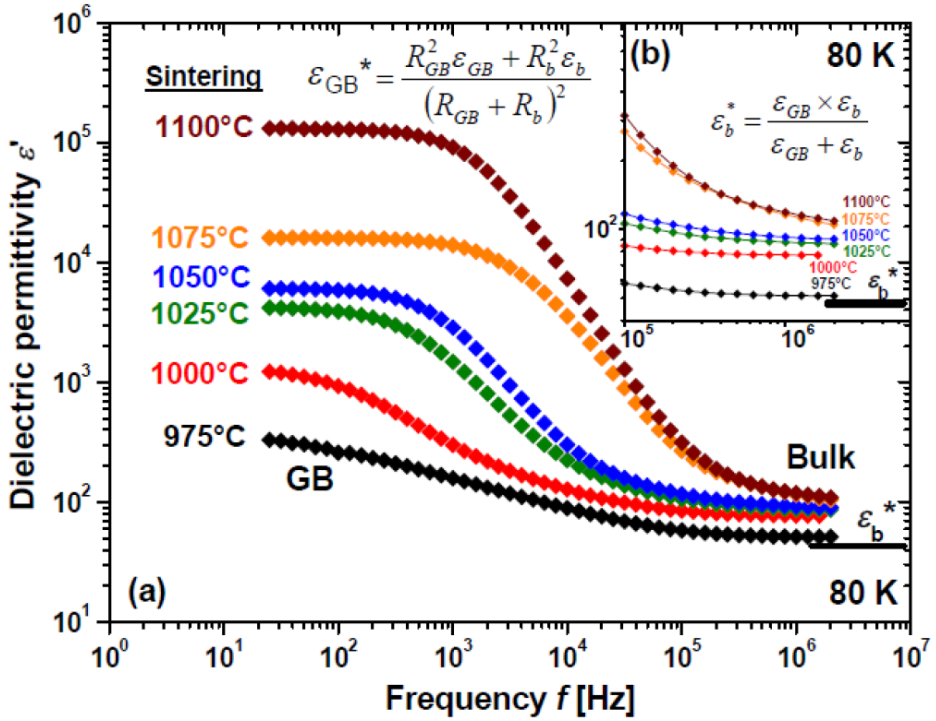

Figure 5.3 (a) ε' vs f for pellets at different sintering temperature T_S, showing ε' increases with T_S. (b) Bulk permittivity with increasing T_S.

It is found that here is substantial increase of GB permittivity with increase of T_S whereas for there is moderate increase of bulk permittivity with T_S. This increase of dielectric permittivity with T_S is also confirmed from Cole-Cole plot where imaginary part of dielectric permittivity is plotted as a function of real part of permittivity and is shown in figure 5.4 below.

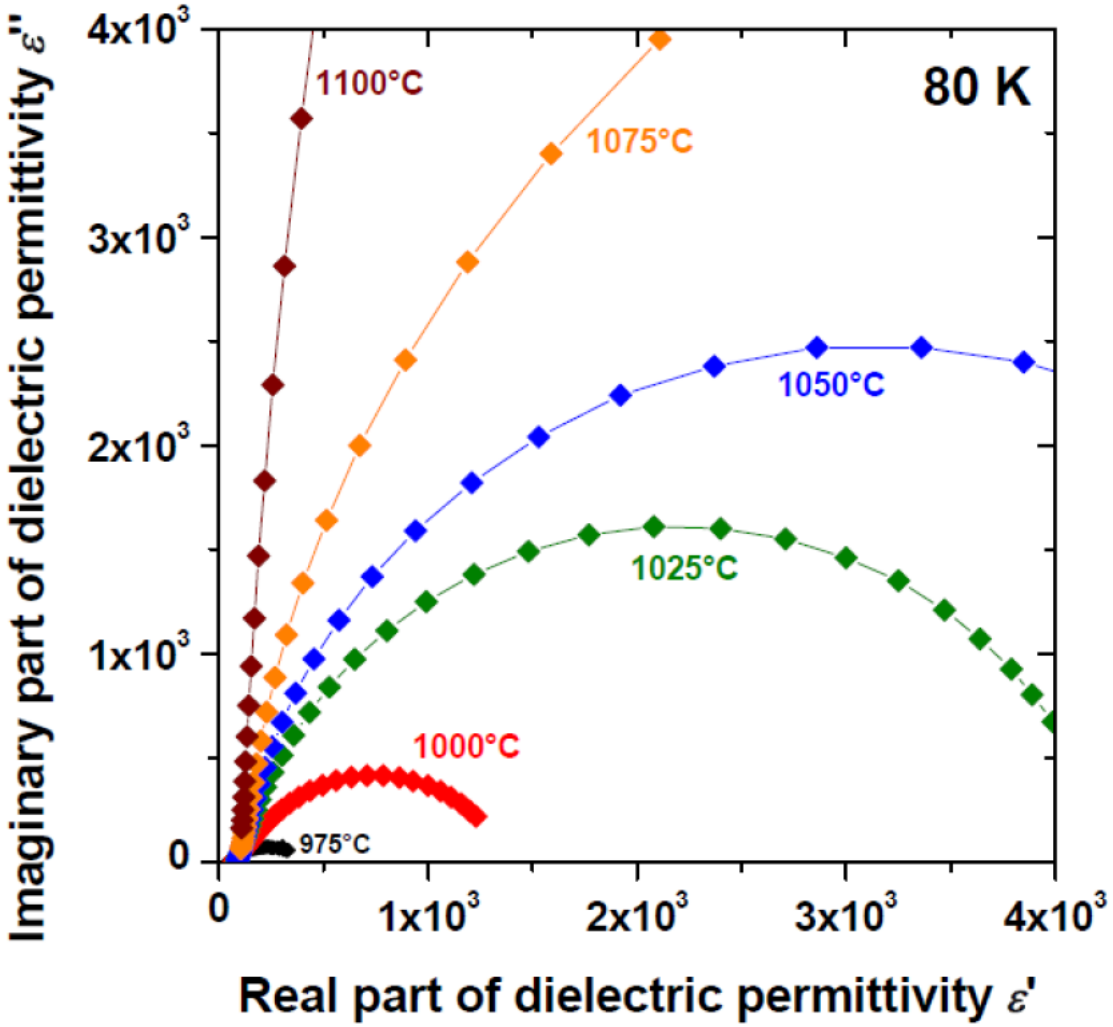

Figure 5.4 Cole-Cole plot of $\varepsilon^{//}$ vs $\varepsilon^{/}$ for pellets sintered at different T_S. The diameter of the semicircle signifies the magnitude of permittivity.

Generally, the grain (domain) resistance (R_g) is smaller than boundary (GB) resistance (R_{GB}) . With increasing T_S, R_g decreases with the sintering temperature which is due to generation of large number of oxygen vacancies that promotes conducting carriers.[108] Figure 5.5 and figure 5.6 shows the SEM image of CCTO as

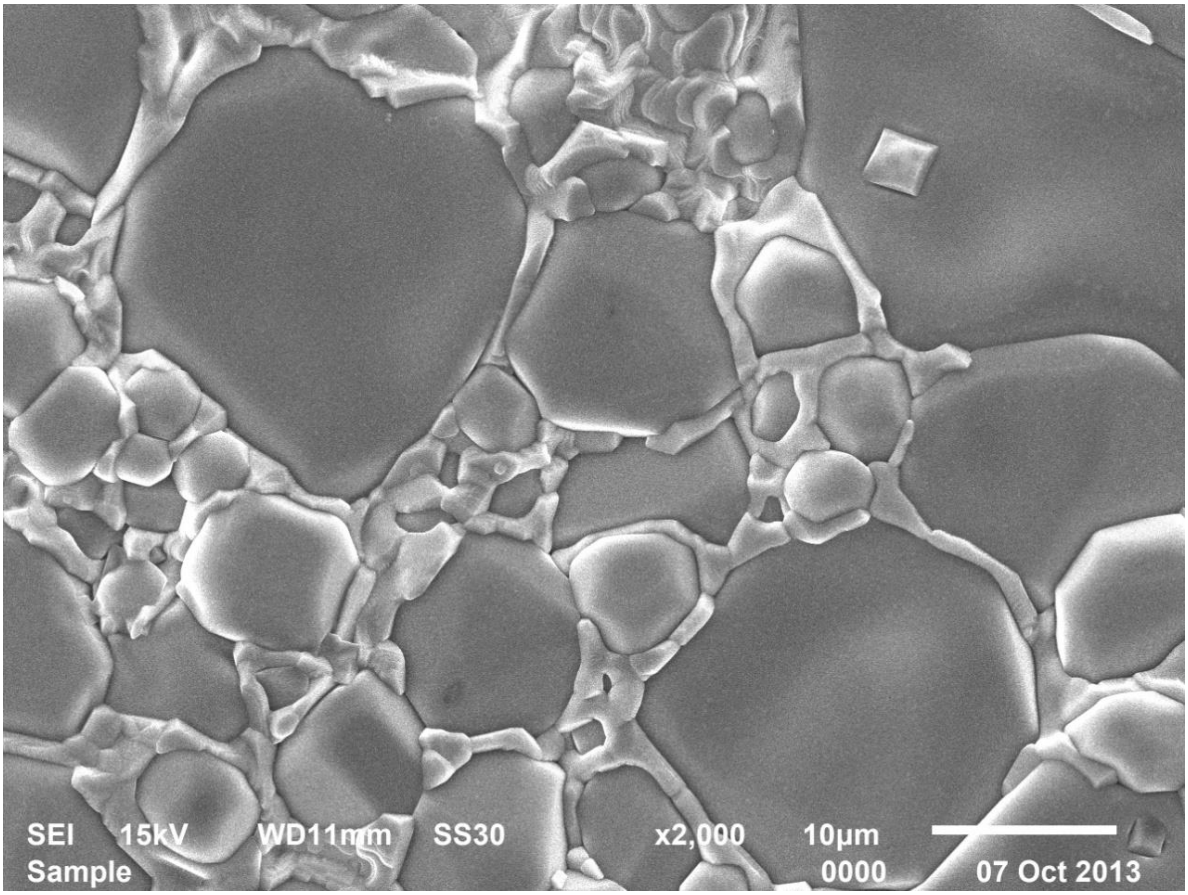

Figure 5.5 Microstructure of CCTO prepared by solid state process. Segregation of copper oxide in between the grains is shown.

prepared by solid state (SS) and sol gel (SG) process and sintered at 1100^{o}C. It is found that there is segregation of CuO at the grain boundary when sintered above 1050^{o}C. This may lead to higher copper content at the GB and thus shows higher resistance than the bulk grains. The EDX point ID analysis confirms the stoichiometric distribution in CCTO. It also reveals that at the grain boundaries,

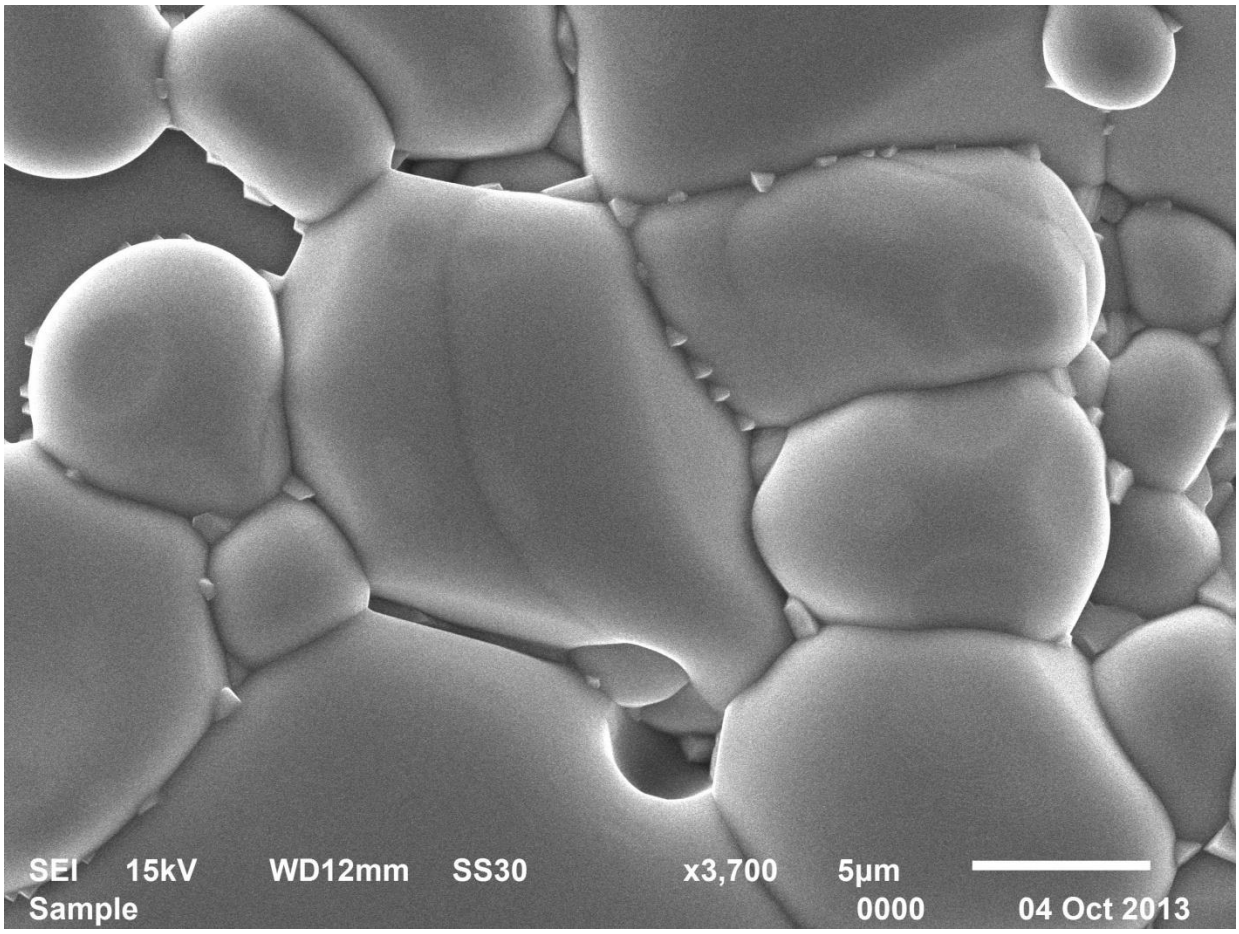

Figure 5.6 Microstructure of CCTO prepared by sol-gel process. The intergranular phase with enriched copper oxide is seen in between the grains.

there is an existence of inter granular phase which is enriched with copper oxide, and at the grains it is more enriched with Titanium oxide.

Impedance spectroscopy performed by Adams et.al. also confirmed presence of electrically heterogeneous phase in CCTO that contains semiconducting grains with insulating grain boundaries.[109] Point EDX analyses on the grains as well as at the grain boundaries were performed and confirmed the presence of copper oxide enriched region in between the grains. With increasing sintering temperature both grain size and inter granular phase becomes large and are uniformly distributed. It was also established that increasing the sintering temperature or the sintering time, both have a similar effect in the fabrication of dielectric CCTO.[108]

5.4 Experimental results

Figure 5.7 demonstrates the real part of dielectric permittivity and dielectric loss for CCTO ceramics prepared by both solid state and sol-gel process at room temperature over frequency range of 1kHz to 1MHz. From figure 5.7 (a) and (c), it is evident that there exhibits giant dielectric permittivity at low frequency. Dielectric permittivity for CCTO prepared by solid state shows value of around 10,000 whereas for CCTO prepared by sol-gel is around 4,500. This shows that the dielectric permittivity is very sensitive to fabrication procedure. Moreover, sharp fall of dielectric permittivity is observed in the frequency range above 30kHz,

which is accompanied by the appearance of corresponding peaks in the dielectric loss spectra as shown in figure 5.7 (b) and (d).

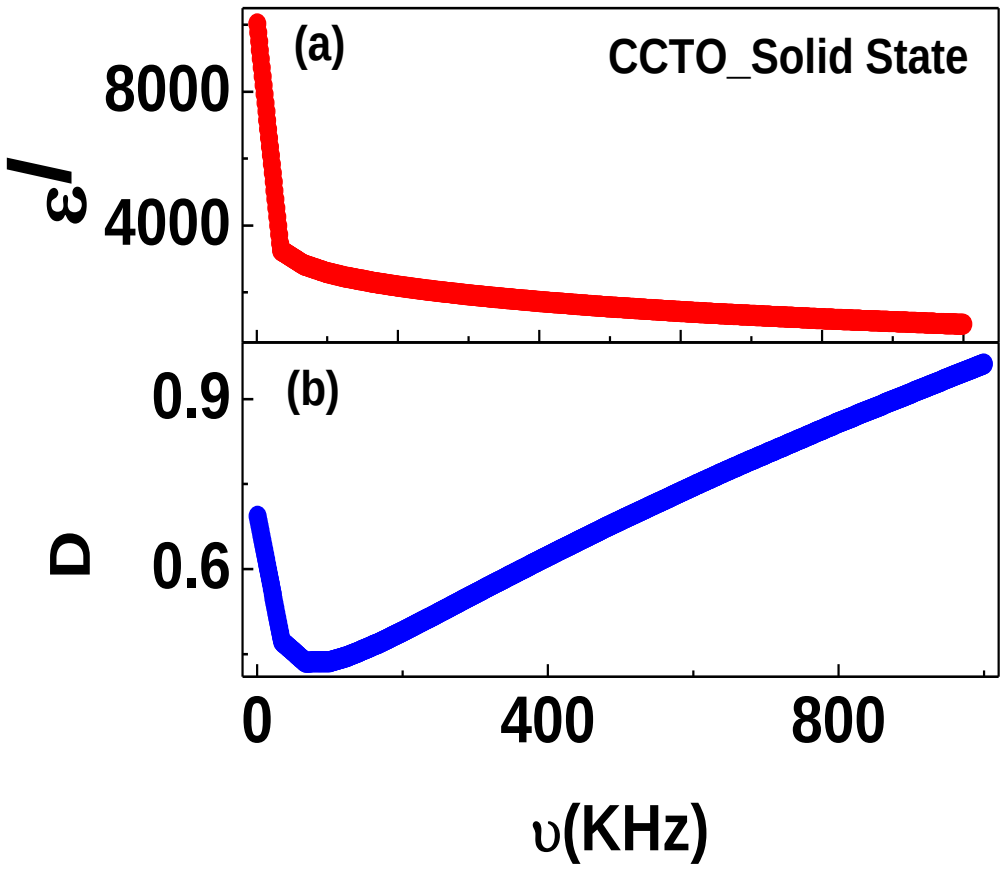

Figure 5.7 Dielectric spectra for CCTO prepared by solid state process. (a) Dielectric permittivity as a function of frequency, at low frequency giant permittivity is observed. (b) Dielectric loss as function of frequency, a peak is observed at high frequency.

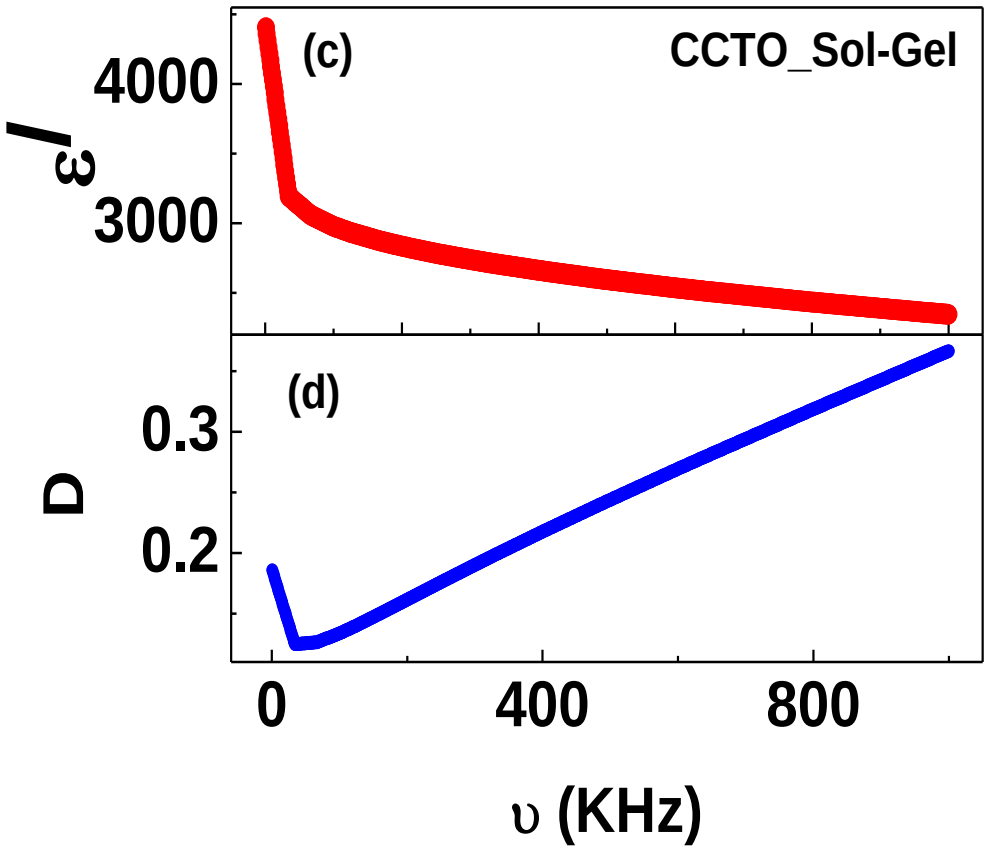

Figure 5.7 Dielectric spectra for CCTO prepared by sol-gel process. (c) Dielectric permittivity as a function of frequency, at low frequency giant permittivity is observed. (d) Dielectric loss as function of frequency, a peak is observed at high frequency.

This giant permittivity at low frequency is considered to be typical feature of hopping conduction of localized charge carriers.[110] Figure 5.8 shows the temperature dependence of dielectric behavior in CCTO. In Figure 5.8 (a) and (c) it is observed that at low temperatures, there is a dramatic decrease of dielectric permittivity which is due to freezing of electric dipoles through relaxation process as evidenced by dramatic increase of relaxation time τ.

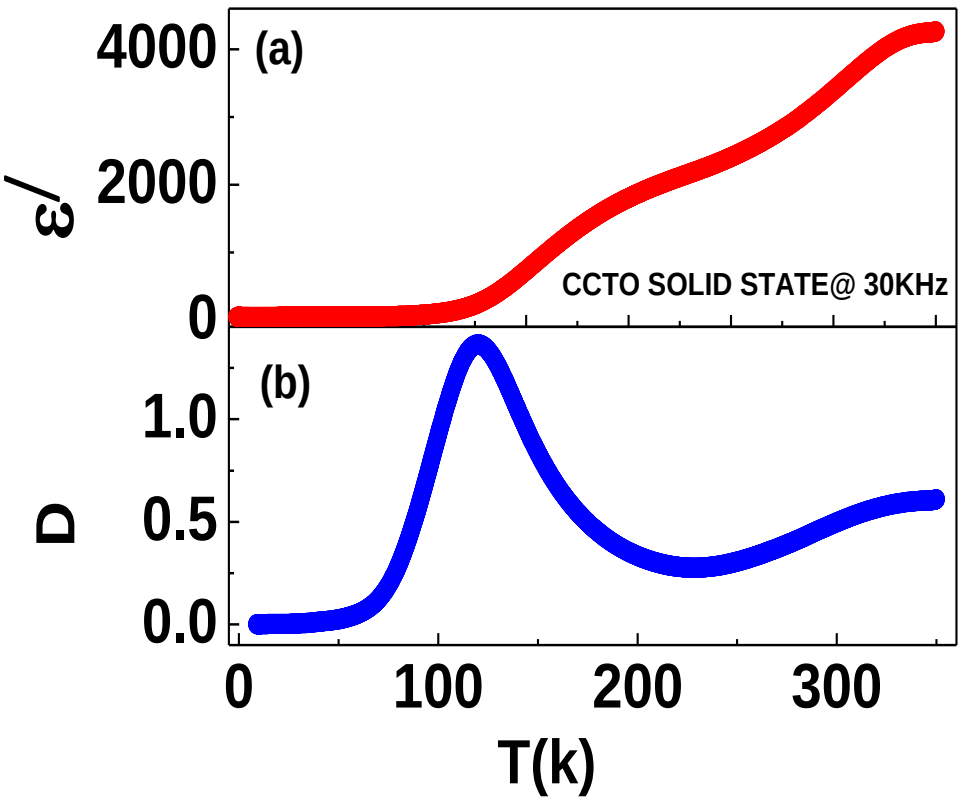

Figure 5.8 Dielectric response of CCTO prepared by solid state process as a function of temperature. (a) Dielectric permittivity shows plateau at 30kHz at temperature below 100K. (b) Dielectric loss shows two relaxation peaks at two different temperatures.

This results in slowing down of dipole fluctuation. This is accompanied by relaxation peak in dielectric loss at low temperatures as shown in figure 5.8 (b) and (d).

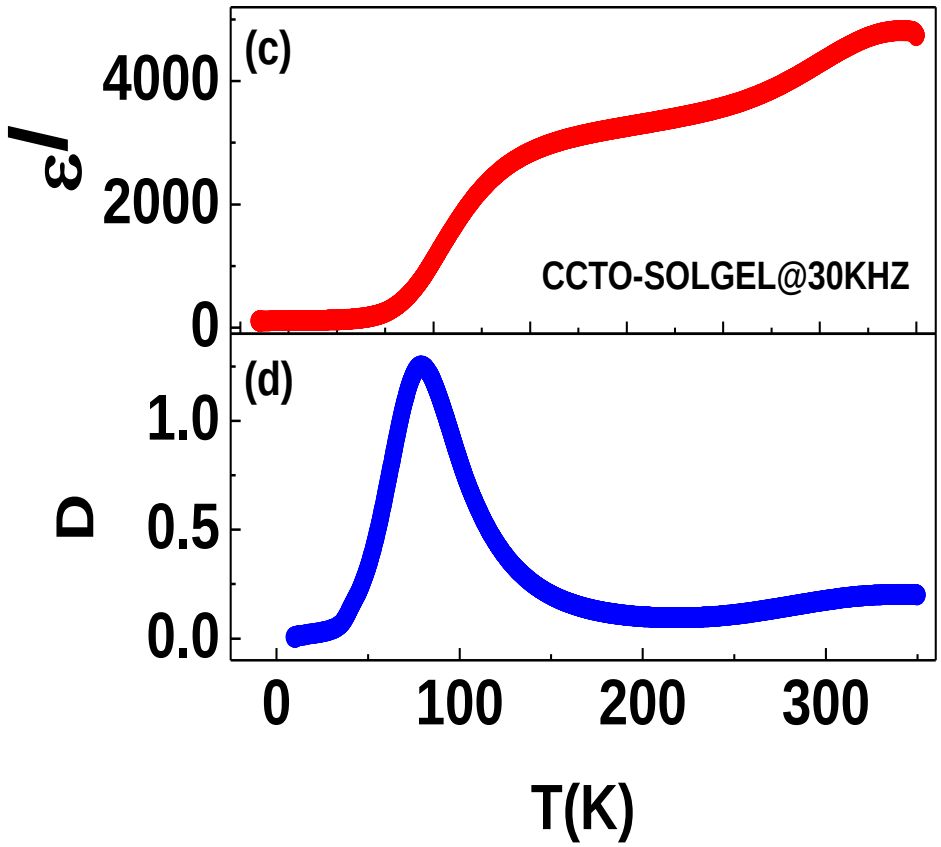

Figure 5.8 Dielectric response of CCTO prepared by sol-gel process as a function of temperature. (c) Dielectric permittivity shows plateau at 30kHz at temperature below 100K. (d) Dielectric loss shows two relaxation peaks at two different temperatures.

In figure 5.9 frequency dependent conductivity for CCTO prepared by solid state and sol-gel process is shown. It is known that frequency dependent conductivity and dielectric constant of disordered mixture originate from two important factors: (a) polarization effects between clusters in the mixture and (b) anomalous diffusion between each cluster. It is shown that ac conductivity increases linearly on a log-

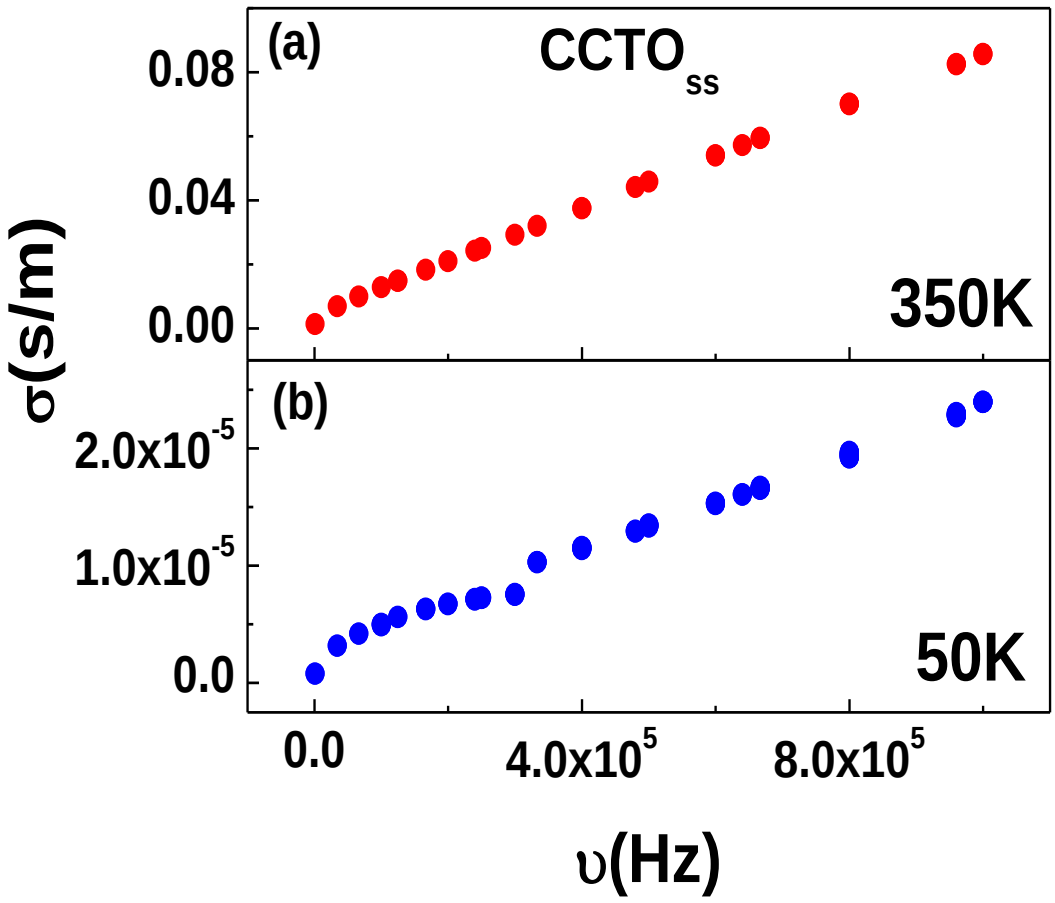

Figure 5.9 (a) and (b) shows the ac conductivity for CCTO prepared by solid state process at 350K and 50K respectively.

log plot, thus demonstrating power law behavior. If the CCTO was conducting, it would have given a flat response with frequency.[111] This means that if there exists many percolating path within the CCTO, then the conductivity is mainly

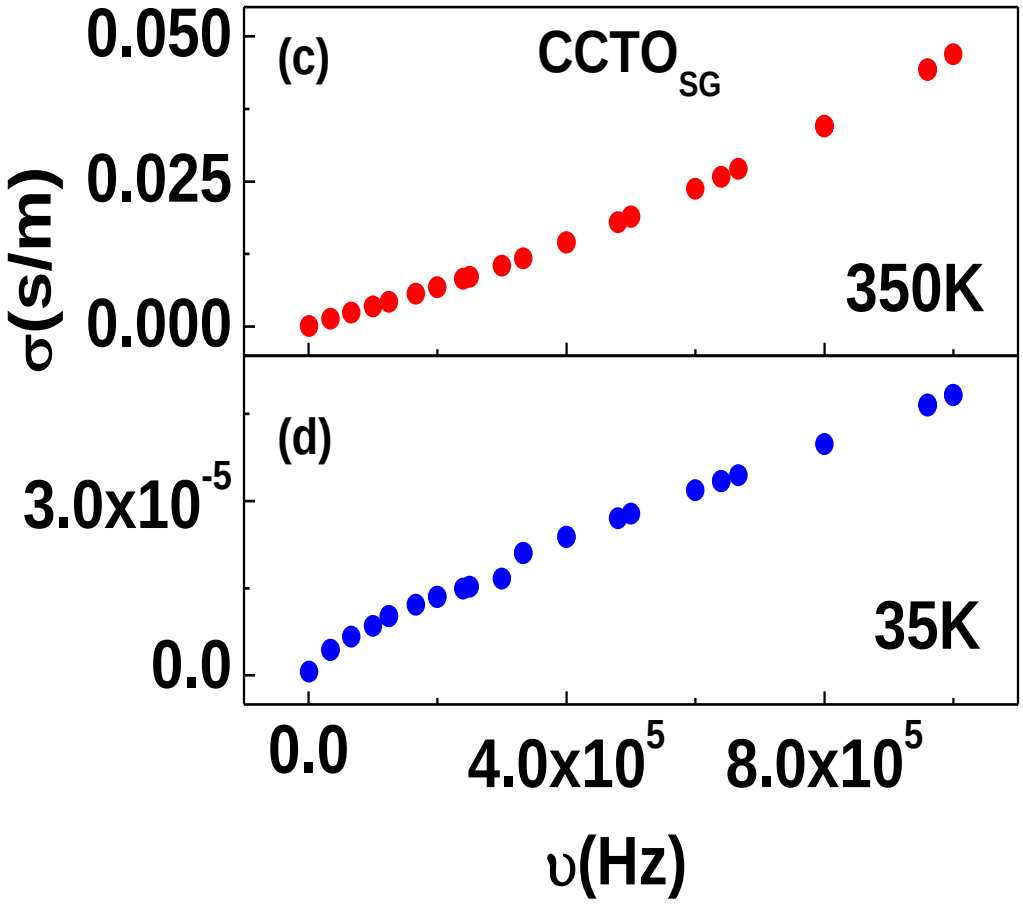

Figure 5.9 (c) and (d) shows the ac conductivity for CCTO prepared by sol-gel process at 350K and 50K respectively.

determined by those percolating path rather than small effects of capacitors. Electrons can move freely independent of some range of frequency. But at high frequency even capacitors contributes in the conductivity.[112] On the other hand, since CCTO is dielectric, contribution from only capacitors plays an important role. With the increase of frequency, the current increases through the capacitors, thus promoting ac conductivity. At a certain frequency ω, electrons will move a

length L_ω. If $L_\omega < \xi$(correlation length), then the conducting clusters appears to be self similar fractals. In this case, the conductivity increases with decrease in L_ω. So conductivity appears to increase with increase of ω.

5.5 Conclusions

Dielectric permittivity of CCTO is found to be very sensitive to its fabrication procedure. Giant permittivity at low frequency is the due to existence of hopping charge carriers. With the increase of frequency, permittivity drops due to increase in relaxation time and it is mainly a bulk permittivity. Temperature dependent dielectric permittivity shows presence of thermally active carriers in the dielectric. Ac conductivity shows a power law behavior with frequency. With increase in frequency, the conductivity increases due to polarization effect.

CHAPTER 6 ENHANCEMENT OF HIGH DIELECTRIC PERMITTIVITY IN $CaCu_3Ti_4O_{12}/RuO_2$ COMPOSITES IN THE VICICNITY OF THE PERCOLATION THRESHOLD

We observe the large enhancement in the dielectric permittivity near the percolation threshold in a composite nanoparticle system consisting of metallic RuO_2 grains embedded into $CaCu_3Ti_4O_{12}$ (CCTO) matrix and annealed at $1100^{O}C$. To understand the nature of the dielectric response, we compare CCTO fabricated by two different techniques, solid state process ($CCTO_{SS}$) and sol-gel process ($CCTO_{SG}$) with the relative permittivity in both cases found to be on the order of 10^3-10^4 at 10 kHz. For $RuO_2/CCTO_{SS}$ and $RuO_2/CCTO_{SG}$ composites, an increase in the real part of the dielectric permittivity by factors of 7 and 5 respectively is observed in the vicinity of the percolation threshold of about 0.1, with moderate losses at room temperature.

The critical exponent of dielectric permittivity and conductivity of these composites are found to be lower than universal values (0.8-1). In these composite systems, both Maxwell-Wagner effect and percolation effect have been found responsible for the enhancement of dielectric permittivity.

6.1 Introduction

Attaining large volumetric capacities (capacities per unit volume), is of crucial importance for a number of applications, such as energy storage and renewable energy.[113] The development of double layer electrolytic capacitors, or supercapacitors, as well a number of other traditional approaches, have been successfully implemented to raise the volumetric capacity to approximately $10^2/cm^3$.[113, 114] However, in order to further increase volumetric capacity, it may be necessary to consider alternative approaches. Recently a different approach to achieve high volumetric capacity based on a rapid increase of the dielectric permittivity near the percolation threshold of a composite system of dielectric and metallic nanoparticles, was proposed by Efros.[115] This approach, which we will refer to as *percolative capacity*, is based on the disappearance of a continuous conduction network (infinite cluster) near the threshold, which results in the divergence of the real part of the dielectric permittivity ε' predicted earlier.[116-118] Experimentally, this idea was successfully demonstrated in a few systems.[19, 119] However, while a large enhancement has been observed, the overall values of ε' achieved near the threshold, up to $8x10^4$, were comparable with the values attainable in a single-component ceramics, such as CCTO.

Here, we show that percolative capacity can be implemented in a composite nanopaticle system consisting of ceramics with very high dielectric permittivity,

such as CCTO, and metallic oxides, such as RuO_2. Using this system, we have achieved both high initial permittivity of CCTO and a significant enhancement of the dielectric capacities near the percolation threshold in the composite system using two alterative synthesis techniques for CCTO, solid state and sol-gel processes. This opens up opportunities for developing new composite materials suitable for fabricating capacitors with high dielectric permittivity.

$CaCu_3Ti_4O_{12}$ (CCTO) is a material with a very high relative dielectric permittivity, ranging from 10^3-10^5 at room temperature with a quadruple perovskite structure.[120-122]. There is a significant effort being made to tune the dielectric properties of CCTO by varying the fabrication procedure, including changing the sintering temperature, time of sintering, and ambient atmosphere.[123-126]. While in the past the origin of the large, relatively temperature independent, dielectric permittivity in CCTO was often attributed to the intrinsic effects, i.e. crystal structure, extrinsic effects, such as an internal barrier layer capacitance and contact – electrode depletion[120, 121, 126, 127] are now believed to play the key role. Specifically, in polycrystalline CCTO ceramics, the internal boundary layer capacitance effect, in which the core grains are semiconductive and the grain boundary is electrically insulating is the most relevant mechanism.[128, 129] Indeed, impedance spectroscopy confirms the existence of semiconducting grains, which

dominate the response at higher frequencies, together with leaky grain boundaries that are more significant at low frequencies.[130-133]

Percolative composite systems are being increasingly used in high charge storage capacitors, embedded capacitor technology, gas sensors, and in spintronics.[117, 134] Earlier an attempt was made to improve the dielectric permittivity in ceramic/polymer hybrid film that contains CCTO as functional filler in polymer host.[135, 136] The value of $\varepsilon' \sim 50$ was obtained at low frequencies. Using CCTO as functional filler dielectric effects in two component systems, such as CCTO/Epoxy, and in three-component systems, such as Al/CCTO/Epoxy and Ni/CCTO/PVDF have also been investigated.[137-139] At room temperature, ε' ~50 and ε' ~700 were reported for two- and three- component system respectively. Recently CCTO/Ag composites were prepared at 1050^{o}C to study the Maxwell-Wagner relaxation effect as well as the enhancement in permittivity in the composite system at low frequency.[140, 141] However, it was found that there is significant loss of Ag in the composite system due to the evaporation of Ag during the sintering process. The distribution of Ag was found to be inhomogeneous with high concentrations at the grain boundaries. The resulting composites showed large dielectric loss with no significant improvement of the dielectric permittivity.

The implementation of the percolation effect in CCTO is significantly complicated by the need to be annealed to the optimized temperature of about

1100^{o}C, thus markedly restricting the number of metallic components one can use. To circumvent this problem, we have loaded ceramic CCTO matrix with metallic Ruthenium Oxide (RuO_2) particles. Since the sublimation temperature of RuO_2 is 1200^{o}C, it is considered to be stable at high temperature, and thus proves to be a good candidate for percolative composite systems with CCTO. In order to better understand the nature of dielectric permittivity enhancement, we have prepared the host CCTO material by two different procedures, solid state process ($CCTO_{SS}$) and sol-gel ($CCTO_{SG}$) process.

6.2 Experimental techniques

Following the solid state process, powder samples of CCTO were prepared by mixing $CaCO_3$ (99.99%, Aldrich,), CuO (99.99%, Aldrich) and TiO_2 (99.99%, Aldrich) in a planetary ball mill with acetone using zirconia balls for two hours. The mixture was then pre-calcined at 1000^{o}C for 12 hours. RuO_2 (99.99%, Aldrich) was then added at different volume fractions (*f*) and mixed thoroughly with agate mortar and pestle in dehumidifying atmosphere to minimize particle agglomeration. After mixing, pellets of $RuO_2/CCTO_{SS}$ composites were prepared by using a cold pressed die with an uniaxial pressure of 1 GP, and then calcined at 1100^{o}C prior to dielectric measurement. To synthesize CCTO composites by Sol Gel technique we used $Ti(OBu)_4$, $Cu(CH_3COO)_2.H_2O$ and $Ca(CH_3COO)_2.H_2O$ reagents as precursors (Aldrich). These starting materials were mixed with hot

glacial acetic acid and ethyl alcohol and were stirred with magnetic stirrer for 8 hrs. A xerogel was obtained at 85^{o}C. This xerogel was then pre-calcined at 1000^{o}C for 12 hours. The rest of the fabrication procedure was the same as in the solid state process. Immediately after fabrication silver paste was used as electrode and gold wires were connected on both sides of pellets for dielectric measurements in parallel plate geometry. Micrographs of composites were obtained using a scanning electron microscope (JEOL, 6610 LV). Electrical properties of the samples were measured by using 4284A precision LCR meter under 1V peak-to-peak AC small signal voltage in the frequency range 10^{1} – 10^{6} Hz. In addition to the electrical conductivity σ, these measurements allowed us to determine the relative dielectric permittivity $\varepsilon = (\varepsilon' + i\,\varepsilon'')/\varepsilon_0$ where ε' and ε'' are the real and imaginary parts of the frequency-dependent permittivity, and ε_0 is the permittivity of vacuum, and the dissipation factor $D = \tan\delta = \varepsilon''/\varepsilon'$, where the loss angle δ is the phase difference between the applied electric field and the induced current.

6.3 Experimental results & Discussions

Figure 6.1 shows the XRD patterns of the CCTO powders prepared by solid state process and sol-gel process after annealing at 1100^{0}C. It indicates the presence of a single phase with a cubic perovskite related structure and thus confirms the absence of any major impurities in as prepared CCTO samples.

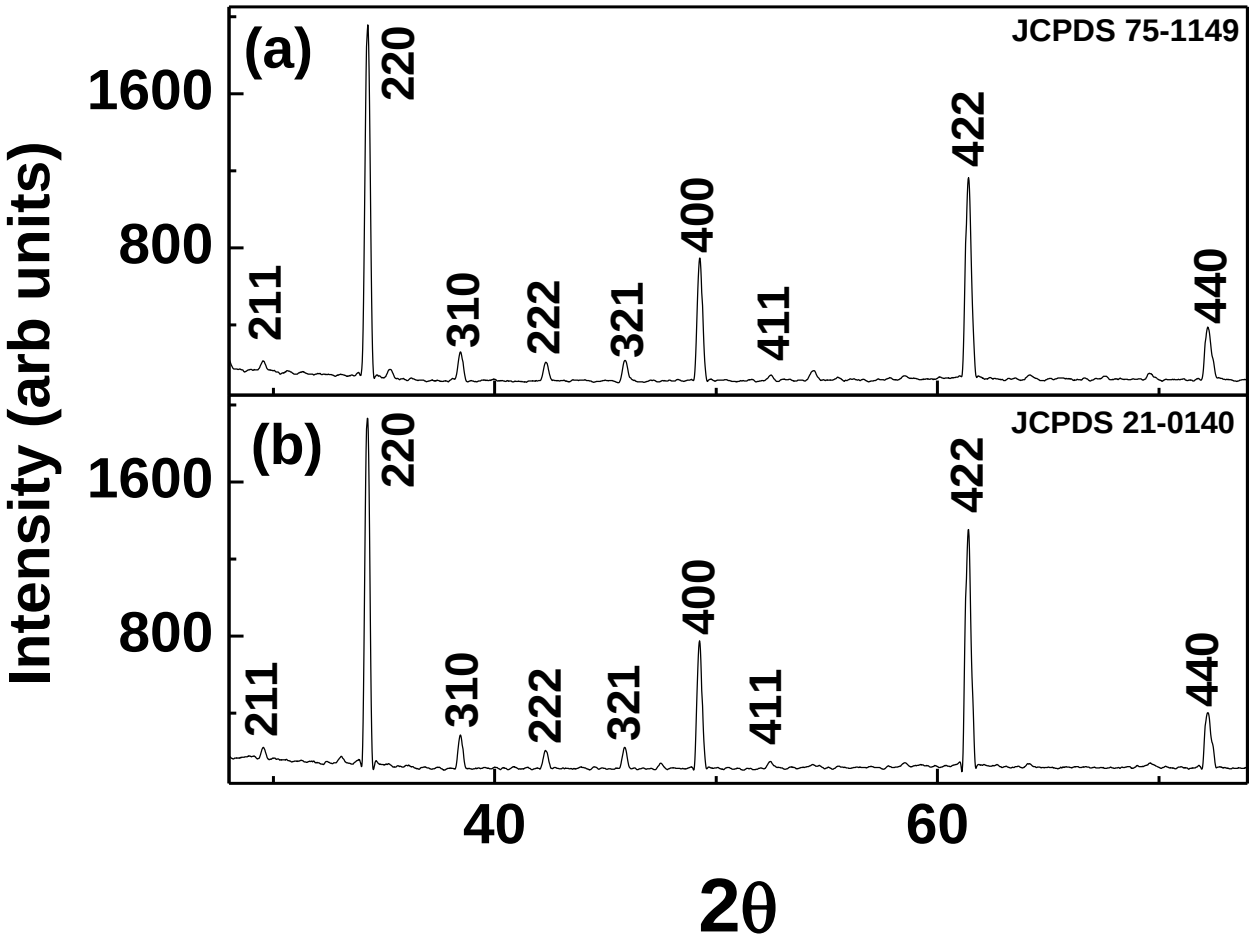

Figure 6.1 (a) XRD patterns of CCTO powders prepared using two different techniques: (a) Solid state process; (b) Sol-gel process.

Fig.6.2a – 6.2d shows selected SEM images of the composites $RuO_2/CCTO_{SS}$ and $RuO_2/CCTO_{SG}$ after annealing. It indicates the presence of isometric shaped RuO_2 particles (some shown with arrows) uniformly dispersed in the host matrix of

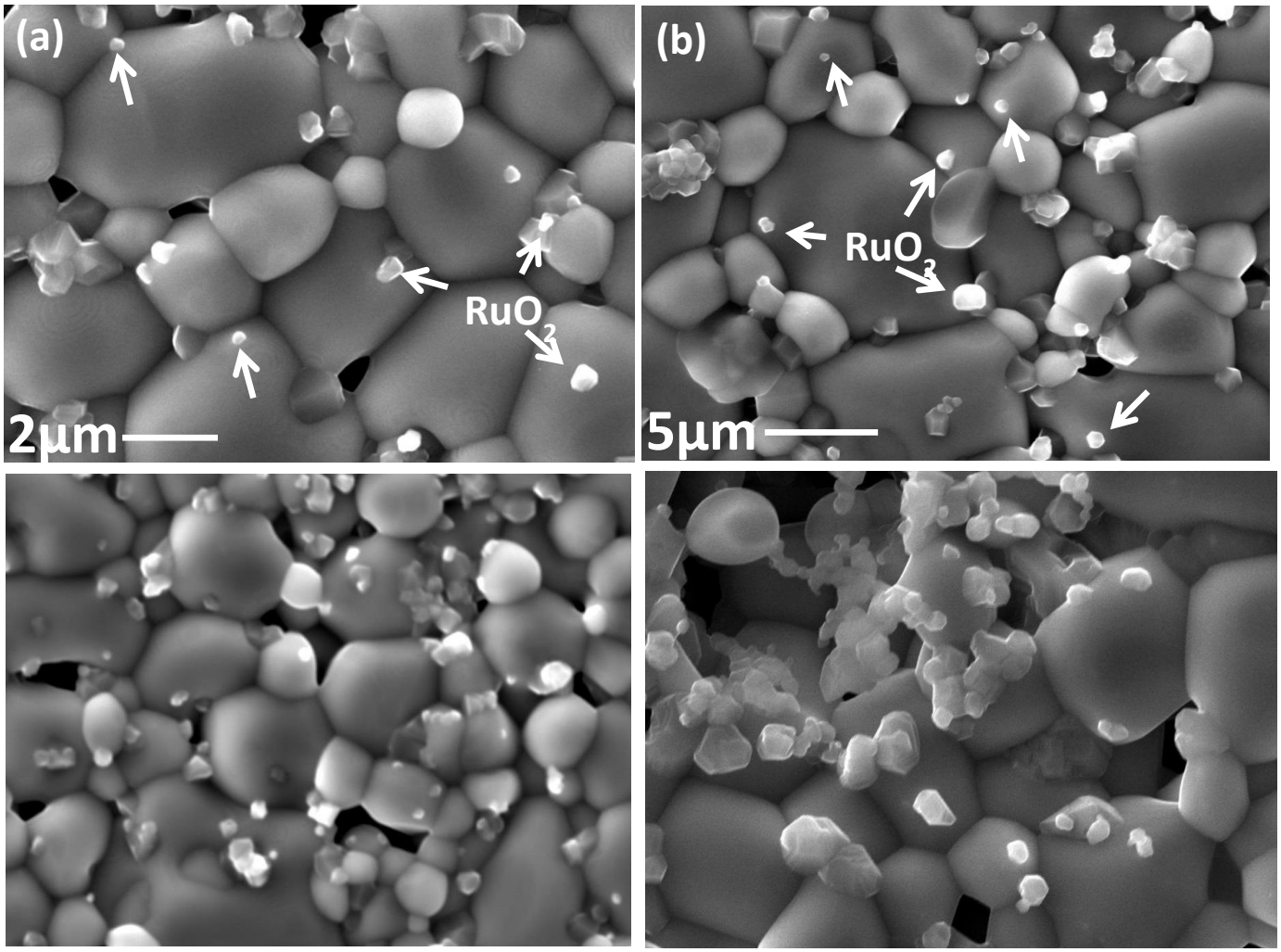

Figure 6.2 SEM images of the composite systems: (a) $RuO_2/CCTO_{SS}$ with 6% RuO_2; (b) $RuO_2/CCTO_{SG}$ with 7% RuO_2. (c) $RuO_2/CCTO_{SS}$ with 10 % RuO_2 ; (d) $RuO_2/CCTO_{SS}$ with 12% RuO_2. RuO_2 particles are represented by arrows.

respective $CCTO_{(SS/SG)}$. While no agglomeration of CCTO was observed either before or after annealing, some agglomeration of RuO_2 particles can be seen starting from 12% volume fraction of RuO_2. The size of both $CCTO_{SS}$ and $CCTO_{SG}$ particles is found to have a range of 4-10µm, with $CCTO_{SG}$ particles

being slightly larger. The log-normal fitting was done to obtain the most probable size of RuO_2, d = 0.45 ± 0.2 μm and 0.55 ± 0.1 μm in $RuO_2/CCTO_{SS}$ and $RuO_2/CCTO_{SG}$ composites as shown in figure 6.3 (a) and (b) respectively.

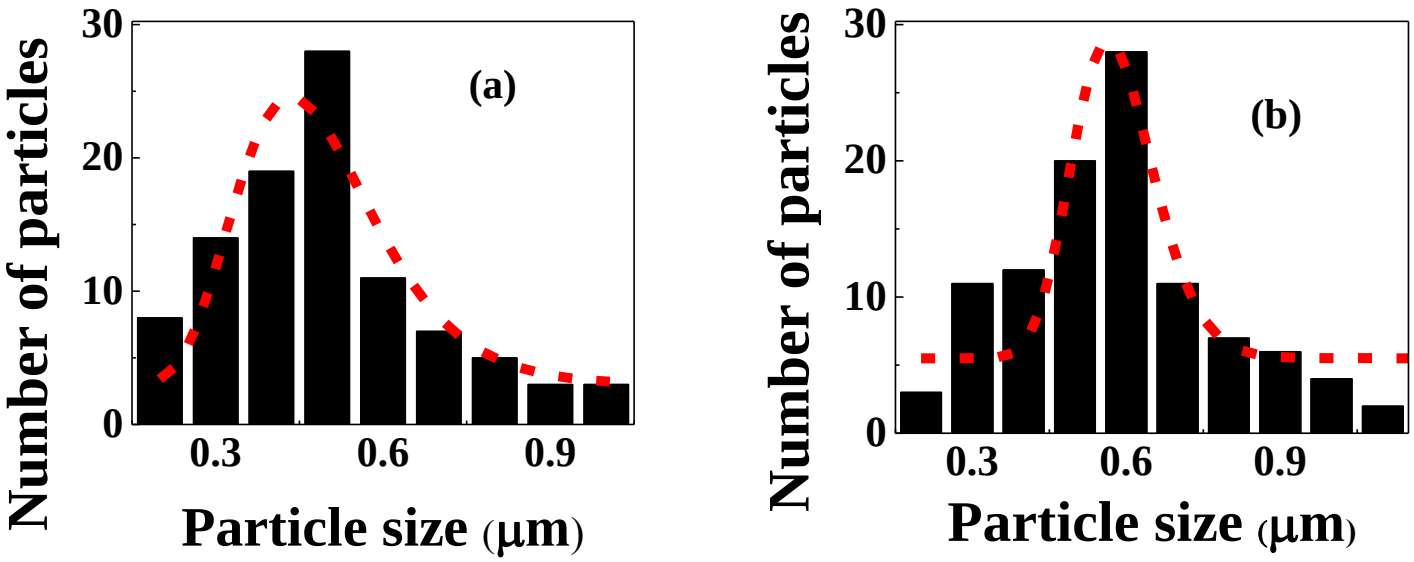

Figure 6.3(a) log-normal size distribution of RuO_2 in $RuO_2/CCTO_{SS}$; (b) log-normal size distribution of RuO_2 in $RuO_2/CCTO_{SG}$.

Importantly, no systematic changes in the microstructure of the composites in the vicinity of the percolation threshold were observed. Energy Dispersive X-ray (EDX) analysis indicates that the compound $CaCu_3Ti_4O_{12}$ is stoichiometric. EDX quantitative analysis was done to parameterize the distribution and connectivity of metallic RuO_2 clusters. We find the presence of strong peak of RuO_2 on $CCTO_{SS}$ grains, which implies that some metallic RuO_2 has diffused into the $CCTO_{SS}$ grain particles, while for the $CCTO_{SG}$ composite, the peak appears to be quite weak,

indicating little diffusion into the $CCTO_{SG}$ grains. We also did the EDX line scan on single RuO_2 particle which appears on the CCTO particles. The EDX line scan strongly confirms presence of diffusive RuO_2 small particles away from the actual RuO_2 particle which is shown in figure 6.4.

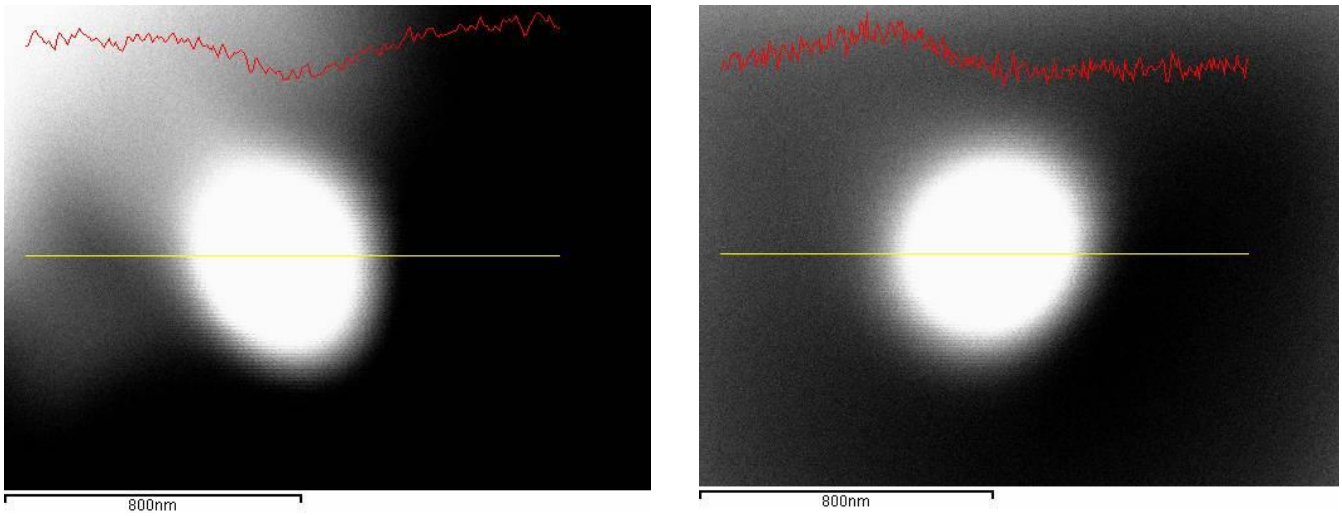

Figure 6.4 Left image shows line scan of RuO_2 on $CCTO_{SS}$ and right image shows line scan of RuO_2 on $CCTO_{SG}$ particle.

It is found that on the surface of RuO_2 particle, the line scan shows a dip rather than showing a peak of RuO_2 spectrum. This asymmetry is found due to isometric shape of RuO_2 particle due to which ejection of RuO_2 X-ray spectrum misalign with the EDX detector. It is to be noted that this diffusion can affect the electrical conduction and modify the Maxwell-Wagner effect across the interface in the matrix, which in turn, will have different dielectric response among two different CCTO hosts. To confirm the dielectric properties of as prepared $CCTO_{SS}$/$CCTO_{SG}$

samples, the temperature dependence of ε' and D at a frequency of 30 kHz were analyzed and are shown in Fig. 6.5a and Fig. 6.5b respectively. It is known that lowering the temperature increases the characteristics relaxation time of dipole moments which results in slower polarization process.[7] This explains the decrease in ε' for T < 200K as observed in the plot. The flat plateau observed in both the cases for T<100K is the direct consequence of freezing of charge carriers. Above 200K, the increase in ε' is mainly due to increase in thermally activated charge carriers, thus enhancing the Maxwell-Wagner polarization effect. The plot also reveals that ε' shows two

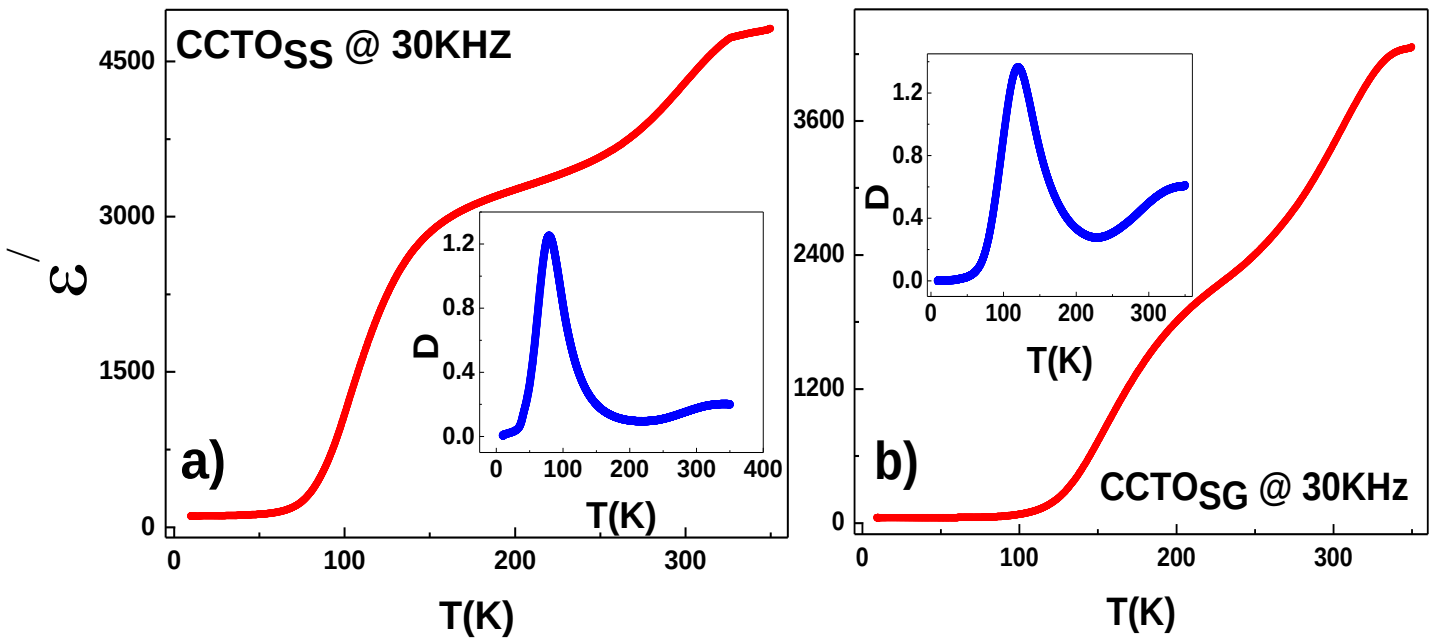

Figure 6.5 The variation of real part of dielectric permittivity with temperature for (a) $CCTO_{SS}$ and (b) $CCTO_{SG}$ at 30KHz. The insets show the temperature dependency of dielectric loss corresponding to the same frequency.

gradual drops coincident with peaks in the dielectric loss. This behavior of CCTO is consistent and confirmed by other groups working on CCTO material.[122, 135] To study the percolation effect, RuO_2 was incorporated into host dielectric matrix ($CCTO_{SS}$/$CCTO_{SG}$) at increasing volume fractions. Fig.6.6 shows the dependence of real part of effective permittivity at intermediate frequency (υ) of 30 kHz as a function of volume fraction of RuO_2, $f(RuO_2)$ in $CCTO_{SS}$ ($CCTO_{SG}$)/RuO_2 composite systems. Both series of composites show a dramatic increase in the effective permittivity at high frequency at a critical volume fraction known as percolation threshold (f_c), consistent with percolation effects. From fig 6.5a and fig. 6.5b ε' for as prepared $CCTO_{SS}$ and $CCTO_{SG}$ is found to be approximately $4x10^3$ and $3.3x10^3$ respectively at room temperature. In the RuO_2/$CCTO_{SS}$ composite, ε' increases by approximately by a factor of 7 at a ~ 10% volume fraction of RuO_2, while for RuO_2/$CCTO_{SG}$, ε' increases by a factor of 5 at 8% volume fraction. At low volume fraction, the increase in permittivity is mainly due to the presence of small isolated metallic clusters which results in strong Maxwell-Wagner effect, whereas on approaching the threshold, the enhancement is mainly dominated by percolation effect in which interparticle distance decreases with increase of cluster size. As the dielectric permittivity tends to diverge at specific metallic volume fractions, the plot confirms the percolation-type behavior.

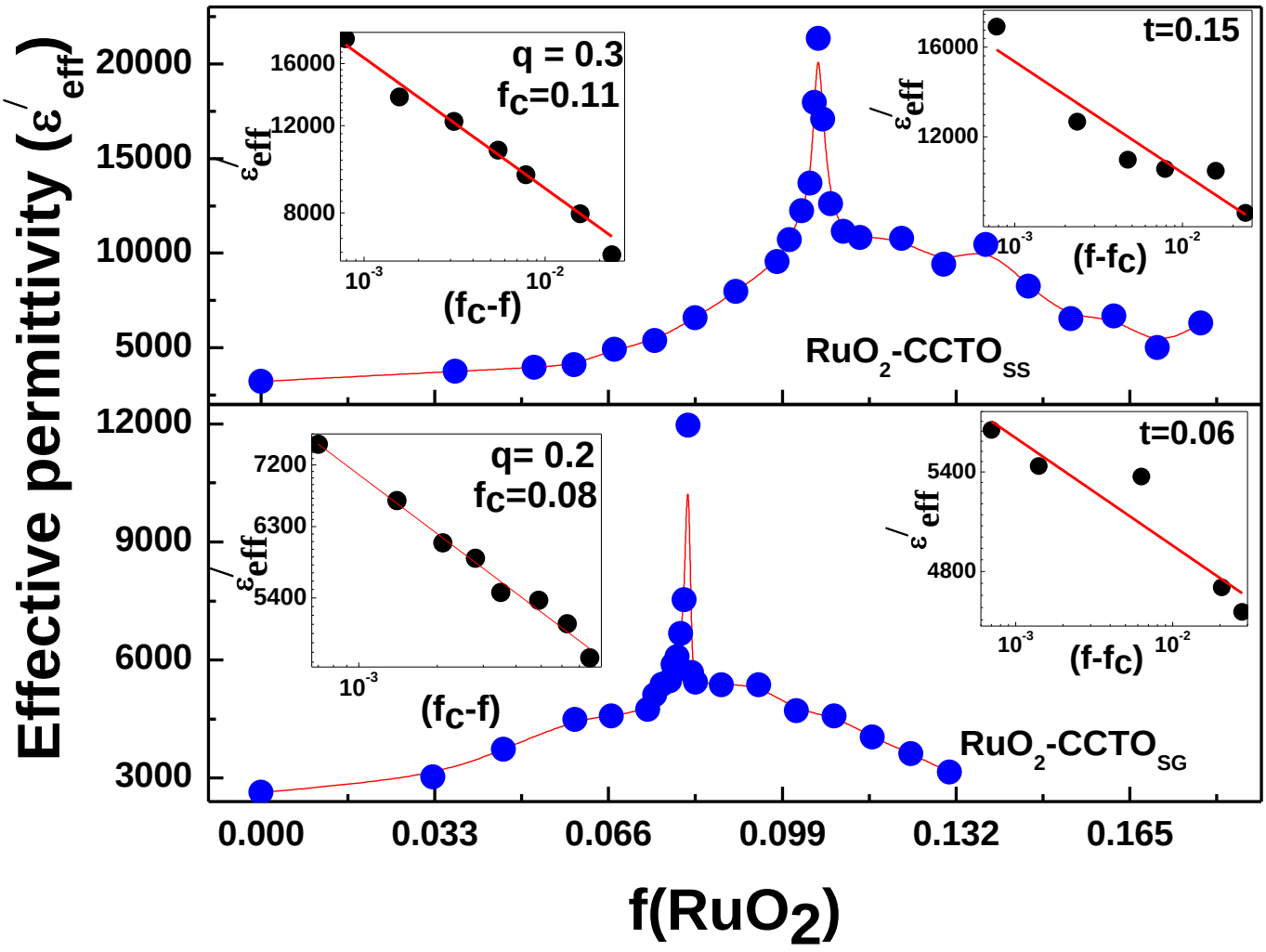

Figure 6.6 Enhancement of effective permittivity with the volume fraction of RuO_2 (f) is shown for (a) RuO_2/$CCTO_{SS}$ composites and (b) RuO_2/$CCTO_{SG}$ composites. Inset: log-log fit for determining the critical exponent below and above f_c.

At the threshold, the enhancement of the dielectric permittivity comes from the formation of microcapacitor networks (the metallic clusters separated by layer of polarized dielectric) in the composite systems.[142-144,117]. This result suggests that effective permittivity of CCTO can be improved even when metallic particles are

incorporated into the host CCTO. This is completely different from other experiments, in which CCTO was used as metallic fillers in host polymers.[135, 137] The increase in the dielectric permittivity of the composite is found to be frequency independent. The effective dielectric permittivity ε' follows a power law scaling as a function of RuO_2 composition and is given as $\varepsilon' \propto (f_c - f)^{-q}$ for $f < f_c$, and $(f - f_c)^{-t}$, for $f > f_c$, where f is the volume fraction of RuO_2, f_c is the percolation threshold, and q and t are the critical exponents. The inset in Fig. 6.6a and Fig. 6.6b shows that for RuO_2/$CCTO_{SS}$ and RuO_2/$CCTO_{SG}$ composites, f_c = 0.11 and 0.08 respectively, while q are 0.3 and 0.2 respectively. The low percolation thresholds in our composites is likely to be due to the finite conductivity of the grains and the grains boundaries in the dielectric CCTO resulted from interfacial RuO_2 diffusion, as well as the RuO_2 size dispersion, which leads to deviation from the universal threshold value of 0.16[145] Due to the same reasons, the critical exponents of the dielectric permittivity q = 0.3 and 0.2 for our composites also differ substantially from the universal value of 0.8-1.[4] We have also determined the critical exponent t on the metallic side of the metal-insulator transition $\varepsilon'_{eff} \propto (f - f_c)^{-t}$, which is found to be about 0.15 and 0.06 for RuO_2/$CCTO_{SS}$ and RuO_2/$CCTO_{SG}$ respectively. Similar to the change of ε' with f, the dielectric loss D of the composite also increases with f, as shown in fig. 6.7a. For RuO_2/$CCTO_{SS}$ composites, it is found that at 30 kHz, the loss $D < 2$ for $f < f_c$ (0.11) and for

$RuO_2/CCTO_{SG}$ composites, D < 1.5 for $f < f_c$ (0.08). It supports the fact that low increase of dielectric loss with volume fraction is the characteristics of low content/high size composites.[146] We note that, while materials with $D > 1$ are not really suitable for applications (as $D < 0.01$ is needed), there are techniques for reducing the loss in composites.[147, 148] Above the percolation thresholds, the dielectric loss increases significantly due to the increase of leakage current. Similarly, as shown in fig. 6.7 (b), the increase of conductivity (σ) in the vicinity of f = 0.11 and 0.08 is clearly seen. The best fit of the conductivity data of $RuO_2/CCTO_{SS}$ and $RuO_2/CCTO_{SG}$ composites to the equation $\sigma \propto (f_c\text{-}f)^{-q}$, for $f < f_c$ yields $q = 0.4$ and $q = 0.27$ respectively. We note that the values of q found from the electrical conductance transition are proportionally higher, compared to the ones found from the dielectric power law shown in Fig.6.6. This is likely to reflect the complex nature of the percolative transition, which will be addressed in more detail elsewhere. The conductivity of the dielectric composites $RuO_2/CCTO_{SS}$ and dependence at the low frequency region, thus implying polarization effect localized hopping among isolated metallic clusters.[149] Close to the percolation thresholds, the conductivity is found to have a relatively weak frequency dependency which is due to delocalization of carriers. The absence of flat response at low frequency at threshold signifies presence of non-percolating polarized clusters.[135]

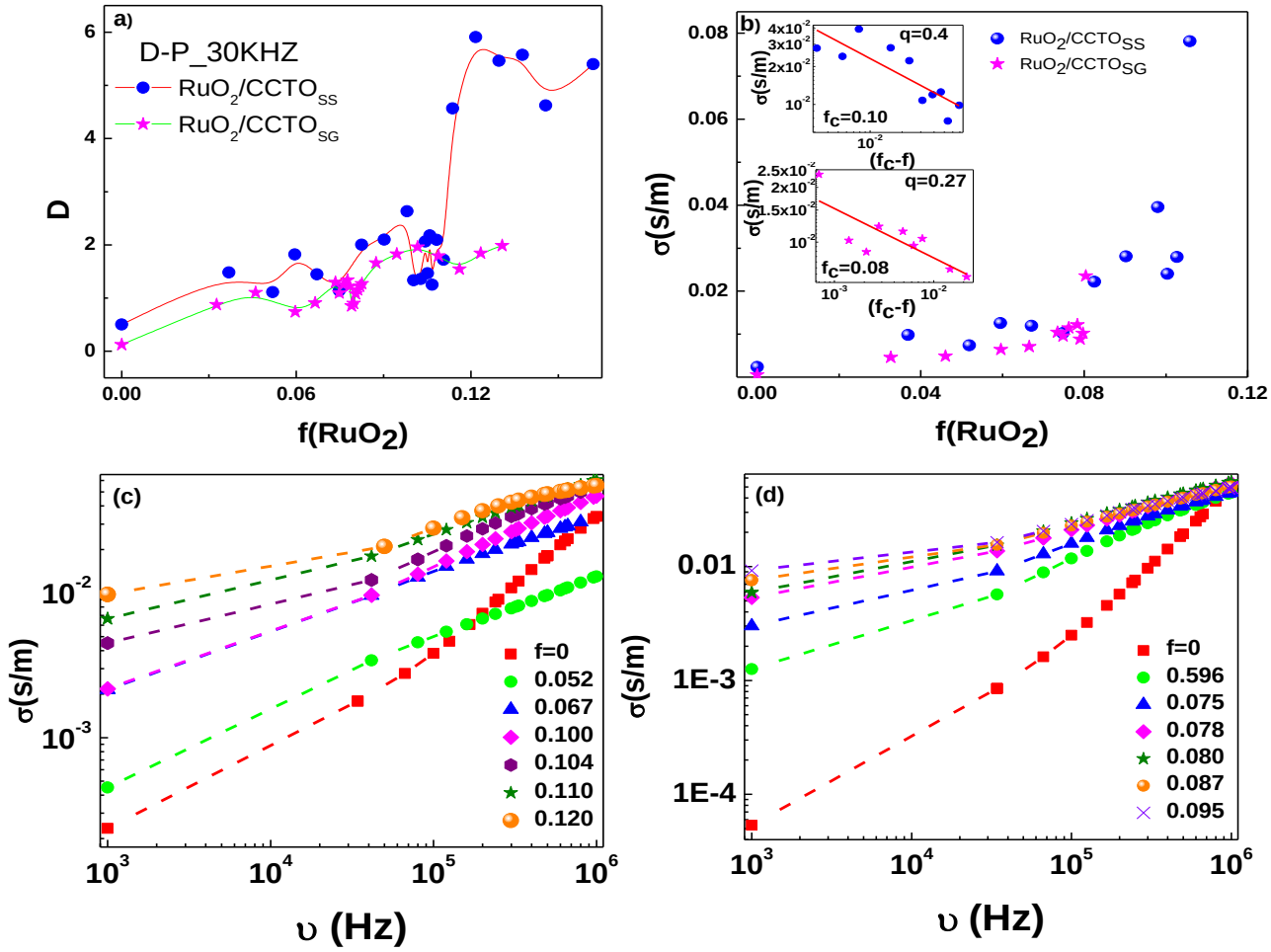

Figure 6.7 (a) Variation of dielectric loss (D) as a function of f(RuO2) in RuO2/CCTOSS and RuO2/CCTOSG composites; (b) conductivity as a function of f(RuO2) at 30KHz for both composites; inset: power law behavior at the percolation threshold; (c) conductivity as a function of frequency for series of RuO2/CCTOSS composites with increasing f(RuO2); (d) conductivity as a function of frequency for RuO2/CCTOSG composites.

6.4 Conclusion

In summary, we have fabricated CCTO by both solid state and sol-gel processes with high values of the dielectric permittivity. By introducing RuO_2 we were able to further increase the dielectric constant in the vicinity of the percolation threshold by about 5-10 times. In both $RuO_2/CCTO_{SS}$ and $RuO_2/CCTO_{SG}$ composites, the dielectric response is found to be frequency independent. The values of the critical exponent *q* for our composite system were found to be lower than in other systems, which can be attributed to different types of interaction between semiconductor (CCTO) and metallic particles (RuO_2). While we were generally successful in using RuO_2 as a metallic component, some diffusion of RuO_2 into the CCTO matrix had occurred, particularly in the case of $CCTO_{SS}$, which was likely to limit the amount of increase of the dielectric permittivity we observed, as it would broaden the percolative transition. One can further optimize the fabrication procedure to control the size and composition of grain boundaries, the degree of inter-diffusion, as well as the size of CCTO nanoparticles, which should be much smaller (about 50-100 nm) to achieve the best results. From this perspective this work is a proof of concept, as the increase of the dielectric effective permittivity near the percolation threshold is fairly modest compared to other systems. By the same token, however, that indicates that there is a lot of room for improvement in this approach, so that it can potentially

lead to dielectric permittivity in the 10^6 range, which would have important implications for various applications.

CHAPTER 7 CONCLUSIONS AND PERSPECTIVES

7.1 Conclusions

In our research percolation effects has been widely used in metal-insulator and metal-dielectric system for the study of electrical transport properties and their corresponding packing behavior. On the one hand in metal-insulator composite system such as CaCO3–CrO2, PMMA-CrO2 we have found percolation behavior to be more classical type where definite percolation threshold exists due to geometrical connectivity of conducting particles. In temperature dependent measurement, the absence of physical contact among metallic particles at particular volume fraction is supported by the fact that the ratio of resistance at low temperature to room temperature sharply increases at that specific fraction. The study of connectivity in these composites also shows that with the increase of ratio of size of insulating particles to metallic particles, the percolation threshold gets lower which supports the fact as the size of insulating particles increases the isolation between metallic particles becomes more difficult.

On the other hand in CCTO-RuO2 composite system, we have found the existence of multiple percolation thresholds that arises from tunneling behavior. This means that despite of absence of any physical contact between metallic particles which is necessary for percolation to occur, the metallic particles are still electrically

connected via tunneling phenomenon. Although tunneling behavior doesn't require physical contact, it still shows power law behavior similar to classical percolation. However, in contrast to the classical percolation behavior, these transitions are non-universal. Also, unlike classical percolation, temperature dependent measurement shows multiple transition regions with staircase-like increase in the low temperature to room temperature resistance ratio.

Since CCTO (Calcium Copper Titanate) is considered to have high dielectric permittivity, the study of its dielectric response in the presence of RuO2 as metallic fillers proved to be very interesting. We observed frequency independent increase of dielectric permittivity in the dielectric regime. The critical exponent corresponding to permittivity is found to be different from universal value which is mainly attributed to diffusion of metallic particles when annealed at 1100oC.

In addition to transport properties, we also studied the packing behavior in these composites comprising of spherical particles and cylindrical shaped nano rods. The filling factor in these composites found to increase till attains maximum and then drops beyond this volume fraction of cylindrical particles. On increasing the cylindrical particle volume fraction, the rods packed to its maximum density which appears as a peak and then beyond that excluded volume dominates and thus filling factor drops. The maximum of filling factor in composites consisting of different

size of spherical particles shows typical non-monotonic dependence on ratio of spherical particle size and cylindrical particle size.

7.2 Future perspectives

In order to better understand the tunneling process, more experiments on two phase composites with different particle shapes and sizes is required. There is plenty of room to study various types of conduction properties in nanocomposite systems. The study of microstructures in composites needs to be done more explicitly to understand the diffusion assisted tunneling process. From the application point of view it would be more interesting to prepare percolative composites with fast switching process from Off mode to On mode. In principle this composites can be structurally modified so that it can be effectively used as memory resistors. In memristors, even if power is turned off, the device can retain its resistance value for long period of time until and unless a reset voltage is applied to change its resistance. So in our lab it is obviously possible to work on this project within our instrumental limitations. Similarly, high dielectric materials can be used as memcapacitors in which even in absence of power it can retain the colossal charge for long period of time. Moreover, the packing behavior in composites can be used to study physical properties such as tensile strength, rigidity for the development of light weight flexible materials.

REFERENCES

1. S. Havlin and D. Ben-Avraham, Advances in Physics **36** (6), 695-798 (1987).

2. M. Sahini and M. Sahimi, *Applications of percolation theory*. (CRC Press, 1994).

3. E. R. C. Reynolds, Journal of Soil Science **17** (1), 127-132 (1966).

4. D. Stauffer and A. Aharony, *Introduction to Percolation Theory*. (Taylor & Francis, 1992).

5. S. R. Broadbent and J. M. Hammersley, presented at the Mathematical Proceedings of the Cambridge Philosophical Society, 1957 (unpublished).

6. A. Bunde and S. Havlin, *Fractals and disordered systems*. (Springer-Verlag New York, Inc., 1991).

7. C.-W. Nan, Progress in Materials Science **37** (1), 1-116 (1993).

8. R. Zallen, *The physics of amorphous solids*. (John Wiley & Sons, 2008).

9. C.-W. Nan, Y. Shen and J. Ma, Annual Review of Materials Research **40**, 131-151 (2010).

10. C. Chiteme and D. Mclachlan, Physica B: Condensed Matter **279** (1), 69-71 (2000).

11. I. Balberg, Carbon **40** (2), 139-143 (2002).

12. I. Balberg, Physical Review Letters **59** (12), 1305 (1987).

13. A. Malliaris and D. T. Turner, Journal of Applied Physics **42** (2), 614-618 (1971).

14. D. He and N. N. Ekere, Journal of Physics D: Applied Physics **37** (13), 1848 (2004).

15. J. Fitzpatrick, R. Malt and F. Spaepen, Physics Letters A **47** (3), 207-208 (1974).

16. H. Ottavi, J. Clerc, G. Giraud, J. Roussenq, E. Guyon and C. D. Mitescu, Journal of Physics C: Solid State Physics **11** (7), 1311 (1978).

17. X. Wang, W. Li, L. Luo, Z. Fang, J. Zhang and Y. Zhu, Journal of Applied Polymer Science **125** (4), 2711-2715 (2012).

18. T. Hanemann and D. V. Szabó, Materials **3** (6), 3468-3517 (2010).

19. C. Pecharromán and J. S. Moya, Advanced Materials **12** (4), 294-297 (2000).

20. Z.-M. Dang, Y. Shen and C.-W. Nan, Applied Physics Letters **81** (25), 4814-4816 (2002).

21. P. Kim, N. M. Doss, J. P. Tillotson, P. J. Hotchkiss, M.-J. Pan, S. R. Marder, J. Li, J. P. Calame and J. W. Perry, Acs Nano **3** (9), 2581-2592 (2009).

22. C. Pecharroman, F. t. Esteban-Betegon, J. F. Bartolome, S. Lopez-Esteban and J. S. Moya, Advanced Materials **13** (20), 1541 (2001).

23. P. K. Jana, S. Sarkar and B. Chaudhuri, Journal of Physics D: Applied Physics **40** (2), 556 (2007).

24. Z. Rubin, S. Sunshine, M. Heaney, I. Bloom and I. Balberg, Physical Review B **59** (19), 12196 (1999).

25. N. Johner, C. Grimaldi, I. Balberg and P. Ryser, Physical Review B **77** (17), 174204 (2008).

26. R. Zhang, M. Baxendale and T. Peijs, Physical Review B **76** (19), 195433 (2007).

27. A. Trionfi, D. Scrymgeour, J. Hsu, M. Arlen, D. Tomlin, J. Jacobs, D. Wang, L.-S. Tan and R. Vaia, Journal of Applied Physics **104** (8), 083708 (2008).

28. S. J. Konezny, C. Richter, R. C. Snoeberger III, A. R. Parent, G. W. Brudvig, C. A. Schmuttenmaer and V. S. Batista, The Journal of Physical Chemistry Letters **2** (15), 1931-1936 (2011).

29. U. Abdurakhmanov, S. Sharipov, Y. Rakhimova, M. Karabaeva and M. Baydjanov, Journal of the American Ceramic Society **89** (9), 2946-2948 (2006).

30. A. Petric and H. Ling, Journal of the American Ceramic Society **90** (5), 1515-1520 (2007).

31. X. Liu, R. P. Panguluri, Z.-F. Huang and B. Nadgorny, Physical Review Letters **104** (3), 035701 (2010).

32. P. I. Sorantin and K. Schwarz, Inorganic Chemistry **31** (4), 567-576 (1992).

33. P. Carcia, A. Suna and W. Childers, Journal of applied physics **54** (10), 6002-6008 (1983).

34. J. Nagamatsu, N. Nakagawa, T. Muranaka, Y. Zenitani and J. Akimitsu, nature **410** (6824), 63-64 (2001).

35. M. E. Jones and R. E. Marsh, Journal of the American Chemical Society **76** (5), 1434-1436 (1954).

36. X.-Y. Qiu, Q.-C. Zhuang, Q.-Q. Zhang, R. Cao, P.-Z. Ying, Y.-H. Qiang and S.-G. Sun, Physical Chemistry Chemical Physics **14** (8), 2617-2630 (2012).

37. Z. Jia, Z. Wang, C. Xu, J. Liang, B. Wei, D. Wu and S. Zhu, Materials Science and Engineering: A **271** (1), 395-400 (1999).

38. P. Auerkari, *Mechanical and physical properties of engineering alumina ceramics*. (Technical Research Centre of Finland Finland, 1996).

39. D. C. Sinclair, T. B. Adams, F. D. Morrison and A. R. West, Applied Physics Letters **80** (12), 2153-2155 (2002).

40. D. L. Sun, A. Y. Wu and S. T. Yin, Journal of the American Ceramic Society **91** (1), 169-173 (2008).

41. Q. Hao, V. Kulikov and V. M. Mirsky, Sensors and Actuators B: Chemical **94** (3), 352-357 (2003).

42. B. E. Warren, *X-ray Diffraction*. (Courier Dover Publications, 1969).

43. B. Abeles, H. Pinch and J. Gittleman, Physical Review Letters **35** (4), 247 (1975).

44. P. Sheng, B. Abeles and Y. Arie, Physical Review Letters **31** (1), 44 (1973).

45. E. Sichel, J. Gittleman and P. Sheng, Journal of Electronic Materials **11** (4), 699-747 (1982).

46. P. Sheng, E. Sichel and J. Gittleman, Physical Review Letters **40** (18), 1197 (1978).

47. Z. Rubin, S. A. Sunshine, M. B. Heaney, I. Bloom and I. Balberg, Physical Review B **59** (19), 12196-12199 (1999).

48. I. Balberg, D. Azulay, D. Toker and O. Millo, International Journal of Modern Physics B **18** (15), 2091-2121 (2004).

49. M. Sahimi, *Heterogeneous Materials I: Linear transport and optical properties*. (Springer, 2003).

50. B. I. Shklovskii and A. L. Efros, Moscow Izdatel Nauka **1** (1979).

51. G. Ambrosetti, I. Balberg and C. Grimaldi, Physical Review B **82** (13), 134201 (2010).

52. G. Ambrosetti, N. Johner, C. Grimaldi, T. Maeder, P. Ryser and A. Danani, Journal of Applied Physics **106** (1), 016103 (2009).

53. G. Ambrosetti, C. Grimaldi, I. Balberg, T. Maeder, A. Danani and P. Ryser, Physical Review B **81** (15), 155434 (2010).

54. D. Toker, D. Azulay, N. Shimoni, I. Balberg and O. Millo, Physical review B **68** (4), 041403 (2003).

55. I. Balberg, Journal of Physics D: Applied Physics **42** (6), 064003 (2009).

56. B. Nettelblad, E. Mårtensson, C. Önneby, U. Gäfvert and A. Gustafsson, Journal of Physics D: Applied Physics **36** (4), 399 (2003).

57. D. Stauffer and A. Aharony, *Introduction To Percolation Theory*. (Taylor & Francis, 1994).

58. A. Hunt and R. Ewing, *Percolation theory for flow in porous media*. (Springer, 2009).

59. S.-I. Lee, Y. Song, T. W. Noh, X.-D. Chen and J. R. Gaines, Physical Review B **34** (10), 6719-6724 (1986).

60. S. Vionnet-Menot, C. Grimaldi, T. Maeder, S. Strässler and P. Ryser, Physical Review B **71** (6), 064201 (2005).

61. B. Derrida, D. Stauffer, H. J. Herrmann and J. Vannimenus, J. Physique Lett. **44** (17), 701-706 (1983).

62. A. Celzard, E. McRae, J. F. Marêché, G. Furdin, M. Dufort and C. Deleuze, Journal of Physics and Chemistry of Solids **57** (6–8), 715-718 (1996).

63. S. Nakamura, K. Saito, G. Sawa and K. Kitagawa, Jpn J Appl Phys 1 **36** (8), 5163-5168 (1997).

64. J. Donnet, R. Bansal and M. Wang, Science and Technology, New York, 62-64 (1993).

65. Y. Fujikura, Polymer journal **21** (8), 609-614 (1989).

66. E. K. Sichel, J. I. Gittleman and P. Sheng, Physical Review B **18** (10), 5712-5716 (1978).

67. Y.-F. Wei and Z.-Q. Li, Applied Physics Letters **102** (13), 131911-131911-131914 (2013).

68. I. Balberg, Physical Review Letters **59** (12), 1305-1308 (1987).

69. I. Balberg, D. Azulay, Y. Goldstein, J. Jedrzejewski, G. Ravid and E. Savir, Eur. Phys. J. B **86**, 1-17 (2013).

70. H. Yu, H. Liu, H. Hao, L. Guo, C. Jin, Z. Yu and M. Cao, Applied Physics Letters **91** (22), - (2007).

71. R. Mukherjee, G. Lawes and B. Nadgorny, Applied Physics Letters **105** (7), - (2014).

72. C. Grimaldi and I. Balberg, Physical Review Letters **96** (6), 066602 (2006).

73. Z.-M. Dang, Y. Zheng and H.-P. Xu, Journal of Applied Polymer Science **110** (6), 3473-3479 (2008).

74. R. Morgunov and A. Dmitriev, Russian Journal of General Chemistry **80** (3), 591-603 (2010).

75. I. Tsuyumoto, Y. Iida and H. Hori, International Journal of Applied Ceramic Technology **8** (6), 1408-1413 (2011).

76. R. Fisch and A. B. Harris, Physical Review B **18** (1), 416-420 (1978).

77. C. H. Grimm, Journal of physics. Conference series **150** (2), 022019 (2009).

78. I. Boro and G. Hinrichsen, Polymer Bulletin **33** (4), 471-478 (1994).

79. H. E. Roman and M. Yussouff, Physical Review B **36** (13), 7285-7288 (1987).

80. M. B. Isichenko, Reviews of Modern Physics **64** (4), 961-1043 (1992).

81. V. Sahni, B. S. Sathyaprakash and S. F. Shandarin, Astrophys J **476** (1), L1-L5 (1997).

82. A. V. Kyrylyuk, M. Anne van de Haar, L. Rossi, A. Wouterse and A. P. Philipse, Soft Matter **7** (5), 1671-1674 (2011).

83. D. He and N. Ekere, Journal of Physics D: Applied Physics **37** (13), 1848 (2004).

84. H. S. Göktürk, T. J. Fiske and D. M. Kalyon, Journal of Applied Polymer Science **50** (11), 1891-1901 (1993).

85. C. W. Nan, Y. Shen and J. Ma, in *Annual Review of Materials Research, Vol 40*, edited by D. R. Clarke, M. Ruhle and F. Zok (Annual Reviews, Palo Alto, 2010), Vol. 40, pp. 131-151.

86. A. Kyrylyuk, A. Wouterse and A. Philipse, in *Trends in Colloid and Interface Science XXIII* (Springer Berlin Heidelberg, 2010), Vol. 137, pp. 29-33.

87. G. M. Paily and S. Neogi, (November, 2005).

88. X. H. Wang, E. Perlsman and S. Havlin, Physical review. E, Statistical, nonlinear, and soft matter physics **67** (5 Pt 1), 050101 (2003).

89. R. Consiglio, R. N. A. Zouain, D. R. Baker, G. Paul and H. E. Stanley, Physica A: Statistical Mechanics and its Applications **343** (0), 343-347 (2004).

90. I. Balberg, N. Binenbaum and N. Wagner, Physical Review Letters **52** (17), 1465-1468 (1984).

91. I. Balberg, C. H. Anderson, S. Alexander and N. Wagner, Physical Review B **30** (7), 3933-3943 (1984).

92. J. Ravez, C. Broustera and A. Simon, J. Mater. Chem. **9** (7), 1609-1613 (1999).

93. S. Anwar, P. Sagdeo and N. Lalla, Solid state communications **138** (7), 331-336 (2006).

94. A. Ramirez, M. Subramanian, M. Gardel, G. Blumberg, D. Li, T. Vogt and S. Shapiro, Solid State Communications **115** (5), 217-220 (2000).

95. M. Subramanian and A. Sleight, Solid State Sciences **4** (3), 347-351 (2002).

96. M. E. Lines and A. M. Glass, *Principles and applications of ferroelectrics and related materials*. (Clarendon press Oxford, 2001).

97. L. He, J. Neaton, M. H. Cohen, D. Vanderbilt and C. Homes, Physical Review B **65** (21), 214112 (2002).

98. G. Chiodelli, V. Massarotti, D. Capsoni, M. Bini, C. Azzoni, M. Mozzati and P. Lupotto, Solid state communications **132** (3), 241-246 (2004).

99. M. Subramanian, D. Li, N. Duan, B. Reisner and A. Sleight, Journal of Solid State Chemistry **151** (2), 323-325 (2000).

100. L. M. Falicov and J. C. Kimball, Physical Review Letters **22** (19), 997-999 (1969).

101. T. Portengen, T. Östreich and L. J. Sham, Physical Review Letters **76** (18), 3384-3387 (1996).

102. G. Czycholl, Physical Review B **59** (4), 2642 (1999).

103. R. Schmidt and D. C. Sinclair, Chemistry of Materials **22** (1), 6-8 (2009).

104. E. Barsukov and J. R. Macdonald, Inc., Hoboken, New Jersey (2005).

105. R. Schmidt, (2007).

106. J. T. Irvine, D. C. Sinclair and A. R. West, Advanced Materials **2** (3), 132-138 (1990).

107. M. Li, Z. Shen, M. Nygren, A. Feteira, D. C. Sinclair and A. R. West, Journal of Applied Physics **106** (10), 104106 (2009).

108. S. Shao, J. Zhang, P. Zheng, W. Zhong and C. Wang, Journal of applied physics **99** (8), 084106 (2006).

109. T. B. Adams, D. C. Sinclair and A. R. West, Physical Review B **73** (9), 094124 (2006).

110. S. Elliott, Solid State Ionics **70**, 27-40 (1994).

111. Y. Song, T. W. Noh, S.-I. Lee and J. R. Gaines, Physical Review B **33** (2), 904 (1986).

112. I. Webman, J. Jortner and M. H. Cohen, Physical Review B **11** (8), 2885 (1975).

113. P. Simon and Y. Gogotsi, Nature materials **7** (11), 845-854 (2008).

114. B. Skinner, M. Loth and B. Shklovskii, Physical review letters **104** (12), 128302 (2010).

115. A. L. Efros, Physical Review B **84** (15), 155134 (2011).

116. V. Dubrov, M. Levinshtein and M. Shur, Soviet Journal of Experimental and Theoretical Physics **43**, 1050 (1976).

117. A. Efros and B. Shklovskii, physica status solidi (b) **76** (2), 475-485 (1976).

118. D. J. Bergman and Y. Imry, Physical Review Letters **39** (19), 1222 (1977).

119. M. Valant, A. Dakskobler, M. Ambrozic and T. Kosmac, Journal of the European Ceramic Society **26** (6), 891-896 (2006).

120. M. A. Subramanian, Solid state sciences **4** (3), 347-351 (2002).

121. A. P. Ramirez, Solid state communications **115** (5), 217-220 (2000).

122. C. C. Homes, Science (New York, N.Y.) **293** (5530), 673-676 (2001).

123. T. B. Adams, Advanced materials (Weinheim) **14** (18), 1321-1323 (2002).

124. T. Fang, Acta materialia **54** (10), 2867-2875 (2006).

125. W. Q. Ni, Journal of materials science **42** (3), 1037-1041 (2007).

126. T. B. Adams, Journal of the American Ceramic Society **89** (10), 3129-3135 (2006).

127. P. Lunkenheimer, Physical review. B, Condensed matter and materials physics **70** (17), 172102 (2004).

128. T. Prodromakis and C. Papavassiliou, Applied Surface Science **255** (15), 6989-6994 (2009).

129. C. C. Wang and L. W. Zhang, Applied Physics Letters **92** (13), 132903-132903-132903 (2008).

130. D. Sinclair and T. Adams, App1. Phys. I ett **8** (12), 2 (2002).

131. J. L. Zhang, Applied physics letters **87** (14), 142901 (2005).

132. M. Li, Z. Shen, M. Nygren, A. Feteira, D. C. Sinclair and A. R. West, Journal of Applied Physics **106** (10), 104106-104106-104108 (2009).

133. T. B. Adams, D. C. Sinclair and A. R. West, Advanced Materials **14** (18), 1321-1323 (2002).

134. R. K. Pandey, W. A. Stapleton, J. Tate, A. K. Bandyopadhyay, I. Sutanto, S. Sprissler and S. Lin, AIP Advances **3** (6), - (2013).

135. Z.-M. Dang, T. Zhou, S.-H. Yao, J.-K. Yuan, J.-W. Zha, H.-T. Song, J.-Y. Li, Q. Chen, W.-T. Yang and J. Bai, Advanced Materials **21** (20), 2077-2082 (2009).

136. Q. Chi, J. Sun, C. Zhang, G. Liu, J. Lin, Y. Wang, X. Wang and Q. Lei, Journal of Materials Chemistry C **2** (1), 172-177 (2014).

137. W. Yang, S. Yu, R. Sun, S. Ke, H. Huang and R. Du, Journal of Physics D: Applied Physics **44** (47), 475305 (2011).

138. B. Shri Prakash and K. B. R. Varma, Composites Science and Technology **67** (11–12), 2363-2368 (2007).

139. M. Panda, V. Srinivas and A. K. Thakur, Applied Physics Letters **99** (4), 042905-042905-042903 (2011).

140. C. C. Wang, Y. J. Yan, L. W. Zhang, M. Y. Cui, G. L. Xie and B. S. Cao, Scripta Materialia **54** (8), 1501-1504 (2006).

141. W. Tuichai, S. Somjid, B. Putasaeng, T. Yamwong, A. Chompoosor, P. Thongbai, V. Amornkitbamrung and S. Maensiri, Nanoscale research letters **8** (1), 494 (2013).

142. D. J. Bergman and Y. Imry, Physical Review Letters **39** (19), 1222-1225 (1977).

143. C.-W. Nan, Y. Shen and J. Ma, Annual Review of Materials Research **40** (1), 131-151 (2010).

144. W. Tuichai, S. Somjid, B. Putasaeng, T. Yamwong, A. Chompoosor, P. Thongbai, V. Amornkitbamrung and S. Maensiri, Nanoscale research letters **8** (1), 1-6 (2013).

145. L. Wang and Z.-M. Dang, Applied Physics Letters **87** (4), - (2005).

146. G. Perrier and A. Bergeret, Journal of Polymer Science Part B: Polymer Physics **35** (9), 1349-1359 (1997).

147. E. A. Patterson, Applied physics letters **87** (18), 182911 (2005).

148. S.-W. Choi, Journal of the American Ceramic Society **0** (0), 070922001308001-??? (2007).

149. Y. Song, T. W. Noh, S.-I. Lee and J. R. Gaines, Physical Review B **33** (2), 904-908 (1986).

ABSTRACT

CORRELATION EFFECTS IN NANOPARTICLE COMPOSITES: PERCOLATION, PACKING AND TUNNELING

by

RUPAM MUKHERJEE

December 2014

Advisor: Boris Nadgorny

Major: Physics

Degree: Doctor of Philosophy

Percolation is one of the most fundamental and far-reaching physical phenomena, with major implications in a vast variety of fields. The work described in this thesis aims to understand the role of percolation effects in various, seemingly unrelated phenomena, such as the dielectric permittivity of metal-insulator composites, tunneling percolation, and the relationship between percolation and filling factors. Specifically, we investigated 1) the very large enhancement of the dielectric permittivity of a composite metal – insulator system, RuO_2 - $CaCu_3Ti_4O_{12}$ (CCTO) near the percolation threshold. For RuO_2/CCTO composites, an increase in the real part of the dielectric permittivity (initially about 10^3-10^4 at 10 kHz) by approximately an order of magnitude is observed in the vicinity of the percolation threshold. 2) In the same system, apart from a classical percolation transition associated with the appearance of a continuous conductance

path through RuO_2 nanoparticles, at least two additional tunneling percolation transitions are detected. Such behavior is consistent with the recently emerged picture of a quantum conductivity staircase, which predicts several percolation tunneling thresholds in a system with a hierarchy of local tunneling conductance, due to various degrees of proximity of adjacent conducting particles distributed in an insulating matrix. 3) The filling factors of the composites of nanoparticles with different shapes have been studied as a function of volume fraction. Interestingly, like percolation, filling factors also obey critical power law behavior as a function of size ratio of constituent particles.

AUTOBIOGRAPHICAL STATEMENT

RUPAM MUKHERJEE

Education: 2009-2014 Ph.D. Wayne State University, Detroit, Michigan

2009- 2012 M.S. Wayne State University, Detroit, Michigan

2006-2008 M.Sc. Indian Institute of Technology, IIT Guwahati, India

2002-2005 B.Sc. Rama Krishna Mission Vidyamandira, Belur, India

Awards: 2014 Summer Dissertation Scholarship, Wayne State University

Professional Membership: 2009-2014 American Physical Society

Publications, poster presentations and conference talk:

- R.Mukherjee, Z-F. Huang, B.Nadgorny; "Multiple percolation tunneling staircase in RuO2-CaCu3Ti4O12 nanoparticle composites" **Applied Physics Letters 105, 173104 (2014)** .
- R.Mukherjee, G.Lawes and B.Nadgorny; "Enhancement of high dielectric permittivity in $CaCu_3Ti_4O_{12}/RuO_2$ composites in the vicinity of the percolation threshold". **Applied Physics Letters 105, 072901 (2014**)
- S.S.Laha, R.Mukherjee, G.Lawes; "Interactions and magnetic relaxation in boron doped Mn_3O_4 nanoparticles. **Material Research Express 1, 025032 (2014)**
- D.Mishra, B.P.Mandal, R.Mukherjee, R.Naik, G.Lawes and B.Nadgorny; "Oxygen Vacancy enhanced room temperature magnetism in Al-doped MgO nanoparticles. **Applied Physics Letters 102, 182404 (2013)**
- "Tunneling percolation behavior and filling factors in metal-insulator nanocomposites", American Physical Society March Meeting, March 4, 2014, Denver, Colorado, USA.
- "Enhancement of dielectric constant at percolation threshold in CaCu3Ti4O12 ceramic fabricated by both solid state and sol-gel process", Poster presentation, American Physical Society March Meeting, March 4, 2014, Denver, Colorado, USA.
- "Giant dielectric constant in CaCu3Ti4O12-MgB2 composites near the percolation threshold" American Physical Society March Meeting, March 20, 2013, Baltimore, Maryland, USA.